Doctoral Thesis

A New Role of Srs2 DNA Helicase, anti-recombinase, during Meiosis

Hana Subhan Memon Sakurai
March 2021

Laboratory of Genome and Chromosome Functions
Department of Biological Science
Graduate School of Science
Osaka University

Table of Contents

List of Abbreviations

AP	Alkaline phosphatase
APC/C	Anaphase promoting complex/cyclosome
ATP	Adenosine triphosphate
BSA	Bovine serum albumin
°C	Degrees Celsius
CHEF	Counter-clamped homogeneous electric fields
CO	Crossover
DAPI	6'-diamidino-2-phenylindole
D-loop	Displacement loop
dHJs	double Holliday Junctions
DNA	Deoxyribonucleic acid
DSB	Double strand break
DTT	Dithiothreitol
EDTA	Ethylene diamine tetra-acetic acid
EtOH	Ethanol
HR	Homologous recombination
IH	Inter-homolog
IS	Inter-sister
JMs	Joint molecules
MI	Meiosis I
MII	Meiosis II
MES	2-(N-morpholino)-ethane sulfonic acid
mJ	milli Joules
ml	milli litre
NCO	Non-crossover
PAGE	Polyacrylamide gel electrophoresis
PBS	Phosphate-buffered saline
PCR	Polymerase chain reaction
PEG	Polyethylene glycol
PFA	Paraformaldehyde
PFGE	Pulse field gel electrophoresis
PLK	Polo-like kinase
RNase	Ribonuclease
RPA	Replication protein A
SC	Synaptonemal complex
S.D	Standard deviation
SEI	Single end invasion intermediate
ssDNA	Single-stranded DNA
TBS	Tris-buffered saline
TCA	Trichloro-acetic acid
UV	Ultra violet
V	Volt
ZMM	Zip-Msh-Mer
µl	Micro litre

Summary

Homologous recombination (HR) is involved in the repair of DNA double-strand breaks (DSBs) in both mitosis and meiosis. HR between homologous chromosomes provides a physical linkage between the chromosomes, which ensures correct segregation of the chromosomes during meiosis I (MI). In HR, Rad51, a RecA homolog, plays a key role in homology search and strand exchange by forming a helical filament on the single-stranded DNA (ssDNA). Rad51 is required for HR in both mitosis and meiosis. In addition to Rad51, a meiosis-specific RecA homolog, Dmc1, is also essential for meiotic recombination. In meiotic recombination, Dmc1 is the main strand-exchange protein for recombination between homologous chromosomes, while Rad51 assists Dmc1-assembly. Assembly and disassembly of Rad51 and Dmc1 filaments are highly dynamic and strictly controlled by several positive and negative factors. In mitosis, Srs2 DNA helicase functions as a negative regulator for HR and indeed has been shown to dislodge Rad51 filaments, thereby inhibiting Rad51-dependent strand invasion. Srs2 is also critical for meiotic recombination. However, its role in HR in meiosis remains to be elusive.

In this study, in order to analyze a role for Srs2 during meiosis, the effect of *SRS2* deletion in S. *cerevisiae* meiosis has been studied in more detail. Previous works have shown that the *srs2* deletion mutant shows reduced sporulation, lowered spore viability, and slight decrease in recombination products. However, the decrease in recombination products does not fully explain the observed low spore viability of the mutant. While the mutant shows wild-type like assembly and disassembly of Rad51 and Dmc1 at early stages of meiosis, it later exhibits a unique defect in the assembly of Rad51: the formation of a large aggregate containing Rad51, but not Dmc1. In this thesis, a new role of Srs2 during meiosis was identified. Srs2 is shown to have dual functions in meiosis, one being in early meiosis and the second role being after the mid-prophase I exit by the induction of the meiotic transcription factor Ndt80. During meiotic DSB repair in early prophase, it was shown that, in the absence of Srs2, abnormal events of strand invasion by Rad51 leads to multiple-invasion. These multiple invasions are prevented by Srs2, by directly disrupted Rad51 mediated strand invasion intermediates and dismantling the structures to ensure proper resolution. The depletion of Srs2 after Ndt80 induction, thus mid-prophase I exit,

was sufficient to induce the formation of the Rad51 aggregates, suggesting that Srs2 plays a novel role in late prophase I. This also indicated that the early defect in Rad51 loading is not a precursor for the formation of Rad51 aggregates observed during late meiosis in the *srs2* mutant. In conclusion, Srs2 regulates the formation of Rad51 filaments at two different stages in meiotic prophase I, in early and late meiotic prophase I separately. Srs2 functions during the meiotic DSB repair event and additionally, at the resolution step of recombination intermediates, most likely by it's translocase activity. In this thesis, the role of Srs2 in coupling the completion of recombination with consecutive chromosomal events will be further discussed.

Section 1: Introduction

1-1 DNA double strand break (DSB) repair

The genome of a cell is subjected to DNA damage induced by exogenous sources such as, ultra-violet (UV) ray, radiation or mutagenic chemicals, as well as endogenous events such as stalled DNA replication and free radical formation, threatening the genomic integrity of the cell if the damage are not properly removed. Genetic stability is pivotal to ensure inheritance of genetic information, and thus the cell has evolved a series of regulatory mechanisms to ensure the maintenance of the genetic information passed down over to the next generation. Out of the different types of DNA lesions, a DNA double strand break (DSB), with two broken DNA ends, is the most detrimental and, thus once formed, induces several responses in the cell (Jackson, 2002; Khanna and Jackson, 2001; van Gent *et al.*, 2001). DSBs pose a threat to the genome stability by eliciting chromosome rearrangement which often disrupts the gene structure and function (Schully *et al.*, 2019).

DSBs are majorly repaired by two distinct repair pathways, non-homologous end joining (NHEJ) and homologous recombination (HR).

1-1-1 Non-homologous end joining (NHEJ)

In non-homologous end joining (NHEJ), the DSB ends are processed by a nuclease and the ends are ligated together with low or no sequence homology between the end sequences. This repair mechanism is error-prone as genetic information is lost by the resection of the DSB ends. Although NHEJ can occur throughout the cell cycle, it is notably dominant in G1 and G2 phases (Chiruvella *et al.*, 2013, Karanam *et al.*, 2012). NHEJ has a distinct role in protecting the genome integrity for most of the repair events, as the repair is quick and importantly, it suppresses chromosomal translocations (Difilippantonio *et al.*, 2000).

1-1-2 Homologous recombination (HR)

In homologous recombination (HR), the 5' DSB end is resected to produce a 3'-overhanging single-stranded DNA (ssDNA), which invades into a template homologous duplex DNA (Intro figure 1). The invaded ends with 3'-OH in the duplex DNA provides a template for the DNA synthesis that recovers DNA information lost in the resection. HR is an error-free repair mechanism as the DNA information is not lost during the repair. DSB repair by HR occurs predominantly during mid-S and G2 phases, when a sister chromatid is available as a template for HR (Karanam *et al.*, 2012). Strand invasion followed by further processing leads to the formation of a double Holliday junction (dHJ), which can be resolved into either crossover (CO) or non-crossover (NCO, a.k.a., gene conversion) in a canonical DSB repair (Matos and West, 2014). Alternatively, in synthesis-dependent strand annealing (SDSA), one end of the resected DNA engages with the duplex DNA while the second end remains idle (Paques and Haber, 1999). The non-invading second DNA end anneals to the displaced strand with an extended ssDNA by DNA synthesis. SDSA does not involve dHJ structures as an intermediate and thus results in non-crossovers.

1-2 Meiosis

Somatic diploid (2n) cells divide to give two identical sister diploid cells by a cell division termed mitosis. Once committed to the division at G1 phase, cells undergo S phase, where the duplication of genome takes places by forming two sister chromatids. During M phase, where the separation of sister chromatids is performed. Mitosis is classified into prophase (G1, S and G2 phases) and M phase of metaphase, anaphase and telophase. Sexual reproduction in eukaryotic cells requires the fertilization of male and female gametes, with half the number of chromosomes relative to somatic cells, to form diploid zygote with a full number of chromosomes. To produce haploid germ cells, the eukaryotic organism makes use of a specialized form of cell division called, 'meiosis'. Meiosis begins with one round of chromosome duplication, followed by two rounds of chromosome segregation, meiosis I and II. In meiosis I (MI) homologous chromosomes

are segregated followed by segregation of sister chromatids in meiosis II (MII), producing four haploid cells, from a single diploid cell.

Importantly, during meiosis, the formation of DNA double-strand breaks (DSBs) is a part of the meiotic program to induce HR between homologous chromosomes, which is important for the increase genetic diversity of the gametes and also to provide a physical linkage between the homologous chromosomes. Recombination brings each homologous chromosome pair into close end-to-end proximity and thus facilitating their association (Romanienko and Camerini-Otero, 2000; Peoples *et al.*, 2002; Tessé *et al.*, 2003; Henderson and Keeney, 2004; Zickler and Kleckner, 2015). The exchange of DNA between the two homologous chromosomes results in the formation of crossovers (COs) forming a connection called, 'chiasmata' (Roeder, 1997; Smith and Nicolas, 1998; Zickler and Kleckner, 1999). Chiasmata are essential for proper segregation of homologous chromosomes at the first meiotic division (MI) as they allow for stable biorientation of the homologous chromosome pair on the MI-spindle (Carpenter, 1994), similar to how cohesion aids in stably bi-orienting the sister chromatids on the mitotic-spindle (Petronczki *et al.*, 2003; Hunter, 2013). Additionally, physical linkage at chromosome arms, which holds sister chromatids together, and monopolar attachment of microtubules to sister kinetochores ensure accurate segregation of the chromosomes during MI (Petronczki, Siomos, and Nasmyth, 2003). Segregation of sister chromatid in MII is followed by the release of cohesion between them. Defects in meiotic recombination can lead to de novo germline mutations, gametes with abnormal chromosome numbers, and infertility. Additionally, aneuploidy in meiosis is detrimental. In mice, loss and gain of somatic chromosome is embryonically lethal. In humans, most meiotic aneuploidy leads to spontaneous abortions in early pregnancy or miscarriages in the first trimester (Ljunger *et al.*, 2005). However, gain and loss of small chromosome can be viable but display severe congenital diseases such as in Down's syndrome (trisomy 21), which is a gain of chromosome 21, the smallest somatic chromosome.

In addition to proper chromosomal segregation, HR in meiosis plays a core role in increasing genetic diversity by creating new allele combinations by both homologous crossover and gene conversion, and also contributes to evolution of genes (Haber, 2014; Giurouilh-Barbat *et al.*, 2014; Lambert and Lopez, 2001). Through HR, linked deleterious

mutations are selectively eliminated and the beneficial variants are preserved and repaired. A higher rate in recombination leads to higher genetic diversity at a specific genomic region, population or even species.

1-3 Meiotic recombination

During meiosis, Spo11, a meiosis-specific topoisomerase-like protein, catalyzes DSB formation to initiate meiotic recombination (Keeney *et al.*, 1997) (Intro figure 2). All three members of the Mre11-Rad50-Xrs2/Nbs1 (MRX/N) complex in addition to Spo11 are required for the formation of meiotic DSBs in *S. cerevisiae* (Keeney, 2001). Mre11's nuclease activity is important for meiotic recombination (Tsubouchi and Ogawa, 1998; Furuse *et al.*, 1998; Moreau *et al.*, 1999; Usui *et al.*, 1998). Sae2 is also shown to have intersecting roles with MRX/N complex (McKee and Kleckner, 1997; Prinz *et al.*, 1997). Mre11 and Sae2 mediate the endo-nucleolytic processing of Spo11 bound DSBs (Neale *et al.*, 2005). Resection of the 5'-end of DSBs results in the generation of a 3'-overhanging ssDNA, which is used for homology search and strand exchange. An ssDNA binding protein, Replication protein A (RPA), binds to the exposed ssDNA. Then, to the RPA-coated ssDNA, Rad52 is recruited and mediates the loading of Rad51, a bacterial RecA homolog, on to the RPA-coated ssDNA (Sung, 1997; Shinohara and Ogawa, 1998; New *et al.* 1998). Rad51 forms a right-handed filament on the ssDNA, called the pre-synaptic filament. Rad51 is required for homology search and strand exchange, which is the key step in HR (Shinohara, 1992). In mitotic recombination, Rad51 filament catalyzes homology search between the ssDNA and a homologous duplex DNA, and then invades the ssDNA into the duplex DNA. On the other hand, meiotic recombination, in addition to Rad51, requires a meiosis-specific RecA homolog, Dmc1, which also forms pre-synaptic filaments on ssDNA and mediates strand exchange in meiosis (Bishop, 1992). During meiosis, HR mainly occurs between homologous chromosomes rather than sister chromatids. This biased partner choice of HR unique to meiosis is mediated by the cooperative action of Dmc1 and Rad51 (Cloud *et al.*, 2012). The invasion of ssDNA into the duplex DNA leads to the formation of the D(displacement)-loop. The D-loop is then converted to a stable joint-molecule, which is accompanied with DNA synthesis. Further

processing gives rise to a recombination intermediates with double Holliday junctions (dHJs). Although, in theory, dHJs can be resolved to give either CO, reciprocal exchange of DNAs, or NCO (gene conversion) products, during meiosis it is biased to resolve only into COs. This biased resolution is a part of meiotic program which guarantees chiasma formation, which is essential for chromosome segregation.

1-4 DNA damage response and repair

In the presence of DNA lesions, the eukaryotic cell has a set of biological regulative processes collectively termed as DNA damage response (DDR) (Ciccia and Elledge, 2010). DNA damage signaling pathway, which ensures efficient and timely damage repair and cell cycle regulation, is essential for cell survival. The DDR comprises of a kinase-dependent signaling cascade. Kinases responsible in this pathway in mammals include ATM, ATR and DNA-PK (Blackford and Jackson, 2017) and, in *S. cerevisiae*, the homologs of ATM (Mec1) and ATR (Tel1) (Weinert *et al.*, 1994; Greenwell *et al.*, 1995). These kinases act as transducers, identifying damage to DNA, initiating a signaling cascade from the DNA damage site by phosphorylating hundreds of proteins (Falck *et al.*, 2005; Marechal and Zou, 2013). At the DNA damage sites, a ring shaped, heterotrimeric complex protein called the 9-1-1 clamp (Rad9, Hus1 and Rad1 in mammals and Ddc1, Mec2 and Rad17 in *S. cerevisiae*) loads first close to the damaged sites. In meiotic cells, the 9-1-1 clamp also loads close to the meiotic DSB sites (Roeder and Bailis, 2000; Hong and Roeder, 2002) and these sites are deliberately induced by Spo11 to trigger meiotic recombination (Keeney *et al.*, 1997; Prieler *et al.*, 2005). Once loaded, the 9-1-1 clamp triggers the downstream DDR signaling cascade such as, Mec1 activation.

1-5 Meiotic Prophase I

To ensure accurate segregation of homologous chromosomes in the first meiotic division, it is crucial that a pair of homologs has at least one crossover. To ensure this, the eukaryotic system has developed a series of regulatory control mechanisms; 1) more DSBs than the required number of COs are formed in the genome, for example; for 16

homolog pairs in the budding yeast, *S. cerevisiae*, ~160 DSBs are formed, while for 20 homolog pairs in mice ~250-300 DSBs are formed (Pan *et al.*, 2011; Keeney *et al.*, 2014), 2) inter-homolog recombination is promoted as opposed to inter-sister, 3) balanced distribution of crossovers throughout the genome is regulated by a specialized recombination pathway, 4) lastly, DSBs that do not resolve to crossovers are either resolved to non-crossovers or repaired by inter-sister recombination prior to chromosome segregation in MI. In *S. cerevisiae*, the coordination between the recombination process and meiotic progression is regulated by the meiosis-specific kinase, Mek1 (Rockmill and Roeder, 1991; Leem and Ogawa, 1992; Wu *et al.*, 2010; Hollingsworth, 2016; Chen *et al.*, 2018).

To connect two chromosomes necessary for the formation of inter-homolog CO during meiosis, strand invasion is biased to form between homologs (Lao and Hunter, 2010). This inter-homolog bias is also regulated by Mek1. After the formation of DSBs, Mec1 and Tel1 are recruited and phosphorylate the chromosome axial element, Hop1 (Carballo *et al.*, 2018). Phosphorylated Hop1 binds to Mek1, followed by auto-phosphorylation to form Mek1 dimer required for its activation (Carballo *et al.*, 2018; Niu *et al.*, 2005; Niu *et al.*, 2007). In addition to Hop1, another axial element Red1 and Hop1-Red1 interactions is also required for full Mek1 activation (Niu *et al.*, 2007). The absence of Mek1, Hop1 or Red1, results in defect in interhomolog bias (as well as reduced DSB formation) resulting in inviable spores (Hollingsworth and Byers, 1989; Rockmill and Roeder, 1990; Schwacha and Kleckner, 1994; Kim *et al.*, 2010).

Mek1 might promote interhomolog recombination directly and indirectly. Due to the spatial distance between homologs as compared to the neighboring sister chromatid, repair through inter-sister is easier to occur, which is seen in mitosis. Mek1 inhibits inter-sister repair by interfering Rad51. Rad54 is an essential accessory protein required for Rad51's strand invasion activity during mitosis. Mek1 inhibits Rad51-Rad54 interaction by; 1) directly phosphorylating Rad54 by which reduces the affinity to Rad51 (Niu *et al.*, 2009), and 2) by phosphorylating meiosis-specific Hed1, which binds to Rad51 to prevent the interaction with Rad54 (Callender *et al.*, 2016).

1-5-1 Synaptonemal Complex (SC)

The coordination between the resolution of recombination intermediates and changes in chromosome morphology is important for the regulation of meiotic recombination, to establish homologous pairing and the formation of at least one crossover per homologous chromosome pair (Bolcun-Filas and Schimenti, 2012; Borde and de Massy, 2013). According to the changes in meiotic chromosome dynamics, meiotic prophase I can be classified into four stages. First, in leptotene, DSB formation takes place (Padmore *et al.*, 1991), the resulting individual interacting DNA filaments link together leading to the co-alignment of the whole chromosomes, this is called as "pairing." Second, in zygotene, the homologous chromosomes become more closely associated with each other. This is termed as "synapsis," which corresponds to the formation of the synaptonemal complex (SC). SC forms a tripartite structure and assembles along the entire length of the condensed chromosome (Zickler and Kleckner, 1999; Page and Hawley, 2004). The SC consists of two lateral elements running along the chromosome axis and flanking the central region, which connects the homolog pair axes (Intro figure 3A). The central region consists of transverse filaments and the central element. The chromatin is organized into loop structures and their bases are tethered to the chromosome axes. SC components include; 1) axial element proteins that bind to the chromosome axes, 2) transverse filaments bridging between the two parallel homolog axes, and 3) central element present along the center of SC. Additionally, cohesin protein complex holds the two sister chromatids together. In *S. cerevisiae*, the lateral elements include proteins Hop1 and Red1, while the coiled coil protein Zip1 forms homodimers as the transverse filaments of the SC in the central region. During zygotene, the SC starts forming and in pachytene stage the elongation of SC is completed (Intro figure 3B). SC is usually formed at the sites for recombination pairing interactions. Once the COs are formed in the end of pachytene, the SC starts disassembling and only remain at the CO sites (chiasmata), which marks the diplotene stage. The SC induced chromosome structure promotes genetic exchange between homologous chromosomes rather than sister chromatids. Pairing and homologous recombination can take place in the absence of intact SCs (Hawley and Arbel, 1993). The function of the SC structure is considered to influence the number and

distribution of COs and the conversion of COs to stable chiasmata, which ensures the correct segregation of homologous recombination (Heyting, 1996).

1-5-2 Ndt80: meiotic prophase I exit

During meiosis, programmed DSBs introduced by Spo11 initiates recruitment of Rad51 and Dmc1, which mediates repair by HR (Shinohara 1992; Bishop 1992). DSB repair, thus meiotic recombination, is tightly coupled with cell cycle progression program of meiosis. This regulatory pathway is referred to as, "recombination checkpoint," which is mechanistically similar to DNA damage checkpoint during mitosis. Progression through prophase-I such as the exit from mid-pachytene stage is mediated by a meiosis-specific transcription activator, Ndt80. Ndt80 activates the resolution of double-Holliday junction and the disassembly of SCs (Xu *et al.*, 1997) by activating two key cell cycle kinases, cyclin-dependent protein kinase (CDK) and Cdc5, a polo-like kinase (PLK) (Sourirajan and Lichten 2008; Okaz *et al.*, 2012). Mek1 regulates the activity of Ndt80 and thereby indirectly influences the timing of the dHJ resolution (Chen *et al.*, 2015; Hollingsworth 2016). As described above, Mek1 activity, which is regulated by Mec1/Tel1-dependent DNA damage response to meiotic DSBs, in turn couples pachytene exit with meiotic DSBs. Thus, the deletion of the *NDT80* induces pachytene arrest with full length SCs and dHJs with persistent DSB formation. The residual DSBs in the *ndt80* arrest are repaired by Rad51-Rad54 mediated pathway (Subramanian *et al.*, 2016).

1-6 Resolution of meiotic recombination intermediates

CO formation and biased resolution to crossovers during meiosis is mediated by a specialized recombination pathway controlled by the ZMM proteins (Börner *et al.*, 2004; Lynn *et al.*, 2007). ZMM-mediated dHJs generates crossovers specifically (Allers and Lichten, 2001; Börner *et al.*, 2004). ZMM stands for Zip-Mer-Msh and includes Zip1/2/3, Zip4/Spo22, Msh4/5, Mer3, and Spo16. The ZMM proteins also make up the synapsis initiation complex (SIC), which is a protein structure that controls the initiation of synapsis formation at crossover-designated inter-homologous arrangements. Key role in

the ZMM pathway is to deposit ZMM protein, Zip1, which in turn becomes the SC transverse element which connects the pairs of sister chromatids together to form the SC (Sym *et al.*, 1993; Dong and Roeder, 2000; Börner *et al.*, 2004). Zip1 phosphorylation is required for ZMM-mediated crossovers and synapsis (Chen *et al.*, 2015). In the presence of the ZMM, the D-loops are stabilized to form single end invasions (SEI) (Hunter and Kleckner, 2001), followed by DNA synthesis and second-end capture resulting in a double Holliday junction formation (Schwacha and Kleckner, 1995) and biased resolution to give crossovers (Allers and Lichten, 2001; Börner *et al.*, 2004) (Intro figure 4). In the presence of ZMM, the double Holliday Junctions is resolved in a biased manner by Mlh1-Mlh3 (MutLγ) endonucleases complexed with Msh4-5 and Exo1 (Zakharyevich *et al.*, 2010; Keelagher *et al.*, 2011; Zakharyevich *et al.*, 2012; Alani, 2008; Wanat *et al.*, 2004). In the ZMM pathway which majorly resolves to COs, the SC structure provides for a stable association of homologous chromosomes (Börner *et al.*, 2004). The resulting COs are distributed along the chromosome uniformly by the phenomenon, 'interference' (Kohl and Sekelsky, 2013).

On the other hand, in the absence of ZMM, the double Holliday Junctions can also be resolved unbiasedly by structure-selective endonucleases (SSN), such as Mus81-Mms4, to give both CO and NCO (De Muyt *et al.*, 2012; Chen *et al.*, 2015) (Intro figure 4). This pathway also contributes some COs in wild-type meiosis.

NCO in meiosis is produced by the SDSA pathway. The D-loop structure after strand invasion and DNA synthesis can be processed in different ways from ZMM-dependent CO formation. In the pathway, the extended invading strand is disassembled from the D-loop by the Sgs1-Top3-Rmi1 (STR) complex (Allers and Lichten, 2001; McMahill *et al.*, 2007; Oh *et al.*, 2007; De Muyt *et al.*, 2012; Kaur *et al.*, 2015; Tang *et al.*, 2015) (Intro figure 4). The displaced strand with the extension is annealed to the 3' end of the other DSB end, resulting in an intermediate for NCO. The ZMM proteins at these sites protect the D-loop from dissolution by the STR complex (De Muyt *et al.*, 2012).

1-7 Regulation of Rad51 assembly

HR is tightly regulated because unrestrained recombination can result in chromosome aberration and loss of heterozygosity, which are linked with carcinogenesis in somatic cells (Abeysinghe *et al.*, 2006). Some type of familial breast and ovarian cancer is caused by the inactivation of genes involved in HR such as BRCA2 (Moynahan *et al.*, 2001). Among various reactions during HR, the assembly of Rad51 on ssDNA is a key decision step to commit HR. In order to control HR, the dynamic assembly and disassembly of Rad51 filaments on ssDNA is highly regulated at various levels. Rad51 assembly onto the ssDNA is inhibited by pre-binding of RPA to the ssDNA, which is thus alleviated by the action of Rad51 mediators, such as Rad52, Rad55-57, PCSS/Shu (Psy3-Csm2-Shu1-Shu2) complex (Sung, 1977; Liu *et al.*, 2011; Sasanuma *et al.*, 2013a) in budding yeast (Intro figure 5A). In the case of human (mammals), RAD51 paralogs, RAD51BCD-XRCC2, RAD51C-XRCC3, SWSAP1-SWS1, SWI5-SFR1, and BRCA2-DSS1 complexes are known to be Rad51 mediators (Masson *et al.*, 2001; Martin *et al.*, 2006; Akamatsu and Jasin, 2010; Zhao *et al.*, 2015). While Rad51 mediator functions during the assembly of Rad51, during homology search and strand exchange, Rad51 requires Rad54 chromatin remodeler, as a positive regulator, which belongs to the SWI2/SNF2 helicase family (Heyer *et al.*, 2006) (Intro figure 5A).

On the other hand, the assembly of Rad51 is negatively regulated to avoid hyper-recombination and crossover-generated chromosomal rearrangements. The yeast Srs2 DNA helicase protein was the initial protein identified as a negative regulator of Rad51 function and thus, recombination. Srs2 dislodges Rad51 from presynaptic filaments through ATP hydrolysis together with DNA unwinding (Krejci *et al.*, 2003; Chiolo *et al.*, 2005) (Intro figure 5B). In mammalian cells, the helicase and Proliferation Cell Nuclear Antigen (PCNA)-interacting factor (PARI) has shown to remove RAD51 nucleofilaments through ATP hydrolysis (Moldovan *et al.*, 2012). Srs2 and PARI also promote error-prone repair pathways such as alternating end joining (alt-EJ), trans-lesion synthesis (TLS), and single-strand annealing (SSA) (Lee and Lee, 2007; O'Conner *et al.*, 2013). Anti-recombinase activities are shown by several mammalian helicases such as the RecQ helicases. RECQL5 disrupts RAD51 filaments in an ATP-dependent manner (Schwendener *et al.*, 2010). RECQL5 limits HR by alleviating the RAD52 inhibition by

RAD51 thus, promoting SDSA repair pathway (Paliwal *et al.*, 2014). Similarly, BLM, another RecQ helicase, displaces RAD51 from ssDNA in an ATP-dependent manner, thus inhibiting early recombinogenic step (Sommers *et al.*, 2009). Other helicases include FANCJ and FBH1, which also promote disassembly of RAD51 filaments (Sommers *et al.*, 2009; Simandlova *et al.*, 2013).

Other than at the level of Rad51 nucleofilament formation, HR can also be regulated at the step of strand exchange. Specific DNA helicases displace D-loop during DSB repair thereby preventing CO formation (Intro figure 5B). RTEL1 helicase displaces D-loop through an ATP-hydrolysis dependent mechanism (Barber *et al.*, 2008). FANCM can dislodge Rad51-coated D-loops (Gari *et al.*, 2008). RTEL1 and yeast FANCM homolog, Mph1, inhibit HR and also promote the SDSA repair pathway (Stafa *et al.*, 2014; Adelman and Boulton, 2010). After strand exchange, Rad51 is removed from the double-stranded DNA (dsDNA), which is important for the next steps of strand extension, resolution of recombination intermediates and chromatin reassembly. The HELQ helicase removes RAD51 from dsDNA and promotes strand extension in an ATP-independent manner (Moldovan *et al.*, 2010; Ward *et al.*, 2010).

These extensive mechanism for positive and negative regulation emphasizes Rad51's central role in deciding the DSB repair pathway choice, in both the control of non-HR pathway as well as the tight regulation of HR repair steps.

1-8 Srs2 DNA helicase

Srs2 of *Saccharomyces cerevisiae*, was first identified as the suppressor of *rad6* from the Rad6-Rad18 complex, involved in DNA damage check point and UV sensitivities (Lawrence and Christensen, 1979) Later, the genes *RADH* identified as a suppressor of *rad18* (Aboussekhra *et al.*, 1989) and *HPR5* identified as a hyper-recombination mutant and the suppressor of *rad18* (Rong *et al.*, 1991) were realized to be alleles of *SRS2*. Srs2 is a SF1A (Super family 1A) family helicase, where it's N terminus shares homology with the bacterial UvrD helicase protein family (Aboussekhra *et al.*, 1989; Rong *et al.*, 1991) and the C terminus contains the post translational regions and mediates protein-protein interactions (Chiolo *et al.*, 2005). Two hybrid analysis has shown that Srs2

interacts with more than 70 proteins including Mre11 nuclease, Sgs1 and Mph1 (Chiolo *et al*., 2005). The C terminus contains a Rad51-interaction domain, and proliferating cell nuclear antigen (PCNA-) interaction motif (PIP) and small-ubiquitin-like modifier (SUMO)-interaction motif (SIM). Both PIP and SIM domains together provide maximal binding of SUMO-modified PCNA by Srs2, which recruits Srs2 to the sites of stalled replication forks to suppress HR (Papouli *et al.*, 2005; Pfander *et al.*, 2005; Armstrong, Mohideen and Lima, 2012). Similar to UvrD, Srs2 is a 3'-to-5' helicase, which translocates on the ssDNA to unwind the duplex DNA (Aboussekhra *et al.*, 1989), which requires ATP binding and hydrolysis (Rong and Klein, 1993). Srs2 helicase can unwind various DNA structures involved in DNA replication and repair such as, Flap, fork and Holliday junctions (Marini and Krejci, 2012).

In the absence of *SRS2*, the repair of DNA lesions is channeled towards recombination repair pathway rather than gap-repair pathway, which is mediated by Srs2 (Aboussekhra *et al.*, 1989; Schiestl *et al.*, 1990; Rong *et al*, 1991), demonstrating an anti-recombinase phenotype. *RAD51* gene was found to be a suppressor of the *srs2* mutant (Aboussekhra *et al.*, 1992), suggesting that the anti-recombinase function of Srs2 is attained by the removal of Rad51 from ssDNA, which has been shown *in vitro* (Krejci *et al.*, 2003; Veaute *et al.*, 2003) and *in vivo* (Sasanuma et al 2013b). This activity of Srs2 in removing Rad51 filaments is called 'strippase' activity. Both the strippase and the helicase activity require the translocase activity of Srs2. Many of the *srs2* mutant phenotypes are thus accredited to failure to prevent homologous recombination (HR) during repair and rescue of stalled replication forks (Barbour and Xiao, 2003; Watts, 2006; Lambert *et al.*, 2010) and in some cases during mitotic HR (Robert *et al.*, 2006; Le Breton *et al.*, 2008; Burgess *et al.*, 2009; Kerrest *et al.*, 2009; Urulangodi *et al.*, 2015). The strippase activity of Srs2 requires both the translocase activity as well as interacting with Rad51. Mutants which fail to interact with Rad51 observe defect in dismantling Rad51 nucleofilaments (Antony *et al.*, 2009; Colavito *et al.*, 2009; Islam *et al.*, 2012). Physical interaction of Srs2 with Rad51 stimulates Rad51's ATPase activity which facilitates it's turnover as Rad51's binding to ATP is required for efficient DNA binding (Antony *et al.*, 2009). Rad51 mediators, Rad55-Rad57 have shown to antagonize Srs2's strippase activity (Liu *et al.*, 2011) and Rad52 is also reported to function similarly (Burgess *et al.*, 2009; Seong *et al.*,

2009). Srs2's role in genome stability revolves around two key activities: the Rad51 strippase activity to regulate the use of HR and the DNA helicase activity.

1-9 Role of Srs2 in replication, recombination and repair during Mitosis

Srs2 stimulates single-strand annealing, ectopic gene conversion, synthesis-dependent strand annealing (SDSA) and non-homologous end joining (NHEJ) (Vaze *et al.*, 2002; Carter *et al.*, 2009; Hedge and Klein, 2000). Srs2 is also involved in post-replication repair (PRR) (Chanet *et al.*, 1996; Schild *et al.*, 1995; Milne *et al.*, 1995). At replication forks, Srs2 acts as the molecular switch between PRR and HR (Chanet *et al.*, 1996; Schild *et al.*, 1995; Milne *et al.*, 1995). Srs2 functions in the error free gap repair branch of the post replication repair (PRR) pathway (Ulrich, 2001; Broomfeild and Xiao, 2002).

srs2 deletion mutant observes synthetic lethality or slow growth with many genes implicated in the double-strand break repair or DNA replication such as, *MMS4*, *MUS81*, *SGS1*, *MRE11*, *POL32* among many others (Gangloff *et al.*, 2000; Klein, 2001; Ooi *et al.*, 2003; Tong *et al.*, 2004; Pan *et al.*, 2006). The synthetic lethality phenotype is attributed to the formation of toxic recombination intermediates (Aboussekhra *et al.*, 1989; Rong *et al.*, 1991; Gangloff *et al.*, 2000; Klein, 2001) as deletion of *RAD51* recues the phenotype. *srs2 rad54* double lethality due to inappropriate recombination is rescued by *rad51* mutation, indicates a pro-recombination role of Srs2 overlapping with Rad54's role during the many steps of HR (Klein, 2001; Ira *et al.*, 2003; Kolesar *et al.*, 2016). At DNA gaps Srs2 inhibits repair through recombination and promotes the synthesis-dependent strand annealing (SDSA) pathway, which results in non-crossovers and reduced crossover formation. Loss of Srs2 thus leads to a reduction in non-crossover formation by SDSA events and a subsequent increase in crossovers. Srs2 regulates recombination by limiting crossovers and promoting SDSA (Ira *et al.*, 2003; Robert *et al.*, 2006; Miura *et al.*, 2013), thus, preventing loss of heterozygosity events during mitotic repair of DNA lesions by HR. The anti-recombination and pro-recombination activities of Srs2, *in vivo*, maintains a tight balance, which in a part is achieved by Rad51 filaments which are resistant to Srs2's strippase activity (Liu *et al.*, 2011).

Srs2 regulates stalled replication fork repairs through the recruitment of SUMO-modified PCNA (Papouli *et al.*, 2005; Pfander *et al.*, 2005), although it can remove toxic recombination intermediates irrespective of this interaction (Le Breton *et al.*, 2008; Kolesar *et al.*, 2016). At stalled replication forks, Srs2 prevents DNA gaps from being used for HR initiation. Srs2 functions in the replication checkpoint, which is modulated by phosphorylation. Phosphorylated Srs2 is recruited to the DNA breaks, where it disassembles any recombination intermediates predisposed to crossovers formation and promotes repair through the non-crossover generating SDSA pathway (Saponaro *et al.*, 2010). The SUMO-like protein Esc2 regulates Rad51 filament formation at stalled forks by counteracting Srs2's ability to remove Rad51 from stalled forks (Urulangodi *et al.*, 2015). The regulation of removal and degradation of Srs2 and through Srs2 modification determines the balance between Rad51 filament formation and recombination repair as opposed to gap repair at stalled or damaged forks.

1-10 Objective of this research study

Studies in mitosis have shown that the Inactivation of Srs2 causes spontaneous hyper-resection (Aboussekhra et al., 1989; Rong et al., 1991; Aguilera and Klein, 1988; Palladino and Klein, 1992). Mutations in Srs2 gene observes a hyper-recombination phenotype caused by aberrant recombination (Aboussekhra et al, 1992; Chanet et al., 1996; Fabre et al., 2002; Rong et al., 1991). Absence of Srs2 function exhibits a range of phenotype from anti-recombinogenic in some cases (Aboussekhra et al, 1992; Chanet et al., 1996; Fabre et al., 2002; Rong et al., 1991), to pro-recombinogenic in others, illustrating Srs2's diverse role in the HR repair pathway.

While Srs2's role in mitosis and/or mitotic recombination is well known, its role during meiosis is still unclear. Previous works from my and other labs revealed the following meiotic defects of the *srs2* deletion mutant of the *S. cerevisiae*: reduced sporulation and spore viability (Rong *et al.*, 1991), delayed meiotic DSB repair and a decrease in recombination products (Sasanuma *et al.*, 2013a). The mutant shows wild-type like appearance and disappearance of Rad51 and Dmc1 foci, suggesting completion of meiotic DSB repair. However, interestingly, the mutant observes Rad51 aggregations at

late times of meiosis, which appear to carry on to the haploid progeny as well (Sasanuma and Sakurai *et al*., 2019). This suggests a novel role of Srs2 during late stage of meiotic prophase-I. In my thesis, the nature of the Rad51 aggregates in the *srs2* mutant and the mechanism behind its formation has been studied. I showed that DNA damage accumulates at late times of meiosis in the *srs2* deletion mutant, which corresponds to the appearance of the Rad51 aggregates in the mutant. The Rad51 aggregation occurs prior to meiosis I and is independent of chromosome segregation at the onset of anaphase I. Rad54 may play a role in the processing of part of the intermediate structures giving rise to the Rad51 aggregates observed in the mutant. The Rad51 aggregates are formed in the *srs2Δ* mutant after mid-pachytene exit. Abnormal structure of Rad51, termed as 'Rad51 bridges' was observed in early prophase in the *srs2Δ* mutant cells. Rad51 bridge structure in the *srs2* deletion mutant may result from the formation of multiple invasion intermediates. The Rad51 aggregate formation is independent to loss of Srs2's role before mid-pachytene exit and appears to be related to Srs2's secondary role after exit from mid-pachytene. Based on results described in this thesis, I will introduce Srs2's dual function in yeast meiosis and discuss about the role of Srs2 in coupling the completion of recombination with consecutive chromosomal events.

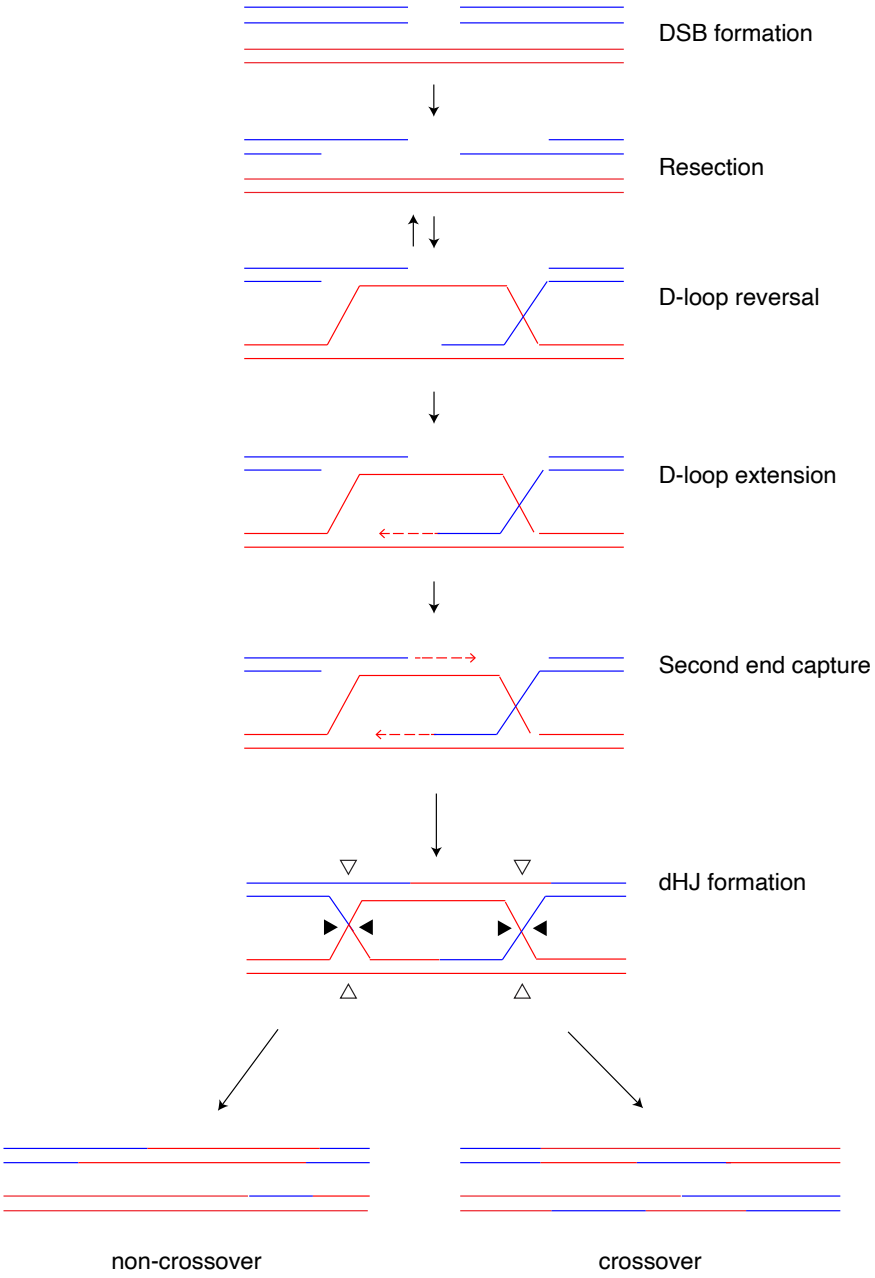

Intro figure 1: Homologous recombination (HR)

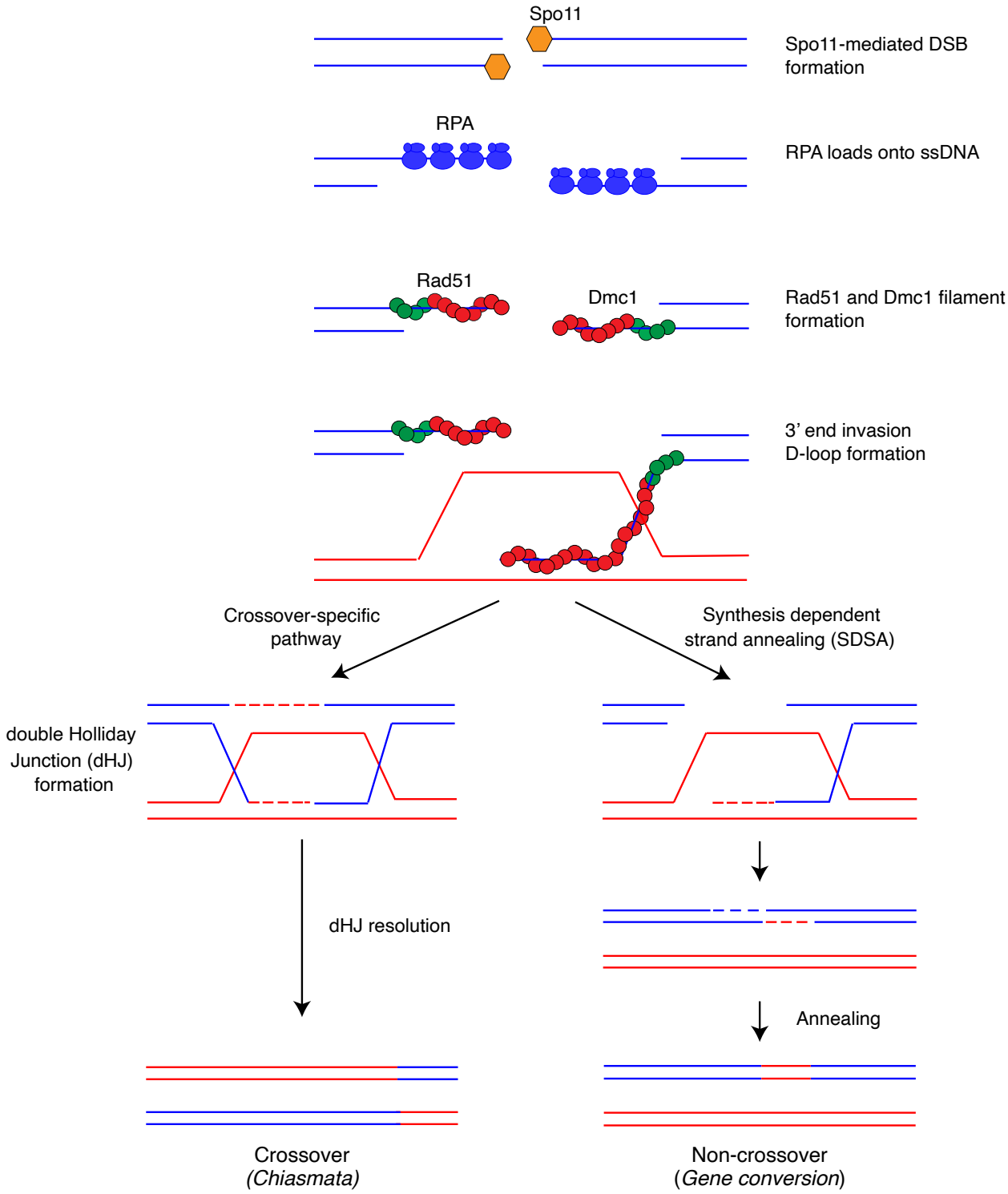

Intro figure 2: Meiotic Recombination pathway.

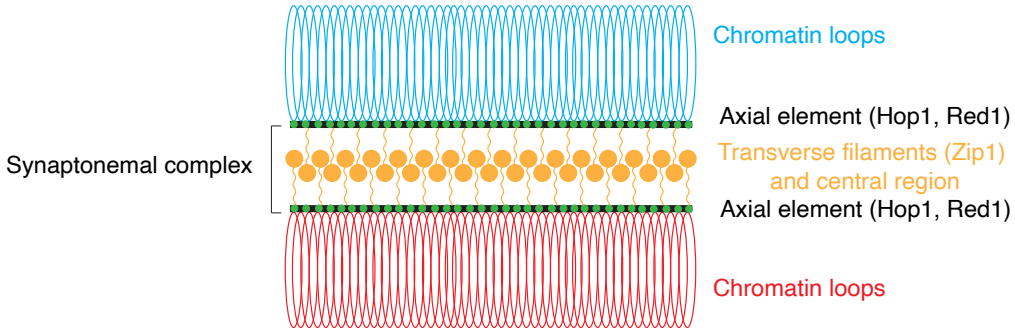

Intro figure 3A: Diagrammatic representation of synaptonemal complex structure (Adapted from Gao and Colaiácovo, 2018)

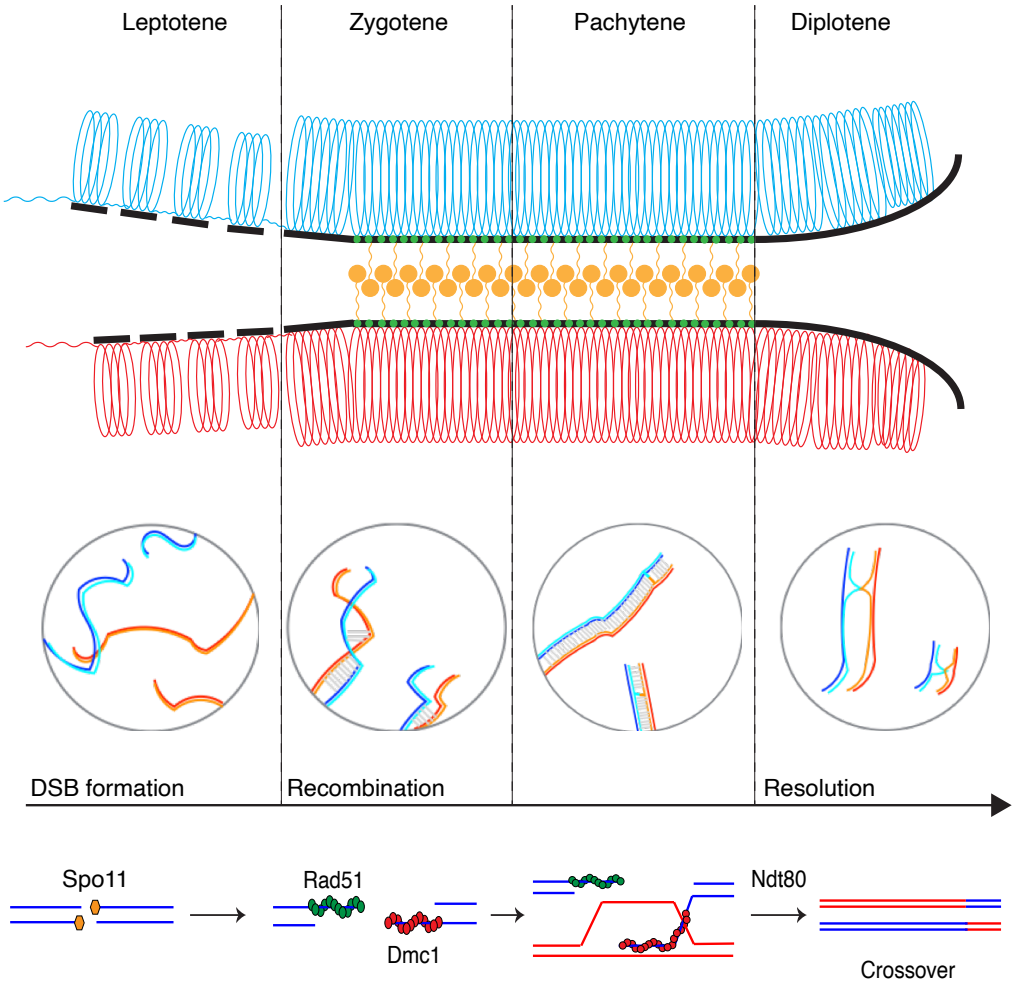

Intro figure 3B: Diagrammatic representation of changes in the synaptonemal complex structure during meiotic prophase I stage (Adapted from Henderson and Keeney, 2005; Baudat *et al.*, 2013)

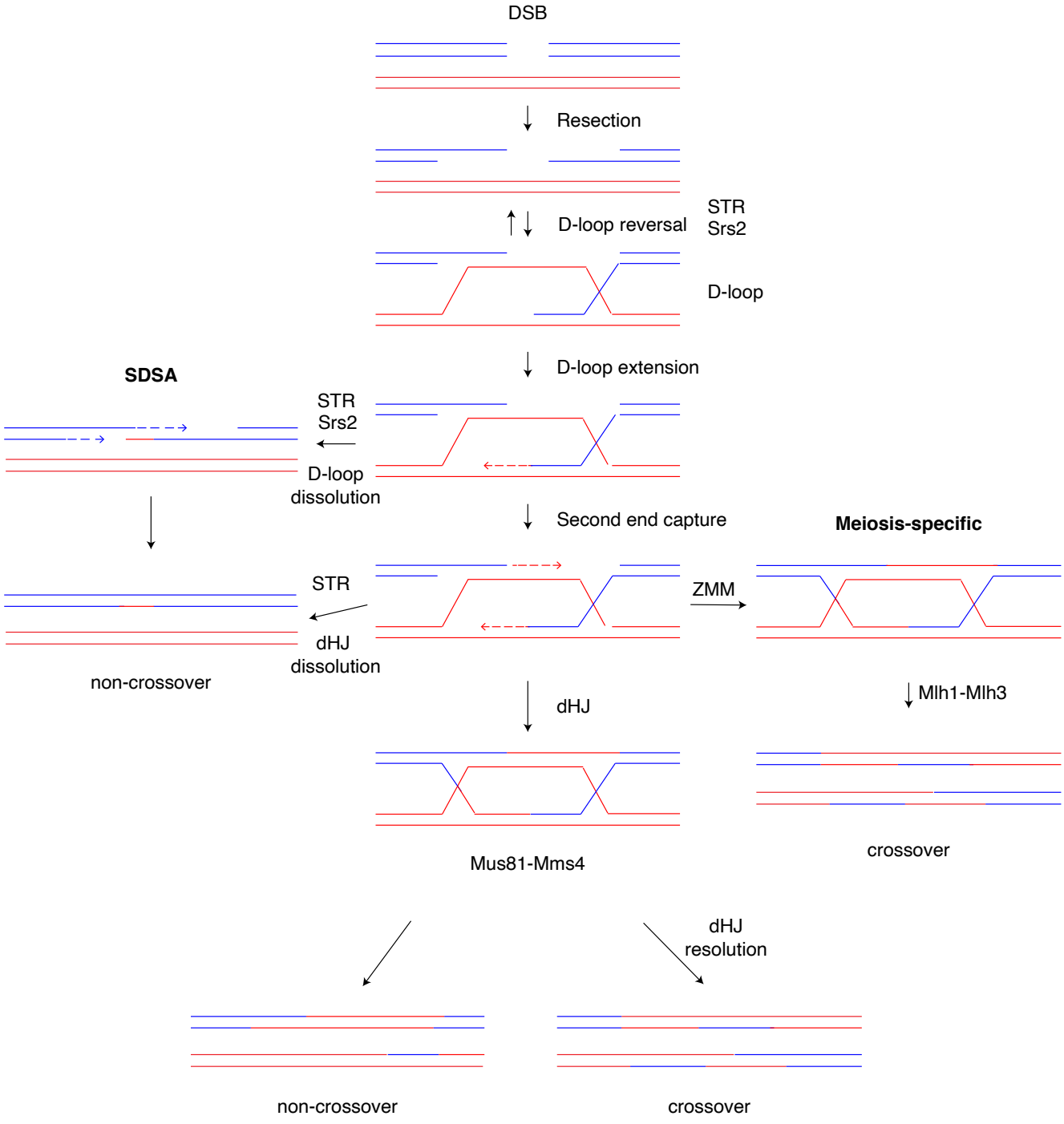

Intro figure 4: DNA double strand break repair and resolution.

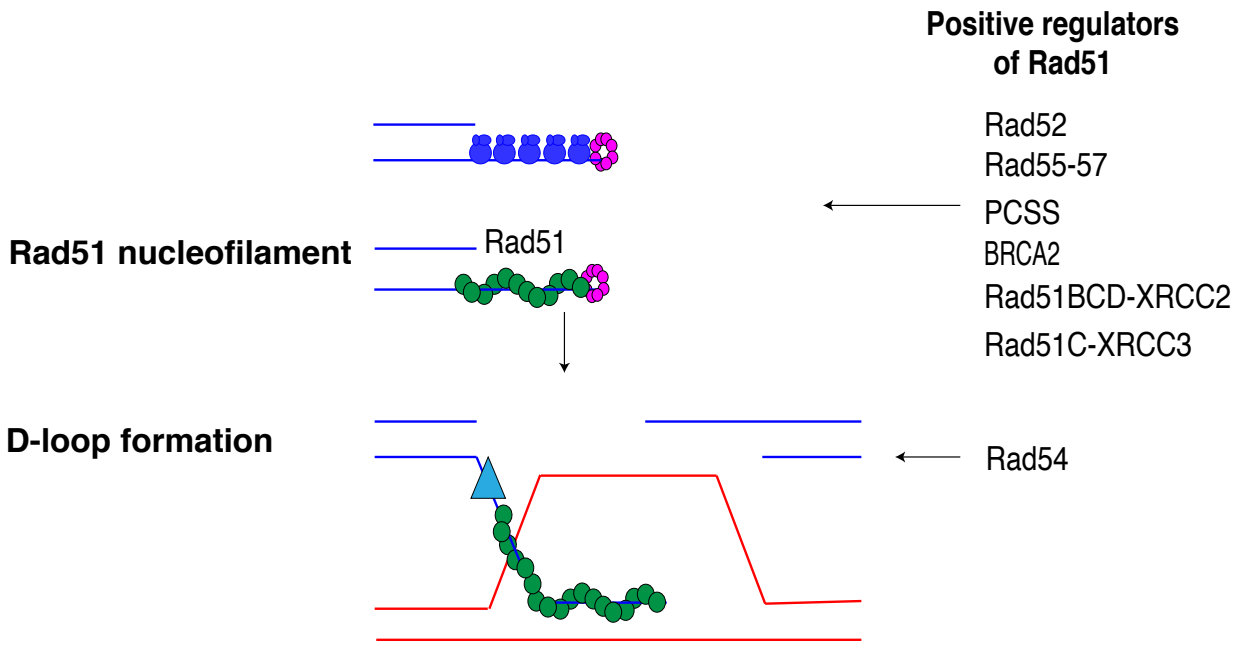

Intro figure 5A: Positive regulation of Rad51 filament assembly.

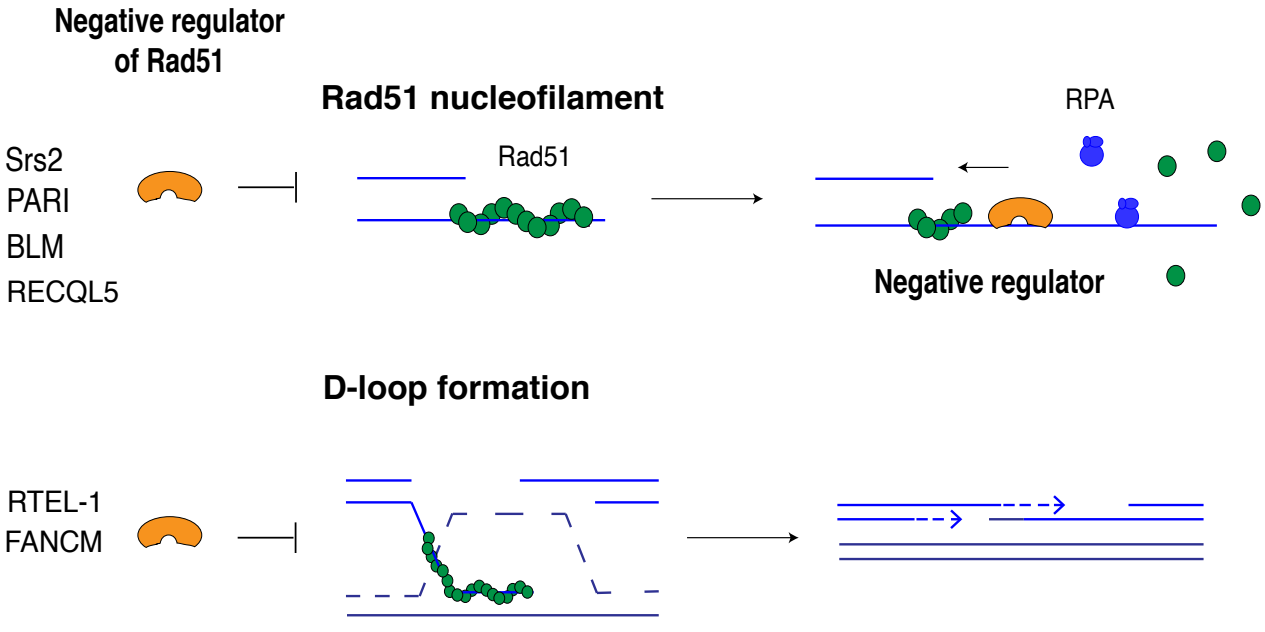

Intro figure 5B: Negative regulation of Rad51 filament assembly.

Section 2: Materials and Methods

2-1 Yeast strains and constructs

All yeast strains used in this study were isogenic derivatives of *S. cerevisiae* SK1 diploid strains, MSY 833/832 (Shinohara *et al.*, 2003) (MATa/ α , ho:: LYS2/", ura3/", leu2::hisG/", trp1::hisG/", lys2/") and NKY 1303/1543 (Storlazzi *et al.*, 1996) (MATa/α, ho:: LYS2/", ura3/", leu2::hisG/", lys2/", his4B-LEU2(MluI)/his4X-LEU2(BamHI)-URA3, arg2-bgI/arg4-nsp). *srs2*Δ strain was provided by Dr. H. Sasanuma (Sasanuma *et al.*, 2013a), *ndt80*Δ was provided by Dr. Kiran Challa (Challa *et al.* 2016), *pCLB2-CDC20* was provided by Dr. H. Sasasunama, *srs2*Δ*ndt80*Δ and *pCLB2-CDC20 srs2*Δ was provided by previous lab members, *RAD54-FRB* strain was provided by Dr. Andreas Hochwagen (Subramanian *et al.*, 2016). *RAD54-FRB srs2*Δ strain was constructed by manual dissection of tetrads and the positive clones were selected by replica plating to appropriate marker plates and the genotype was confirmed by PCR check with the appropriate primers. The AID system (Nishimura et al., 2009) optimized for meiosis by replacing the promoter of PADH1-OsTIR1 with the CUP1 promoter was provided by Dr. Neil Hunter (Tang *et al.*, 2015). Srs2 fusion to a minimal AID degron was constructed using plasmid p7aid-9m, provided by Dr. Neil Hunter, as template for PCR-mediated allele replacement (Morawska and Ulrich, 2013). Estrogen-inducible IN-NDT80 GAL4-ER has been described (Benjamin et al., 2003; Carlile and Amon, 2008; Picard, 1994). Table 1 lists the genotype of the strains used in this study and Table 2 lists the primers used.

2-2 Spore viability

For spore viability check, haploid parental strains were patched together on a YPAD plate (1% Bacto Yeast Extract, 2% Bacto Peptone, 2% Glucose, 1% Adenine) for minimum 5 hours for mating after which it was streaked and left at 30°C for two days to obtain single diploid colony, which was later patched onto SPM plate (0.3% Potassium acetate, 0.02% Raffinose) and incubated at 30°C for minimum one day to obtain tetrads. The tetrads were manually dissected using the Zeiss Axioskop 40 microscope. The plates were incubated

at 30°C for two days after which the viable spores were counted for spore viability. A total of 100 tetrads were dissected for each respective strain.

2-3 Yeast genomic DNA preparation

Yeast cells were cultured in 2 ml YPAD liquid medium overnight (at 30°C) and the cells harvested in Eppendorf tubes. The pellet was suspended in 500 µl Zymolyase buffer (10 mM Sodium phosphate (1.4 mM Na_2HPO_4 $12H_2O$ (Wako 196-02835), 16 mM NaH_2PO_4 $2H_2O$ (Wako 192-02815)), 10 mM EDTA (Dojindo, 345-01865), 0.1 M β–Mercaptoethanol (nacalai Tesque, 21418-55), 100 mg/ml Zymolyase 100T (nacalai tesque, 07665-55)), mixed by vortex and incubated at 37°C for 30 mins. The cells were then lysed by adding 5 µl Proteinase-K (1mg/ml, Wako, 165-21043) and 100 µl of Lysing buffer (0.25 M EDTA (Dojindo, 345-01865), 0.5 M Tris base (nacalai tesque, 35434-34), 2.5% (w/v) SDS (nacalai tesque, 31607-65)), mixed well by shaking and incubated at 65°C for 1 hr, during which the tubes were mixed by inverting at least 4 times. 100 µl of 5M potassium acetate was added, mixed thoroughly and incubated on ice for 15 mins. The cells were centrifuged (15000 rpm, 10 mins, 4°C) and the resulting supernatant was transferred to new Eppendorf tube containing 500 µl cold 100% (V/V) ethanol (EtOH, Wako, 057-00451). The sample was gently inverted 5 times and centrifuged (12000 rpm, 2 mins, 4°C). The supernatant was removed and the DNA pellet was washed with 70% (V/V) EtOH followed by 100% (V/V) EtOH. The pellet was dried with centrifugal concentrator for 10 mins. The DNA pellet was suspended with 500 ml 1X TE buffer (10 mM Tris-Cl (pH 8.0), 1 mM EDTA).

2-4 Meiosis time course

Haploid yeast cell strains were opened on YPG plate (1% Bacto Yeast Extract, 2% Bacto Peptone, 2% Glycerol) from -80°C stock, incubated at 30°C for overnight, then streaked on YPAD plate and incubated for further two days at 30°C. Haploid parental strains were patched together on a YPAD plate for minimum 5 hours for mating, after which it was streaked and left at 30°C for two days to obtain single diploid colony. A single diploid

colony was inoculated in 3 ml liquid YPAD medium and incubated in rotator at 30°C overnight. 1 ml of the overnight YPAD culture was added to 200 ml of SPS medium (0.5% Bacto Yeast Extract, 1% Bacto Peptone, 0.17% Yeast nitrogen base, 1% Potassium acetate, 1% Potassium hydrogen phthalate, 0.5% Ammonium sulfate) and incubated in shaker (Innova® 44) at 30°C, 230 rpm for 16~17 hrs. Next day, the SPS culture was centrifuged using a 50ml screw cap tube and the pellets were washed twice with sterilized distilled water. Yeast cells were suspended in 250 ml SPM (0.3% Potassium acetate, 0.02% Raffinose) and incubated at 30°C, 230 rpm to enter meiosis, and the samples were collected at each time point.

2-5 Meiotic Progression: DAPI analysis

1 ml of meiotic cell culture was collected, centrifuged and the pellets was fixed with 70% (V/V) EtOH. After centrifugation, 100 µl of 1 M Sorbitol (D-Glucitol, nacalai tesque, 32021-95) with DAPI (1 mg/ml, 1:1000, Wako, 045-18803) was added. 5 µl of sample was spotted on to the slide (S2226 micro slide glass, Matsunami glass, IND., LTD), covered with cover glass and sealed with nail polish. The slide was observed with epi-fluorescent microscope (ZIESS Axioplan2). 200 nuclei were counted for each sample.

2-6 Meiotic chromosome spreads: Lipsol method

To prepare chromosome spread slides, 5 ml of diploid yeast cells (SPM culture) was collected, centrifuged in a 15ml screw cap tube and suspended in 1 ml ZK buffer (25 mM Tris-Cl (pH 7.5), 0.8 M Potassium chloride) and 20 µl of 1 M DTT (Dithiothreitol, nacalai tesque 14128-62) was added, left at room temperature for 2 mins, and centrifuged. The pellet was resuspended in 1 ml ZK Buffer and 5 µl of 5 mg/ml Zymolyase 100T was added, mixed and incubated at 30°C for 30 mins. The samples were spin downed and washed with 1 ml cold MES/Sorbitol (0.1 M MES (pH 6.5) (Dojindo, 345-01625), 1 M Sorbitol (D-Glucitol, nacalai tesque, 32021-95), 0.5 mM $MgCl_2$ (nacalai tesque, 20909-55), 1 mM EDTA (Dojindo, 345-01865)) with pasteur pipettes, centrifuged to remove supernatant and suspended in 1 ml cold MES/Sorbitol and stored on ice till lipsol

treatment. For chromosome spreads, 20 µl of the cell suspension was spotted on a clean glass slide (S2441 micro slide glass, Matsunami glass, IND., LTD) using a micropipette, to which 40 µl of PFA/sucrose (3.5% PFA (pH 7.0) (Paraformaldehyde, SIGMA ALDRICH, 158127-500G), 3.4% sucrose (Wako, 196-00015), freshly prepared) was added and gently swirled. 80 µl of 1% Lipsol and 80 µl of PFA/sucrose was added at the same time and gently swirled to spread throughout the slide making sure to not leave any gaps. After confirming that about 80~90% of the cells have been lysed under light microscope, the slide was dried overnight and stored at -20°C.

2-7 Immunostaining of chromosome spreads

Prepared chromosome spread slides were dipped in 0.2% Photoflo (Photo-Flo 200 solution Kodak) for 2 mins in Coplin jar. The slides were air dried for 10 mins, and blocked with TBS/BSA (1X TBS (Tris-buffered Saline, 20 mM Tris-Cl pH 7.5 (nacalai tesque, 35434-34), 0.15 M NaCl (Wako, 195-01663)) 1% BSA (Bovine serum bovine, SIGMA, A8022-100G)) for 15 mins. Blocking buffer was drained in a paper towel and 90 µl of TBS/BSA solution with primary antibody (1:1000 dilution) was added to the slides and covered with a coverslip. The slides were incubated at 4°C overnight. The cover glass was removed by immersing the slides at an angle of 45° in 1X TBS washing buffer. The slides were washed in 1X TBS using Coplin jar for 10 mins twice. 90 µl of TBS/BSA solution with secondary antibody (1:2000 dilution of fluorochrome-conjugated IgG) was added to the slides and covered with a coverslip, and incubated at room temperature for 2 hours in a dark moist chamber. The coverslip was removed and the slides were washed as described above, and then washed with sterilized distilled water for 2 mins. The slides were air dried for 10 mins and 10~15 µl of mounting medium Vecta shield (Vector laboratories Inc., H-1000) with 0.2 µg/ml DAPI (Wako, 045-18803)) was added to the slides and covered with cover glass, sealed with nail polish and stored in dark at 4°C till use. The sample slides were observed using an epi-fluorescence microscope.

2-8 Immunostaining of whole cell

Immunostaining of whole cell was carried out using pre-coated poly L-lysine (1 mg/ml) slides. The slide was prepared by adding 200 µl of 1 mg/ml poly L-lysine solution on a glass slide (S2441 micro slide glass, superfrost Matsunami glass, IND., LTD), covered with cover glass and incubated at room temperature for 15 mins. The cover glass was removed by immersing it in MilliQ water and washed with MilliQ water for 2 mins twice. The slides were dried in room temperature for 15 mins.

For whole cell immunostaining, 900 µl of meiotic SPM culture was collected and 100 µl of 37% formaldehyde (Wako, 064-04845) was added for cell fixation. The sample tube was centrifuged and the pellet was suspended in 1 ml ZK buffer and 20 µl of 1 M DTT was added, left at room temperature for 2 mins, and centrifuged. The pellet was re-suspended in 1 ml ZK Buffer and 5 µl of 5 mg/ml Zymolyase 100T was added, mixed and incubated at 30°C for 1.5 hr. Cells were collected and suspended in 1X PBS (Phosphate Buffered Saline, 0.05 mM KH_2PO_4 (Wako, 169-04245), 0.15 mM Na_2HPO_4 $12H_2O$ (Wako, 196-02835), 7.75 mM NaCl (Wako, 195-01663)). 200 µl of the cell suspension was added to the poly L-lysine coated slides, covered with a coverslip and incubated at room temperature for 15 mins. The cells were then fixed with cold 100% Methanol (nacalai tesque, 21915-64) for 6 mins, 30 secs with cold 100% Acetone (Wako, 016-00346) and 2 mins with cold 1X PBS. The slides were blocked with 5% BSA in 1X PBS for 15 mins. Blocking buffer was drained in a paper towel and 90 µl of PBS/BSA (1X PBS, 1% BSA) solution with primary antibody (1:1000 dilution) was added to the slides and covered with a coverslip. The slides were incubated at 4°C overnight. The cover glass was removed by immersing the slides at an angle of 45° in PBST (1X PBS, 0.1% Tween 20 (nacalai tesque, 28353-85)) washing buffer. The slides were washed with PBST using Coplin jar for 10 mins twice. 90 µl of PBS/BSA solution with secondary antibody (1:2000 dilution of fluorochrome-conjugated IgG) was added to the slides and covered with a coverslip, and incubated at room temperature for 2 hours in a dark moist chamber. The coverslip was removed and the slides were washed as described above, and then washed with sterilized distilled water for 2 mins. The slides were air dried for 10 mins and 10~15 µl of mounting medium Vecta shield (Vector laboratories Inc., H-1000 with 0.2 µg/ml DAPI (Wako, 045-18803)) was added to the slides and covered with cover

glass, sealed with nail polish and stored in dark at 4°C till use. The sample slides were observed using an epi-fluorescence microscope.

2-9 Cytological analysis and antibodies

The immunostained samples were observed using an epi-fluorescence microscope (BL51; Olympus) with a 100X objective lens (NA1.4). The images were captured using a CCD camera (Cool Snap; Roper) and processed using iVision software. A minimum number of 100 nuclei were analyzed. Nuclei with more than five foci were counted as "a positive cell" (Shinohara *et al.*, 2003). Primary antibodies against Rad51 (anti-guinea pig 1:1000 and anti-rabbit 1:1000) (Sasanuma *et al.*, 2013a; Shinohara *et al.*, 2003), Dmc1 (anti-rabbit, 1:1000), Hed1 (anti-rabbit, 1:200), Rad52 (anti-rabbit, 1:500) was used. For secondary antibodies, fluorescent-labeled antibodies (Alexa-fluor-488, Alexa-fluor-594, Molecular probes) against the primary antibodies originating from the different species was diluted at 1:2000 and used.

2-10 Western blot analysis

5 ml of SPM culture was collected, the precipitated cells were washed with water, then resuspended in 1 ml of 20% (w/v) trichloroacetic acid (TCA, Wako, 208-16215). Cells were disrupted using a Multi-beads shocker (2500 rpm, on 60 secs, off 60 secs, repeat 10 times) (Yasui kikai Co. Ltd., Osaka, Japan). The precipitated proteins samples obtained after centrifugation was suspended in 100 µl of Tris-Cl (pH 8.8) to adjust to neutral pH, followed with 100 µl of 2X SDS Buffer (120 mM Tris-HCl (pH 6.8) (nacalai tesque, 35434-34), 4 % SDS (nacalai tesque, 31607-65), 10 % β-mercaptoethanol (nacalai tesque, 21418-55), 10 % glycerol (nacalai tesque, 17018-83), 0.04 % bromophenol blue (Wako, 029-02912)). Samples were boiled to 95°C for 10 mins, kept on ice for about 10 mins and centrifuged at 150,000 rpm, 4°C for 10 mins. 100 µl from the top was collected. 5 µl of sample was loaded and run on SDS-PAGE. The proteins were transferred from gel to Nylon membrane (Immobilon-P, MILLIPORE, IPVH00010) with semi-dry transfer unit (ATTO TRANSWESTERN). Antibodies against Hop1 (anti-guniea pig, 1:1000)

(Iwasaki *et al.*, 2016), Dmc1 (anti-rabbit, 1:1000), Mei5 (anti-rabbit, 1:1000), (Hayase *et al.*, 2004), Tub (anti-Rat, 1:2000) (αMCA77G; AbD Serotec, UK), Myc tag for Srs2-AID-9Myc (anti-mouse, 1:1000) (nacalai Tesque, 04362-34), Ndt80 (anti-rabbit, 1:1000) (Benjamin *et al.*, 2003), Cdc5 (1:1000) (Santacruz, sc-33625) were used (Shinohara *et al.*, 2008). For secondary antibodies, conjugated Alkaline Phosphatase were used, anti-rabbit (1:7500) (Promega, S373B), anti-Rat (1:5000) (Proteintech, SA00002-9), anti-guinea pig (1:7500) (SIGMA, A-5062), anti-mouse (1:7500) (Promega, S372B). The membrane blot was detected by BCIP/NBT reaction with a kit (nacalai Tesque, 03937-60). For Hop1 quantification analysis, HRP antibody for anti-Rat (1:5000, Thermo scientific, 31470) and anti-guinea pig (1:5000, Invitrogen, A18769) was used.

2-11 CHEF analysis and Southern hybridization

For chromosome-wide meiotic DNA resolution CHEF (clamped homogeneous electric field) gel electrophoresis was performed as described previously (Bani *et al.*, 2014; Gothwal *et al.*, 2016). Plug DNA of meiotic culture samples were prepared with 1.8% LMP (low melting point) agarose (SeaPlaque Agarose, LONZA, 50100) in 125 mM EDTA (pH 7.5) (Dojindo, 345-01865). LMP agarose gel for plugs was melted and kept at 45°C until use. Meiotic cell culture (15 ml for 0 h time point, 7.5 ml for the rest) was collected and washed twice with 5 ml of 50 mM EDTA (pH 7.5). Samples were centrifuged and the cell pellet suspended in 1 ml of 50 mM EDTA, transferred to a 1.5 ml Eppendorf tube, centrifuged and the cell pellets re-suspended in 50 mM EDTA to a total of 100 µl. To prepare the plug DNA, 100 µl of cell suspension was warmed at 45°C for 30 secs, followed by addition of pre-warmed (at 45°C) LMP/Solution I (for 4 samples, 0.67 ml of 1.8% LMP in 125 mM EDTA (pH 7.5), 0.13 ml of Solution I (5% β-mercaptoethanol (nacalai tesque, 21428-55), 1.5 mg/ml Zymolyase 100T (nacalai tesque, 21418-55) in SCE (1 M sorbitol (D-Glucitol, nacalai tesque, 32021-95), 0.1 sodium citrate (Wako, 191-01785), 60 mM EDTA (pH 7.5), pH 7.0 with HCl (nacalai tesque, 18321-05)) was added. 90 µl of the cells/LMP/Solution I was inserted into the plug mold and left to set at room temperature. After set, the plug DNA was transferred to 3 ml of Solution II (7.5% β-mercaptoethanol, 450 mM EDTA (pH 7.5), 10 mM Tris-HCl (pH

7.5) (nacalai tesque, 35434-34), 0.01 mg/ml RNaseA (SIGMA, R5000)). Sample tubes were inverted gently and kept at 37°C overnight. Solution II was removed and washed once with 3 ml Solution III (1% SDS (nacalai tesque, 31607-65), 250 mM EDTA (pH7.5), 10 mM Tris-HCl (pH 7.5)) by gently inversion. Plug DNA was transferred to 1 ml Solution III with 1 mg/ml Proteinase K (Wako, 165-21043) and incubated at 50°C overnight. The plug DNA was rotated for 15 mins twice with 50 mM EDTA (pH 7.5), 20 mins with Storage solution (50% glycerol (nacalai tesque, 17018-83), 50 mM EDTA (pH 7.5)) and stored in storage solution at -20°C. For gel electrophoresis, 1% gel (Pulse Field Certified Agarose, BIORAD, 64161360) in 150 ml of 0.5X TBE (45 mM Tris base, 44 mM Boric acid (Wako, 021-02195), 5 mM EDTA (pH 8.0)) was prepared and left at 55°C for a few hours to equilibrate. Plug DNA was placed on the comb and the gel was poured to the mold of size (14 cm W x 21 cm H) and left to set at room temperature for 30 mins. Before electrophoresis the gel was placed in the CHEF apparatus and equilibrated in 1X TBE buffer at 14°C for 30 mins. CHEF apparatus (CHEF-DR III system BIORAD) and condition was set at 60 sec initial switch time, 120 sec final switch time, 120° switch angle, 6 V/cm, run time 24 h, pump speed 90 for all yeast chromosome detection and 15.1 sec initial switch time, 25.1 sec final switch time, 120° switch angle, 6 V/cm, run time 41 h, pump speed 90 for short chromosome detection. After electrophoresis, the gel was stained with ethidium bromide (0.5 μg/ml, SIGMA ALDRICH, E1510-10ML) for 30 mins and washed with distilled water for 20 mins thrice, gel was detected with ImageQuant LAS4000 (GE Healthcare) and processed with ImageQuant TL. Before transfer to membrane, the gel was placed in a UV crosslinker (Stratelinker® UV crosslinker) and UV irradiated with 1800 μJ/cm^2 was equilibrated in 500 ml of PFGE transfer buffer (0.6 M NaCl (Wako, 195-01663), 0.4 M NaOH (Wako, 198-13765)) for 20 mins, followed by 20 mins in 25 mM Na-Phosphate buffer (pH 6.5) (0.3 M $Na_2HPO_4.12H_2O$ (Wako, 196-02835), 0.7 M $NaH_2PO_4.2H_2O$ (Wako, 192-02815)) twice. Gel was capillary transferred to membrane (Hybond N) (Clear Trans® Nylon membrane 0.45 μm, Wako, 039-22673) for two days. To crosslink the DNA, the membrane was UV crosslinked by UV irradiation of 120 mJ/cm^2 (Autocrosslink mode: 1200 μJ (x100)) and was hybridized with RI by southern blotting. The membrane was inserted in a hybridization bottle with 20 ml hybridization buffer (7% SDS, 1M Na-Phosphate buffer

(pH 7.2) (0.5 M $Na_2HPO_4.12H_2O$ (Wako, 196-02835), 0.16 M $NaH_2PO_4.2H_2O$ (Wako, 192-02815)), 0.5M EDTA (pH 8.0)) and equilibrated at 65°C for 30 mins. For the preparation of DNA probe, 10.5 µl of 25 ng/µl probe DNA (dissolved in 1X TE buffer), 2.5 µl of primer DNA (Megaprime DNA labelling kit; GE Healthcare) was added and boiled at 95°C for 5 mins. 2.5 µl of Reaction Mix, 2 µl each of dCTP, dTTP, dGTP (Takara Bio), 2.5 µl of α^{32}P-dATP (3000Ci/mmol) (Perkin Elmer, NEG512H) was added to the sample followed by 1 µl of Klenow fragment (3→5-exo) (NEB, M212S) was added, incubated at 37°C for 15 mins. To remove the unbound the sample was applied to G-50 spin column and collected in a new Eppendorf tube. Probe was boiled at 95°C for 5 mins, chilled on ice for 5 mins and then added to the bottle with membrane and fresh 20 ml hybridization buffer. The membrane was incubated 65°C for more than 12 hours. The membrane was washed with wash buffer (0.1% SDS, 0.04 M Na-Phosphate buffer (pH 7.2), 0.01 M EDTA (pH 8.0)) thrice at 65°C. The membrane was dried and contacted with IP plate (BAS imaging plate) for more 5~8 hours. Membrane was scanned using the IP reader (Typhoon FLA7000, GE Healthcare). For chromosome III, *CHA1* probe was prepared using F-CHA1-IIIL primer; 5'-GTGGTTCCTACAGCGACAAAG-3' and R-CHA1-IIIL primer; 5'-CCAACGCTTCT TCCAAGTCC-3'.

2-12 Benomyl treatment

Sporulation medium containing Benomyl was always freshly prepared on the experiment day. Dimethyl sulfoxide (DMSO; Dojindo, 349-01025) or benomyl (30 mg/ml stock in DMSO; methyl 1-[butylcarbamoyl]-2-benzimidazolecarbamate; Sigma Aldrich, PCode 1002355429) was dissolved in SPM medium and mixed at 30 for an hour, and left to slowly cool down to room temperature. At the time of drug treatment (T = 4 h), the cells were collected and immediately resuspended in the medium containing either benomyl or DMSO.

2-13 Conditional nuclear depletion or inactivation

Nuclear proteins were conditionally depleted from the nucleus upon addition of rapamycin using the anchor away technique (Haruki *et al.*, 2008). Dimethyl sulfoxide (DMSO; Dojindo, 349-01025) or Rapamycin (1 mM concentration stock in DMSO; LC Laboratories, R-5000) was added to the meiotic cell culture during pachynema (T = 4 h).

2-14 Southern blot analysis for DSB detection

DNA was isolated from 10 ml of SPM culture as per the yeast genomic DNA extraction method. To the resuspended DNA in 500 µL of 1X TE (10 mM Tris-Cl (pH 8.0) (nacalai tesque, 35434-34), 1 mM EDTA (Dojindo, 345-01865)), 1 µl of RNase A (10 mg/mL, sigma, R5000) was added, incubated at room temperature for 30 mins. 500 µl of Isopropanol (2-Propanol, Wako, 164-13765) was added and centrifuged (15000 rpm, room temperature, 15 mins). The supernatant was removed and the DNA pellet was washed with 70% (V/V) EtOH followed by 100% (V/V) EtOH. The pellet was dried with centrifugal concentrator for 10 mins. The DNA pellet was suspended with 200 µL of 1X TE buffer.

10 µL of DNA sample was digested with PstI (NEB, R0140L), incubated at 37 for 2 h. 50 µL of 7.5 M Ammonium acetate (nacalai tesque, 02406-95), 100 µL of Isopropanol was added, the tubes inverted to mix and centrifuges (15000 rpm, room temperature, 10 mins). The supernatant was removed and the DNA pellet was washed with 70% (V/V) EtOH and the pellet was dried with centrifugal concentrator for 10 mins. The DNA pellet was suspended with 20 µL of 1X TE buffer and left to dissolve for 30 mins. 5 µL of 10X loading dye (0.37 M Bromophenol blue (Wako, 029-02912), 0.37 M Xylene cyanol FF (Wako, 242-00462), 50 % glycerol (nacalai tesque, 17018-83)) was added. All 20 µL of the sample was loaded on the wells of 0.7 % Agarose S (Wako, 318-01195) gel and run electrophoresis (50 V, 500 mA) in 1X TAE buffer (50X TAE; 1.7 M Tris, 5.7 % Acetic acid, 0.05 M EDTA pH 8.0). The run is stopped when the sample dye has 17 cm from the top. The gel is treated with 500 mL of 0.25 M of HCl (nacalai tesque, 18321-05) for 20 mins, followed by 15 mins neutralization with alkali salt solution (0.2 M NaOH, (Wako, 198-13765) 0.25 M NaCl (Wako, 195-01663)), followed by 20 mins in 25 mM Na-

Phosphate buffer (pH 6.5) twice. Gel was capillary transferred to membrane (Hybond N) (Clear Trans® Nylon membrane 0.45 µm, Wako, 039-22673) for two days. To crosslink the DNA, the membrane was UV crosslinked by UV irradiation 120 mJ/cm^2 (Autocrosslink mode: 1200 µJ (x100)). Probes used for Southern blotting was "Probe 291" for DSBs detection (Storlazzi *et al.*, 1995). Image Gauge software (Fujifilm Co. Ltd., Tokyo, Japan) was used to quantify the DSBs bands. The Southern hybridization method is same as mentioned above (2-11).

2-15 Rad51 tail and bridge analysis

Immunostaining of Chromosome spreads was performed as described above (2-7). The cells were stained with anti-Rad51 (1:1000, anti-rabbit) (Shinohara *et al.*, 2003), and secondary antibody fluorescent-labeled antibodies (Alexa-fluor-488, Molecular probes) was used with 1:2000 dilution. For Rad51 bridges and lines analysis, images were taken by a computer-assisted fluorescence microscope system (Delta vision, Applied Precision), with 100X objective lens (NA 1.35). Image deconvolution was carried out by Image Workstation (Soft Works, Applied Precision). For the distance measurement analysis of Rad51 tail and bridge, 40 chromosome spreads positive for Rad51 were chosen at random. Distance was measured with the Velocity^{TM} program (Applied Precision). For Rad51 tail, the distance from the center of the foci to the end of the protruding tail was measured. For Rad51 bridge, the distance from the center of one focus to the center of the other, or the last focus in the case of bridge between multiple foci, was measured.

2-16 Auxin induced degradation of Srs2

For Auxin-Induced Degradation of Srs2 at 7 h and 8 h after meiotic induction, 50 µM CuSO4 (Wako, 033-04415) was added to induce expression of *pCUP1-OsTIR1*, 30 minutes prior to the addition of auxin. Cell cultures were split and 2 mM auxin (3-indoleacetic acid, Wako 096-00182, dissolved in DMSO) or equal amount of Dimethyl sulfoxide (DMSO; Dojindo, 349-01025) alone was added to the control at indicated times. A follow up 1 mM auxin was added after 30 minutes of the first addition. At 7 h, 1 µM

β-estradiol (sigma, E8875-250MG) in 100% ethanol (Wako, 057-00451) was added to induce IN-NDT80. Cell samples were processed to monitor Srs2-AID-9Myc protein levels, meiotic divisions and Rad51 kinetics.

2-17 GAL-promoter inducible Srs2 system

For inducible Srs2 system, cell culture was split at 7 h and 1 μM β-estradiol (sigma, E8875-250MG) in 100% ethanol (Wako, 057-00451) was added to induce SRS2. Cell samples were processed to monitor meiotic division and Rad51 kinet

Section 3: Results

3-1 *srs2Δ* mutant completed meiotic DSB repair with the formation of abnormal Rad51 aggregates at late times of meiosis

Previous works from my and other labs have revealed that *srs2Δ* mutant shows reduced sporulation and spore viability (Rong *et al.*, 1991), and delayed meiotic DSB repair (Palladino and Klein, 1992). Immunostaining of chromosome spreads revealed that the number of Rad51 foci were slightly reduced in the mutant compared to wild-type (Sasanuma *et al.*, 2013a). Previous works from my lab also reported that the meiotic progression (Sasanuma and Sakurai *et al.*, 2019), observed by staining the cells with a DNA dye called DAPI, of the *srs2Δ* mutant showed a delay of 1 h and the percentage sporulation at 24 h into meiosis was reduced to 81.3 % (± 2.9 %, n = 3) relative to 96.9 % (± 1.4 %, n = 3) of wild type ($p = 0.021$, n = 3, unpaired t-test with Welch's correction) (Figure 1A). The spore viability of the *srs2Δ* mutant was observed to be reduced to 34.9 % as compared to 96.9 % for wild type (Figure 1B). The mutant also observed a reduction in recombination products (CO and NCO) to half of that observed in wildtype (Sasanuma *et al.*, 2013a). However, this reduction cannot explain the low spore viability of 34.9 % observed in the mutant. Immunostaining of chromosome spreads for Rad51 revealed that, in the *srs2Δ* mutant at early hours, Rad51 appear as dotty-like staining termed as, "foci" (Figure 1C). The Rad51 foci in wild type start to appear from 3 h and peak at 4 h with 75.2 % (± 1.0 %, n = 3) of nuclei being Rad51 focus-positive, following reduction and disappearance of the foci by 8 h into meiosis (Figure 1D). The Rad51 foci in the *srs2Δ* mutant similarly exhibited a peak at 4 h (Figure 1D). While at 6 h, the foci start to decrease similar to wild type, a second distinct Rad51 staining was observed at late hours, which was cytologically visualized as a single or more than one clustered staining of Rad51 hereby termed as, "Rad51 aggregates" (Figure 1C). The kinetics of the aggregates revealed that they first appear at 5 h, peak at 52.3 % (± 11.2 %, n = 3) at 6 h and continue to persist even till 12 h of meiosis, at 8.6 % (± 1.4 %, n = 3), although reduced levels of Rad51 aggregates are seen at late time such as 10 and 12 h (Figure 1D). Previous immuno-staining analysis of the recombination proteins Rad51 and Dmc1 on chromosome spreads

revealed unique specificity to these proteins, which works together in early prophase I (Sasanuma and Sakurai *et al.*, 2019). Interestingly, while Rad51 is observed to form aggregates in the *srs2Δ* mutant, no aggregates of Dmc1 was observed (Sasanuma and Sakurai *et al.*, 2019). Dmc1-focus kinetics for the *srs2Δ* was similar to wild type. The absence of Srs2 does not appear to affect the assembly of Dmc1 onto the DNA (Sasanuma and Sakurai *et al.*, 2019). To know the inability of the *srs2Δ* to form Dmc1 aggregate, the expression of the Dmc1 protein along with its mediator Mei5 (Hayase *et al.*, 2004) was analyzed by western blotting. Dmc1 and Mei5 protein expression in the *srs2Δ* was similar to the expression observed in wild type cells (Figure 1E). Rad51-aggregate formation is observed uniquely in the *srs2Δ* mutant and have not been reported in other DNA helicase mutants; e.g. *sgs1* mutant, which also show meiotic recombination defects (Sasanuma and Sakurai *et al.*, 2019). Thus, in my thesis, I focused on the mechanism of Rad51-aggregate formation in the *srs2Δ* and its physiological implications.

Cytological analysis using chromosome spreads reveals only two-dimensional (2D) structure accompanied with detergent treatment, which may alter any structure inside of the nuclei. Thus, immunostaining analysis of a whole cell was carried out. Yeast diploid cells were induced to undergo meiosis by incubating with sporulation medium (SPM) and sample was collected at different time points. The cells were fixed and subjected to immuno-staining. The kinetics of cells containing Rad51 and Dmc1 foci in both wild type and the *srs2Δ* mutant was analyzed. In wild type, dotty staining of Rad51 and Dmc1, called foci, inside of nuclei, detected by DAPI staining, was observed at early times such as 3, 4, and 5 h (Figure 2A, B, C). Like wild-type cells, the *srs2Δ* mutant exhibited appearance of Rad51 and Dmc1 foci in the nucleus at early time points of 3, 4, and 5 h. Importantly, the analysis revealed the presence of a bright clustered staining of Rad51 aggregates inside the *srs2Δ* nuclei at 6 h. The peak was observed at 8 h with 58.4 % (± 8.1 %, n =3) of mutant cells positive for the Rad51 aggregates and then gradually decreased to 34.5 % (± 6.6 %, n = 3) of cells positive for the aggregates at 12 h (Figure 2C). As expected, Dmc1 did not form aggregates at the late times in the mutant. Rad51 aggregates appeared after the disappearance of the Rad51 and Dmc1 foci (Figure 2B). The wild-type like appearance and disappearance of the Rad51 and Dmc1 foci in the

srs2Δ mutant suggests completion of the meiotic DSB repair. Therefore, the Rad51 aggregates in the *srs2Δ* mutant seems to be formed after DSB repair or meiotic recombination. Moreover, the whole-cell staining analysis showed that the Rad51 aggregates are not an artifact of chromosome spreads, rather *de novo* structure in a meiotic nucleus of the *srs2Δ* cells.

3-2 Rad51 aggregates appear to carry on to cells undergoing Meiosis I and II

It has been previously reported that, during mitosis in the absence of Srs2, cells undergo DNA damage checkpoint arrest and are not able to recover even when the DNA had been repaired (Vaze *et al.* 2002), suggesting that Srs2 is required to turn off the checkpoint. Through whole-cell immunostaining analysis cells can be classified into prophase I, meiosis I (MI) and II (MII) by checking the number of DAPI bodies inside of a cell. Meiotic *srs2Δ* cells, which contain the Rad51 aggregates, were classified into the three distinct categories of cells before meiosis I (MI), post MI cells and cells post meiosis II (MII). The aggregates in cells with 1, 2 and, 3 and 4 DAPI bodies, corresponding with before MI, post MI cells and cells post MII, respectively, were observed (Figure 2D). In cells undergoing MII (3 or 4 DAPI bodies), Rad51 aggregates in a middle region of 4 dense DAPI bodies were often seen (Figure 2D). At 12 h, when 88 % of cells finished MII, 70.2 % (± 10.3 %, n = 3) tetra-nucleated cells contained the aggregate while 29.0 % (± 9.8 %, n = 3) cells with the aggregate were mono-nucleated (Figure 2E). This suggests that the DNA damage, which is associated with Rad51 aggregates in *srs2Δ* cells, does not induce a cell-cycle arrest during meiosis and the cells are capable of progressing towards meiosis II.

3-3 Aggregation of Rad51 is completely dependent of meiotic DSBs

To test whether the aggregation of Rad51 in the *srs2Δ* mutant is a consequence of the meiotic DSB repair event, the formation of Rad51 aggregates was observed in the *spo11-Y135F*, a catalysis-defective mutant and thus deficient in DSB formation (Bergerat *et al.*, 1997). Interestingly, no aggregates of Rad51 were observed in the late hours in the *spo11-Y135F srs2Δ* double mutant cells (Figure 3A). This indicates that meiotic DSB formation and its repair events may trigger the Rad51 aggregate formation in the absence of Srs2 (Sasanuma and Sakurai *et al.*, 2019).

3-4 Rad52 and Hed1 colocalize with Rad51 aggregates in the *srs2Δ* mutant

Rad52, a Rad51 mediator, functions to remove RPA from the ssDNA tracts and promotes the assembly of Rad51 (Gasior *et al.*, 1998; Hays *et al.*, 1998). In addition to Rfa2 (a subunit of RPA) (Sasanuma and Sakurai *et al.*, 2019), Rad52 was also observed to colocalize with Rad51 aggregates in *srs2Δ* cells and showed near identical overlapping with Rad51 (Figure 3B). At 6 h, 58.0 % (± 2.7 %, n = 3) of nucleus exhibited Rad52 colocalization with Rad51 aggregates (Figure 3C). This suggests that the abnormal intermediate in late prophase I of the *srs2Δ* cells elicits the assembly of RPA, which in turn promotes the action of Rad52, which mediates the binding of Rad51 for repair, which is very similar to normal DSB repair during mitosis and meiosis (Shinohara and Ogawa 1998; Lao *et al.*, 2008). While these abnormal intermediates appear in the absence of Srs2 and trigger the assembly process of recombination proteins, Rad51 seems to be unable to repair these intermediates since Rad51 aggregates do not turn over (Figure 1D, 2C).

It is known that the meiosis-specific protein Hed1 is one of the substrates of the meiosis specific checkpoint kinase, Mek1. Mek1 phosphorylates Hed1, which in turn binds to Rad51 and inhibits its activity for recombination (Callender *et al.*, 2016). The phosphorylation of Hed1 helps suppress Rad51 activity in *dmc1Δ* mutants by promoting the stability of the Hed1 protein (Callender *et al.*, 2016). Similar to RPA and Rad52, Hed1

also colocalizes with the Rad51 aggregates (Figure 3D, E). This suggests that Rad51's repair activities at the aggregates may be inhibited by Hed1. Hed1 inhibition prompted by the inter-sister inhibition promoted by the meiotic checkpoint kinase Mek1 would cause the cells to arrest at mid prophase I. However, the Hed1 and Rad51 aggregates are continued to be observed even in the dividing cells (Figure 2D, E). This may suggest that the binding of Hed1 to the Rad51 aggregates may be independent to the prophase 1 checkpoint.

3-5 Pachytene checkpoint is not activated in the *srs2Δ* mutant

DSB formation catalyzed by Spo11 recruits the 9-1-1 clamp, which binds to the resected DNAs and recruits Mec1/Tel1 kinases. Mec1/Tel1 then phosphorylates Hop1, which promotes Mek1 dimerization. Mek1 is then activated *in trans* by auto-phosphorylation (Carballo *et al.*, 2008; Niu *et al.*, 2007; Subramanian and Hochwagen, 2014). This cascade of phosphorylation is a part of the cellular surveillance response called pachytene checkpoint or recombination checkpoint during meiosis. Hop1 phosphorylation can be used as an indicator of checkpoint activation during meiosis. Western blotting showed the appearance of bands corresponding for Hop1 phosphorylation at 3 and 4 hours, followed by gradual decrease of Hop1 phosphorylation bands in wild type (Figure 4A). Hop1 phosphorylation status in the *srs2Δ* mutant was observed to be similar to that in wild type with slight delay in disappearance. Thus, the pachytene checkpoint is not activated in the *srs2Δ* mutant, suggesting that the damage or breaks that induce the formation of the Rad51 aggregates do not elicit the checkpoint activation. Quantification for Hop1-phosphorylation over the time in meiosis revealed that the *srs2Δ* mutant showed similar pattern of Hop1 to wild type (Figure 4D). However, there is reduction in the Hop1 protein expression in the mutant at 10 h (Figure 4B). The *srs2-101* mutant, which is mutated in the predicted ATP binding site (Rong *et al.*, 1991), also induced the formation of Rad51 aggregates similar to *srs2*Δ. Deletion of *MEK1* in this mutant does not rescue the Rad51-aggregate phenotype. Both of these results indicate that failure in the

processing or the resolution of specifically inter-homologue recombination is not the cause for the Rad51 aggregate phenotype observed in the mutant (Hunt *et al.*, 2019).

3-6 *srs2Δ* mutant accumulated phosphorylated histone H2A

In mammals, histone H2AX, a histone H2A variant is a key factor in the repair process of damaged DNA. DNA damage induces the phosphorylation of histone H2AX at Ser139 (Rogakou *et al.*, 1998). This phosphorylated form of H2AX protein is termed γH2AX, which in mammalian cells is an indicator of DSBs. γH2AX then mediates the recruitment of other DNA repair machinery (Kobayashi, 2004). In *S. cerevisiae*, which does not have histone H2AX, Ser129 of canonical histone H2A, which is encoded by two copies of histone H2A1 and H2A2 genes, is phosphorylated in response to presence of DSBs (Downs *et al.*, 2000; Fink *et al.*, 2007). Western blotting with antibody against γH2AX showed an accumulation of γH2AX in late times in meiosis in the *srs2Δ* mutant, but not in wild type (Figure 4C). This suggests that Rad51 aggregates in the *srs2Δ* induces the formation of γH2AX, thus the activation of DNA damage checkpoint. This is different from Hop1 phosphorylation. Importantly, as described above, although the checkpoint was observed to be activated at late meiotic prophase I, progression into MI and MII was not deterred in the *srs2Δ* mutant.

3-7 Absence of Srs2 does not affect DSB turnover

Analysis of meiotic DSB formation and repair in the *srs2Δ* mutant by Southern blotting at the *HIS4-LEU2* locus, an artificial meiotic recombination hotspot located in chromosome III (Cao *et al.*, 1990) (Figure 4E), revealed that the mutant observed elevated levels of DSBs with hyper resection and delayed disappearance by ~2 h, as compared to wild type (Sasanuma and Sakurai *et al.*, 2019). This indicated that Srs2 is required for efficient meiotic DSB repair. The steady state levels of DSBs in the mutant was analyzed in a *rad50S* background, which has accumulated DSBs without turnover because of the

inability to resect DSBs (Alani *et al.*, 1990). The accumulated DSB levels in the *rad50S srs2Δ* was 13.7 % (± 2.9 %, n = 3) at 8 h, which was comparable to the DSB level observed in the control *rad50S*, 15.2 % (± 2.0 %, n = 3) (p = 0.506, n = 3, unpaired t-test with Welch's correction) (Figure 4F, G). Thus, the role of Srs2 for efficient DSB repair is not linked to its requirement in the initial step of DSB formation, rather it may play a role in the processing of DSBs in the later step of meiotic DSB repair.

3-8 Chromosome tension caused by the microtubules is not a factor for the formation of Rad51 aggregates in the *srs2Δ* mutant

In mammalian cells, chromosome bridges are known to be DNA damage associated with chromosome segregation during M phase (Clarke *et al.*, 1993; Gorbsky, 1994). It is likely that Rad51 aggregates can be induced by chromosome segregation during meiosis since they are observed in pre-meiosis I, meiosis I and meiosis II. To study the effect of microtubule-induced chromosome tension on the formation of the Rad51 aggregates in the *srs2Δ* mutant, I tried to disrupt microtubules by adding (120 μg/ml final concentration of) Benomyl (methyl 1-[butylcarbamoyl]-2-benzimidazolecarbamate), a microtubule depolymerizing drug to the SPM culture. Previous works have reported that a concentration of 80-120 μg/ml concentration of Benomyl causes a delay into Metaphase I in budding yeast meiosis (Hochwagen *et al.*, 2005). At the 4-hour mark (early prophase), cells were re-suspended in the SPM medium containing 120 μg/ml Benomyl and a mock was prepared with DMSO (0.2 %). Meiotic progression was monitored with DAPI staining and ~70 % cells were observed to be arrested at prior to meiosis I with cells with a single DAPI body in the presence of the drug, but not in its absence (Figure 5A).

Cytological analysis of chromosome spreads was carried out to observe the effect of Benomyl on the formation of the Rad51 aggregates. For the mock, wild type showed punctate staining of Rad51, called foci, at early times such as 3, 4, 5 h, which disappears in late hours (Figure 5B, C). As described above for the results from immunostaining of chromosome spreads (Figure 1C), the *srs2Δ* mutant exhibited punctate staining of Rad51

similar to the wild type. In *srs2Δ* mutant, Rad51 foci appear at 3 h, peaks at 4 h and then disappear (Figure 5D). Kinetic analysis showed that Rad51 aggregates were observed to appear after the disappearance of Rad51 foci at 5 h and accumulated during further incubation (Figure 5D). The observed Rad51 aggregates were classified into type I and type II. Aggregate type I was observed to be more dispersed-like; in addition to a larger body of clustered staining of Rad51, grouping of several foci together was also observed, which were either attached together to the larger body of Rad51 staining or present at a distance (Figure 5B). Aggregate type II was observed to be more aggregated-like; included only the larger body of Rad51 staining clustered together (Figure 5B). Rad51 aggregates type I and type II both appear after 5 h; type I is transient and type II persists till 12 h into meiosis (Figure 5D). Upon the addition of Benomyl at 4 h, wild type observed similar disappearance of Rad51 foci as compared to mock (Figure 5B, C, E). For the *srs2Δ* mutant, addition of the drug at 4 h does not prevent the formation of Rad51 aggregates in the mutant (Figure 5B, F). Kinetic analysis of Rad51 foci and aggregates (both type I and type II) showed little significant difference from that observed for the mock (Figure 5D, F). This experiment was repeated three times to check for reproducibility. With the addition of Benomyl, both dispersed-like type I and aggregated-like type II Rad51 aggregates appear to reach a maximum and remain constant (Figure 5F). Since in the absence of Benomyl, type I is transient, it is possible that microtubule dynamics may affect turnover of type-I Rad51 aggregates in *srs2Δ* cells. On the other hand, the kinetics of total Rad51 aggregates (type I and type II) in control DMSO (55.0 % ± 7.8 %) and upon the addition of Benomyl (53.6 % ± 10.3 %) at 8 h is not significantly different ($p = 0.9206$, $n = 3$, unpaired t-test with Welch's correction), suggesting that the drug had little effect on the formation of the aggregates (Figure 5G). In other words, chromosome tension produced by the microtubules for segregation during meiotic division does not induce Rad51 protein to aggregate in the *srs2Δ* mutant.

3-9 *srs2Δ* mutant accumulates broken chromosomal DNAs at late times of meiosis

In order to understand the nature of the DNA structure, which is accompanied with Rad51 aggregates in the *srs2Δ* mutant, counter-clamped homogeneous electric fields (CHEF) electrophoresis was performed for chromosome-wide analysis. CHEF electrophoresis can resolve very large DNA molecules. In the case of budding yeast all of linear chromosomes are resolvable by CHEF. DNA replication status can also be distinguished as branched DNAs of DNA replication and recombination intermediates cannot enter the gel under the condition and remain in the well. Status of a specific chromosome can be monitored by Southern blotting using a chromosome-specific probe. CHEF electrophoresis condition was first set to resolve all 16 chromosomes of the budding yeast, *Saccharomyces cerevisiae*. In wild-type meiosis, smear staining pattern with fuzzy appearance of chromosomal bands was observed at 3 and 4 h time point, which corresponds with fragmentation of chromosomes by meiotic DSBs (Figure 6A). At 5 h in wild type, smear pattern disappeared, consistent with repair of the DSBs. The *srs2Δ* also observed smear band not only at 3, 4, but also at 5 h. At 7 h, full-length size of chromosomes was recovered. This indicates the delayed repair in the mutant. In addition, the *srs2Δ* mutant formed smaller smear DNA bands at late time point such as 12 h, suggesting the presence of some kind of DNA damage at late times of meiosis, such as in spores (Figure 6A).

The CHEF condition was then modified to resolve smaller sized chromosomes (Figure 6C), and Southern blotting analysis was carried out with a chromosome-specific probe for chromosome III (*CHA1* gene located in the end of the chromosome). In wild type, smear shorter DNA bands compared to a full length of chromosome III were detected only at 3 and 4 h, indicating the presence of meiotic DSBs (Figure 6D). In the *srs2Δ* mutant, similar to as observed with EtBr staining mentioned above, bands corresponding to DSBs were observed at 3, 4 and 5 h (Figure 6D). In late meiosis, a smear was observed at 12 h, indicative of the presence of fragmented bands in the mutant (Figure 6D).

It appears that the *srs2Δ* mutant undergoes meiotic DSB repair (or slight delay) similar to the wild type. However, at late times in meiosis some other kinds of DNA breaks or damage might occur, which could be linked with the Rad51 aggregation in this mutant. For the CHEF analysis, the genomic DNA was isolated by treatment of plug DNAs. As spores have a thicker wall, the zymolyase treatment (check methods 2-11) does not effectively work. Thus, it is likely that the observed smear is not a true representative of the late hour (10 and 12 h) samples.

3-10 DNA damage observed in the *srs2Δ* is independent of Meiotic I division

Previous lab results (Sasanuma and Sakurai *et al.*, 2019) have shown that the formation of the Rad51 aggregates in the mutant is independent of the onset of anaphase I, as the *srs2Δ* mutant with the *CDC20mn*, which is a meiosis-specific null mutant of the *CDC20*, where the promoter is replaced with that of mitosis-specific *CLB2* gene. The *CDC20* encodes for the activator of the Anaphase promoting complex/cyclosome (APC/C) (Lee and Amon, 2003). CHEF electrophoresis was additionally performed with the *CDC20mn srs2Δ* mutant. Previous works from my lab have shown that Rad51 aggregate formation is observed in the *CDC20mn srs2Δ* mutant. Similar to the control *CDC20mn* (at 4 and 5h), the *srs2Δ CDC20mn* mutant observed smear bands at 4, 5, and 6 h, indicating meiotic DSB repair in prophase-I. However, unlike the control but similar to the *srs2Δ* single mutant, a smear band was observed additionally at 10 h and 12 h time point in meiosis of the *srs2Δ CDC20mn* mutant (Figure 6B). This supports that DNA damage is present in the late hours of meiosis in the *srs2Δ* cells prior to the progression into meiosis I. This suggests the presence of DNA breaks in late meiosis I stage after the completion of the DSB repair, implying that the formation of the DNA damage at late times of meiotic prophase I in the *srs2Δ* appear to be independent of meiotic I division, thus chromosome segregation.

3-11 *RAD54-FRB srs2Δ* is a conditional mutant

In order to better understand the molecular mechanism behind the aggregation of Rad51, a conditional mutant was used, which depletes Rad54 by the anchor-away technique. In the anchor away technique the desired protein is sequestered from the compartment wherein it functions to a different one, where it is attached to a suitable protein receptor (the anchor) and thus making it non-functional (Haruki *et al.*, 2008). This technique depends on the heterodimer formation between the human FK506-binding protein (FKBP12) to the FKBP12-rapamycin-binding (FRB) domain of the human mTOR, which takes place in the presence of rapamycin (Belshaw *et al.*, 1996; Chen *et al.*, 1995). The gene of interest is tagged with FRB while a suitable anchor protein is tagged with FKBP12. In this case, ribosomal protein RPL13A was used as an anchor, which transports out of the nucleus during the ribosome assembly and thus depletes the target protein from the nucleus (Figure 7A). However, rapamycin is toxic to wild-type yeast cells and thus strains, which have a mutated *TOR1* gene (*tor1-1*) and deleted *FPR1* gene (*fpr1Δ*) must be used. The later *FPR1* is the yeast homolog of the human *FKBP12* gene that encodes for the most abundant FK506- and rapamycin-binding protein in *S. cerevisiae* (Arevalo-Rodriguez *et al.*, 2004), this deletion is necessary to remove rapamycin toxicity and to decrease competition between endogenous FPR1 protein and anchor-FKBP12 protein. While the former mutated *TOR1* (*tor1-1*, amino-acid substitution of Ser-1972 of the Protein kinase C (PKC) site to Arg) has been shown to confer resistance to Rapamycin toxicity (Helliwell *et al.*, 1994). The *rad54Δ* mutant shows mitotic defects similar to *rad51Δ* mutant. However, interestingly, *rad54Δ* shows subtle meiotic defects unlike the *rad51Δ* due to the function of the Rad54-related meiosis-specific protein Tid1/Rdh54 (Shinohara *et al.*, 1997; Klein 1997). Previously, it has been reported that *srs2Δ rad54Δ* double mutant is synthetically lethal (Palladino and Klein 1992) and thus a conditional mutant by using anchor-away method for Rad54 depletion was introduced into the *srs2Δ* mutant. If Rad51-Rad54 functions in the repair process that generates the aggregates, it would be expected that in the absence of *Rad54* more defective turnover of Rad51 aggregates in the *srs2Δ* would be observed.

Dilution assay was performed to check for the lethality of the *RAD54-FRB srs2Δ* only in the presence of rapamycin. The haploid *RAD54-FRB srs2Δ* strain was lethal in the presence of rapamycin, but not in its absence (Figure 7B). In order to know the effect of *RAD54* depletion in Rad51 aggregate kinetics, rapamycin was added at 4-hour (early prophase, mark in Figure 7C). Sporulating cells were re-suspended and added to the SPM containing 1 μM Rapamycin and a mock was prepared with DMSO (0.1 %). While the depletion of Rad54 by the addition of rapamycin at 4 h had no significant effect on the percentage sporulation of the *RAD54-FRB* strain (Mock 96.6 % ± 2.5 %; + rapamycin 95.6 % ± 1.6 %; $p = 0.5798$, n = 3, unpaired t test with Welch's correction), it recovered the efficiency of the *RAD54-FRB srs2Δ* mutant to complete meiosis II from 77.5 % (± 3.7 %) to 86.4 % (± 1.6 %) ($p = 0.0361$, n = 3, unpaired t test with Welch's correction) (Figure 7C). Rad54 depletion only reduced the spore viability negligibly from 96.3 % to 92.2 % observed after rapamycin addition, whereas the spore viability was shown to be reduced from 64.4 % to 56.7 % for the *RAD54-FRB srs2Δ* mutant upon rapamycin addition (Figure 7C). This slight decrease might be a bit surprising given severe lethal defect of *srs2Δ rad54Δ* double depletion in mitosis (Figure 7B). These results show that *RAD54-FRB srs2Δ* is not synthetically lethal in meiosis; Rad54 is not redundant with Srs2 in meiosis, different from mitosis.

3-12 *srs2Δ* mutant forms Rad51 clumps similar to wild type upon Rad54 depletion

Immunostaining of chromosome spreads was performed to observe Rad51 localization upon Rad54 depletion. Without the addition of rapamycin, wild type shows dotty staining of Rad51 foci at early times such as 3, 4, and 5 h inside of chromosome spreads stained with DAPI (Figure 8A). Like wild-type cells, the *srs2Δ* mutant does form Rad51 foci in the nucleus at early time points and disappears (Figure 8B). As described above (Figure 5B), at late hours in meiosis Rad51 aggregates form in the *srs2Δ* mutant with two different kinds of pattern, dispersed like, type I, which contains a larger cluster of Rad51 staining

accompanied with a grouping of several foci together, and the aggregate-like, type II, where only a large cluster of Rad51 staining is observed in the nuclei (Figure 8A).

Upon the addition of rapamycin at 4 h to deplete Rad54, wild-type *RAD54-FRB* showed a novel class of Rad51 staining, in which bright Rad51 foci are associated with fragmented DAPI bodies, which was termed "Rad51 clumps" like staining (Figure 8D). This Rad51 clumps is transient in wild-type background; it appears at 5 h, peaks at 6 h at 29.2 % (± 5.8 %, n = 3) and disappears by 10 h (Figure 8E).

In the *srs2Δ* mutant, Rad51 aggregates start forming at 5 h, peak at 8 h at 48.2 % (± 4.6 %, n = 3), and decrease slightly with persistent fractions (Figure 8C). Upon the depletion of Rad54 in the *srs2Δ* mutant with the addition of rapamycin at 4 h, the Rad51 clumps staining was observed (Figure 8D, F). Like in wild-type *RAD54-FRB*, in the *RAD54-FRB srs2Δ* the clump of Rad51 appears at 5 h, peaks at 6 h at 37.9 % (± 14.5 %, n = 3) and disappears by 10 h (Figure 8G). This suggest the absence of Srs2 does not affect turnover of Rad51 clumps induced by Rad51 deficiency.

On the other hand, upon the Rad54 depletion, Rad51 aggregate type I decreases. However, the kinetics of Rad51 aggregate type II appear to be unaffected (Figure 8G). When comparing the kinetics of the sum of type I and type II aggregates upon the addition of rapamycin, the increase in the *RAD54-FRB srs2Δ* cells with either type I or type II aggregates observed a more delayed increase as compared to without the addition of rapamycin (or mock), although the percentage of cells positive for either type I or type II aggregates at 12 h was similar for both with and without rapamycin addition (Figure 8H). This result suggested that Rad54 may play a role in the processing of intermediates associated with the Rad51 aggregates at late meiosis.

To summarize these results, in the control where *RAD54* is present, the *RAD54-FRB* strain did not form any Rad51 aggregates while the *srs2Δ* mutant formed Rad51 aggregates as shown above. With the addition of rapamycin, which depletes Rad54 protein effectively, the *RAD54-FRB* strain showed Rad51 clumps and under the same condition the *RAD54-FRB srs2Δ* strain upon *RAD54* depletion also formed Rad51 clumps. Additionally, *RAD54-FRB srs2Δ* cells showed an overall decrease in the Rad51

aggregates compared to when Rad54 is present however, a large reduction is observed in the type I aggregates formed in the absence of both Srs2 and Rad54. These suggest that Rad51 clumps, which were observed upon the depletion of Rad54 in both wild type and *srs2Δ* might be related to type I aggregate, which was observed to be greatly reduced.

3-13 Rad51 aggregates form after the mid-pachytene exit

In order to understand the nature of the DNA damage that causes the Rad51 protein to form aggregation on the chromosomes in the *srs2Δ* mutant, it is important to know at what stage in meiotic prophase I the formation of Rad51 aggregates occurs in the mutant; in other words, whether it is during or after meiotic recombination.

To address this question, the *ndt80Δ* mutant was used. *NDT80* is a meiosis-specific gene required for pachytene exit (Xu *et al.* 1995) and the *ndt80Δ* mutant shows mid-pachytene arrest due to the inability to induce a transcriptional program to exit the mid-pachytene stage. Thus, the *ndt80Δ* mutant shows mid-pachytene arrest with fully synapsed chromosomes and accumulation of recombination intermediate with double- Holliday junction structure (dHJ) (Xu *et al.*, 1995; Allers and Lichten, 2001) and exhibits persistent secondary DSB formation, due to lack of shutdown of DSB formation by disassembly of meiotic chromosome structures required for DSB formation (Xu *et al.*, 1995). *srs2Δ ndt80Δ* mutant was confirmed to be arrested at prior to meiosis I with DAPI analysis, similar to *ndt80Δ* single mutant (Figure 9B). Immunostaining of whole cell was then carried out to check for the formation of Rad51 aggregates in the *srs2Δ ndt80Δ* double mutant. In the *srs2Δ ndt80Δ* double mutant, Rad51 foci along with Dmc1 foci persist throughout the late time points of meiosis similar to the *ndt80Δ* single mutant (Figure 9A, C, D), which was expected since the *NDT80* deletion causes the cells to accumulate DSBs at late time points. Importantly, kinetic analysis of Rad51 staining revealed that, unlike the *srs2Δ* mutant, at late time points few Rad51 aggregates were observed in the *srs2Δ ndt80Δ* double mutant (Figure 9A, C). This result suggests that the Rad51-aggregate formation depends on the *NDT80* function, thus the exit of mid-pachytene.

Therefore, it suggests that Rad51-aggregate formation in the *srs2Δ* occurs at or after the processing of dHJ (disassembly of synaptonemal complex).

3-14 Rad51-bridge staining connecting two individual recombination events observed in *srs2Δ* mutant

Although prior to mid-pachytene, Rad51 aggregates do not appear in the *srs2Δ* mutant, careful examination of Rad51 staining during early meiotic prophase revealed a new type of staining in the *srs2Δ* cells. Thin faint lines of staining were observed in between two Rad51 foci, which was termed as "Rad51 bridges" (Figure 9E). These faint lines were even observed to form between three of more foci in the mutant. Although Rad51 bridges was observed in wild type (35 % ± 6.9 %, n = 3), they were present at a lower percentage as compared to *srs2Δ* (79 % ± 4.1 %, n = 3) (p = 0.0017, n = 3, unpaired t-test with Welch's correction) (Figure 9F). The length of the bridge was measured as the distance from the center of one focus to the other. The length of the Rad51 bridge between two foci in the mutant (0.365 μm ± 0.020 μm) was comparable to that observed in the wild type (0.405 μm ± 0.045 μm) (p = 0.39, n = 3, Mann-Whitney U test) (Figure 9G). However, unlike wild type, Rad51 bridge between three or more foci was increased in the *srs2Δ* mutant (Figure 9H).

In addition to Rad51 bridge, faint staining protruding from a single focus was also observed, which was termed as "Rad51 tail". This staining pattern was observed in both wild type and the mutant (Figure 9E). This may be indicative of some additional Rad51 molecules bound in excess at the site of the recombination event.

Rad51 bridge was also observed in the *srs2Δ ndt80Δ* mutant (at 6 h) (Figure 9I). The *srs2Δ ndt80Δ* mutant observed an increased amount of bridge between two or more foci as compared to *ndt80Δ* (Figure 9I). The Rad51 bridges thus form prior to the exit of pachytene. Given the increased Rad51 bridges in the mutant, these structures underlying the Rad51 bridges could be a precursor event, which might lead to the formation of the Rad51 aggregates after the mid-pachytene exit.

3-15 Rad51 aggregate formation is not dependent of Rad55/57-mediated Rad51 assembly

Rad51 paralogs, Rad55 and Rad57, which form a heterodimer, is known to antagonize the anti-recombinase activity of Srs2 by associating with the Rad51 filaments, which is rendered to be more resistant to translocation by Srs2, as compared to Rad51 filaments alone. The heterodimer was also shown to directly bind with Srs2 protein there by blocking translocation (Liu *et al.*, 2011). The formation of Rad51 aggregates was analyzed in the *srs2Δ rad55Δ* mutant to test whether Rad55-57 mediated Rad51 assembly in early meiosis may lead to the late defect observed in the absence of Srs2. *rad55Δ* increased the sporulation efficiency of *srs2Δ* mutant from 68.8 % (± 4.8 %, n = 3) to 84.6 % (± 13.0 %) (p = 0.16, n = 3, unpaired t-test with Welch's correction), as compared to *rad55Δ* (72.7 % ± 12.0 %) (p = 0.31, n = 3, unpaired t-test with Welch's correction) and the wild type (97.8 % ± 1.77 %) (p = 0.22, n = 3, unpaired t-test with Welch's correction) (Figure 10A). The double mutant observed a similar delay in meiotic progression as compared with *rad55Δ* (Figure 10A). Spore viability analysis could not be carried out as *rad55Δ* mutant observed near zero viable spores, which was similarly observed in the double mutant.

As expected of a deletion mutant of a Rad51 mediator gene, *rad55Δ* mutant observed delayed and reduced number of Rad51 foci positive nuclei (Figure 10B, C). Kinetic analysis shows *rad55Δ srs2Δ* mutant shows similar peak to wild type (Figure 10C). The appearance of the aggregates in the *rad55Δ srs2Δ* mutant appeared with a ~2 hr delay as compared to the *srs2Δ* mutant and peaked at 10 h as compared to the peak at 8 h observed for *srs2Δ* (Figure 10E). However, even with reduced loading of Rad51 in early meiosis in the double mutant, the peak value at 10 h for the percentage of cells with Rad51 aggregates in the double mutant (53.6 ± 21.2 %) was observed to be similar to the peak value for *srs2Δ* (58.1 % ± 12.9 %) observed at 7 h (p = 0.66, n = 3, unpaired t-test with Welch's correction) (Figure 10D). Interestingly, *rad55Δ* mutant observed distinct Rad51 staining, which was similar to the observed staining upon Rad54 depletion which was termed as "Rad51 clumps" like staining (Figure 10D and 8D). Interestingly, at late hours

into meiosis (10 h), *rad55Δ* mutant also observed these Rad51 clumps-like staining, which was observed after the disappearance of Rad51 foci in the *rad55Δ* (Figure 10F), which appear similar to those observed in the Rad54 depleted cells.

These results suggest that Rad51 loading mediated by Rad55-57 by antagonizing Srs2 in early meiosis is not the precursor defect which results in the formation of Rad51 aggregates in the absence of Srs2. Although, some defects in Rad51 loading were observed in the absence of the Rad55-57 mediator.

3-16 Dissolution by Sgs1 is not associated with the formation of Rad51 aggregate in the absence of Srs2

Sgs1 helicase, which forms a complex with Top3 and Rmi1, functions to dissolve double Holliday junctions to form non-crossovers (Ira *et al.*, 2003; Wu and Hickson, 2003). The synthetic lethality of the *srs2 sgs1* mutant demonstrates the redundant functions of the two helicases in HR (Gangloff *et al.*, 2000; McVey *et al.*, 2001). Genetic data suggests *srs2 sgs1* accumulate toxic recombination intermediates that cannot be resolved in the absence of Srs2 and Sgs1, as the lethal phenotype is suppressed by the deletion of *RAD51* gene (Gangloff *et al.*, 2000). To investigate whether intermediates that produce Rad51 aggregates in the absence of Srs2 is a by product from the dissolution by Sgs1-Top3-Rmi1 (STR) complex, a meiotic null mutant of *SGS1, pCLB2-SGS1* was used, where the promoter is replaced with that of mitosis-specific *CLB2* gene.

pCLB2-SGS1 srs2Δ mutant observed reduced sporulation of 39.4 % (± 3.6 %) as compared to wild type (97.4 % ± 1.6 %) ($p = 0.0002$, n = 3, unpaired t-test with Welch's correction), *srs2Δ* (74.8 % ± 2.5) ($p = 0.0003$, n = 3, unpaired t-test with Welch's correction) and *pCLB2-SGS1* (87.3 % ± 8.5 %) ($p = 0.0044$, n = 3, unpaired t-test with Welch's correction) (Figure 11A). Low sporulation of the double mutant may be indicative of the "meiotic" lethality of the double mutant. While the Rad51-focus kinetics did not exhibit a significant difference between the double mutant as compared to the single mutants, which were slightly delayed as compared to the wild type (Figure 11B,

C). Meiotic depletion of Sgs1 does not affect the formation of Rad51 aggregates, the double mutant (51.5 % ± 6.8) had similar peak values as compared to *srs2Δ* mutant (50.8 % ± 19.4) (p = 0.96, n = 3, unpaired t-test with Welch's correction) (Figure 11C). However, while, in the *srs2Δ* mutant the Rad51 aggregates plateaued at 10 h and decreased at 12 h, in the double mutant, the Rad51 aggregate continued to plateau at 12 h (Figure 11D). This indicates that a small fraction of Rad51-aggregate positive nuclei observed in the *srs2Δ* mutant after 10 h may have been dissolved by Sgs1.

3-17 Srs2 has a secondary function at pachytene exit to prevent the formation of Rad51 aggregates

Rad51 aggregates in the *srs2* mutant form after the induction of *NDT80*, which marks the exit from mid-pachytene arrest. In order to investigate Srs2's role in late meiosis, which is independent of its role in early meiosis, an inducible Ndt80 system coupled with a conditional degradable Srs2 system was constructed. For the inducible Ndt80 system (*NDT80-IN*), Ndt80's open reading frame was placed under the *GAL1-10* promotor. In cells producing Gal4 estrogen receptor fusion protein (Gal4-ER), transcription from the *GAL1-10* promoter can be induced by the addition of β-estradiol (Picard, 1994; Benjamin *et al.*, 2003; Carlile and Amon, 2008). In the absence of β-estradiol the cells are arrested at pachytene, meiotic progression is restored upon its addition (Figure 12B). For the degradation of Srs2 protein, the Auxin inducible Degron (AID) system was used. The protein was tagged with an AID-9Myc tag to express Srs2-AID-9Myc protein (Morawska and Ulrich, 2013). Upon the addition of auxin (3-indoleacetic acid), its binding with TIR1 protein, promotes TIR1's interaction with E3 ubiquitin ligase (SCF). SCF-TIR1 ubiquitin ligase complex together with E2 enzyme polyubiquitylates an AID tagged protein, which is subjected to rapid degradation by proteosomes (Nishimura *et al.*, 2009) (Figure 12A).

The *SRS2-AID-9Myc NDT80-IN* cells were incubated in nutrient poor sporulation medium for 7 h to allow cells to initiate meiosis and arrest at pachytene. The culture was split into two, with auxin (Aux +) and without auxin (DMSO added as control) (Aux -,

control). For Ndt80 induction, β-estradiol was added to both cultures at the same time (Figure 13 A). Western-blot analysis showed effective degradation of Srs2 after one hour upon addition of auxin, together with confirmed expression of Ndt80 protein as well as its downstream substrate Cdc5 (PLK) kinase (Figure 13B). Meiotic progression was restored upon Ndt80 induction as observed with DAPI analysis (Figure 13C). Degradation of Srs2 in this condition observed an increased delay in the progression and a reduction in sporulation at 12 h from 59.5 % (± 14.7 %) compared to 72.8 % (± 18.3 %) of the control (p = 0.39, n = 3, unpaired t-test with Welch's correction) (Figure 13C). Although nuclear division was observed with DAPI analysis for meiotic progression, even after 72 hours upon meiotic induction, no spores were observed for both control (Aux -) and upon addition of auxin thus spore viability analysis could not be carried out. Immunostaining of chromosome spreads for Rad51 revealed the disappearance of Rad51 foci with control (Aux -) and that Aux + conditions followed similar kinetics (Figure 12D, E). On the other hand, Rad51 aggregates started appearing 1 hour after the addition of auxin and continued increasing to 31.3 % (± 9.3 %, n = 3) at 10 h (Figure 12D, F). Srs2 has a function specific to after the induction of Ndt80 and the inability of this function generates abnormal intermediates that results in Rad51 aggregates. From this observation it can be speculated that the events following induction of Ndt80, such as resolution of recombination intermediates and disassembly of SC, could lead to DNA entanglement of Rad51-bound filaments resulting in the appearance of Rad51 aggregates observed.

To understand further, β-estradiol was added 7 h after meiotic induction to the *SRS2-AID-9Myc NDT80-IN* cells to induce Ndt80 expression. At 1 h after Ndt80 induction, the culture was split into two, with auxin (Aux +) and without auxin (DMSO was added as control) (Aux -, control) (Figure 14A). Western-blot analysis showed effective degradation of Srs2 and confirmed protein expression of Ndt80 as well as the downstream Cdc5 (PLK) kinase (Figure 14B). Meiotic progression was restored upon Ndt80 induction as observed with DAPI analysis (Figure 14C). Degradation of Srs2 in this condition observed an increased delay in the progression and a reduction in sporulation of 42.8 % (± 22.2 %) compared to 79.7 % (± 10.9 %) of the control (p = 0.084, n = 3, unpaired t-test with Welch's correction) (Figure 14C). Similar to auxin addition at 7 h, spore viability analysis could not be carried out as no spores were observed in the culture at even 72

hours after meiotic induction. Similar to auxin addition at 7 h, Rad51 foci was observed to disappear in control (Aux -) and Aux + conditions showing similar kinetics (Figure 14D, E). On the other hand, Rad51 aggregates started appearing 1 hour after the addition of auxin and continued increasing to 14.5 % (± 5.5 %, n = 3) at 10 h (Figure 14F), which was lower than the observed percentage for auxin addition at 7 h (Figure 13F). Interestingly, the percentage increase 1 h after auxin addition was higher in the case of Aux + at 8 h (11.1 % ± 3.2 %, n = 3) (Figure 14F), as compared to Aux + at 7 h (3.1 % ± 1.6 %, n = 3) (Figure 13F). This could be a consequence of the late addition of auxin as at 2 h after the addition of Aux (9 h) in Aux + at 7 h, 20.9 % (± 3.6 %, n = 3) of aggregate positive cells were observed (Figure 13F). The decreased percentage of aggregate-positive cells when Srs2 was degraded after the Ndt80 induction suggests that post Ndt80 induction events could result in the accumulation of aberrant recombination intermediates which may lead to the Rad51 aggregates or these events may influence the formation of the Rad51 aggregate structure from Rad51 bound DNA structures. There is also the possibility of some residual Srs2 remaining which resolves the aggregate structure as the degron system could be leaky and low amounts of Srs2 protein, which is not detectable with western was still present in the cell.

3-18 Srs2 induction in late meiosis reduces Rad51 aggregation

To investigate if Srs2 plays a role in directly resolving the Rad51 aggregate structures, the *SRS2* gene was placed under the inducible ER-driven *GAL1-10* promoter for induction by the addition of β-estradiol (Picard, 1994). *CDC20mn* was used to ensure accumulation of Rad51 aggregates in late meiosis. β-estradiol was added at 7 h. Srs2 induction could not be confirmed with western due to the unavailability of a working Srs2 antibody. Sporulation efficiency was low as *CDC20mn* cells arrest at anaphase I onset (Figure 15B). Induction of Srs2 at 7 h does not completely resolve all aggregates (Figure 15A). However, a decrease in the total aggregate percentage was observed from 38.7 % (± 19.8 %, n = 3) at 10 h to 18.7 % (± 4.8 %, n = 3) upon the addition of estradiol (Figure 15C). This result indicates that, although Srs2 is not able to resolve the Rad51 aggregates

completely, Srs2 functions to prevent the formation of the aggregates at late meiosis. As observed from a reduction in the aggregate percentage, Srs2 could also possibly resolve the Rad51 aggregates to some minor extent.

Section 4: Discussion

4-1 Nature of Rad51 aggregates in *srs2Δ* mutant

The assembly of the Rad51 filaments on to the chromatin is more firmly regulated during meiosis as compared to the vegetative growth period (Sasanuma *et al.*, 2013b). Several past studies have elucidated the mechanism by which Rad51 is positively regulated by the aid of proteins called, Rad51 mediators (Sung, 1997a; Sung, 1997b; Hays *et al.*, 1995; Cole *et al.*, 1989; Sasanuma *et al.*, 2013a). Alternatively, Srs2 DNA helicase is known to function as a negative regulator of Rad51 and it has been reported that Srs2 has the ability to dismantle Rad51 *in vitro* as well as *in vivo* (Krejci *et al.*, 2003; Veaute et al., 2003 Sasanuma *et al.*, 2013b), which is the basis for the possible mechanism by which the protein functions as an anti-recombinase. Studies on *srs2* deletion and overexpression during meiotic recombination have shown that Srs2 has at least two distinct roles during meiosis: anti-recombinase activity in regulating the dynamic assembly/disassembly of Rad51, and pro-recombinase activity in processing recombination intermediates post synapsis. It has been previously reported that the *srs2* deletion mutant have reduced formation of crossovers (COs) and non-crossovers (NCOs) resulting from meiotic recombination, indicating Srs2's role in promoting efficient interhomolog recombination (Sasanuma *et al.,* 2013a, Sasanuma and Sakurai *et al.*, 2019). The mutant is reported to observe delayed meiotic DSB repair with normal assembly of Rad51 and Dmc1, which was also shown by this study, suggesting that Srs2 helicase functions at post assembly stage of Rad51 (Sasanuma *et al.,* 2013ab, Sasanuma and Sakurai *et al.*, 2019). This is supported by the fact that the *srs2* mutation is synthetically lethal with a mutation of the *RAD54* gene, which works at the post-assembly step (Palladino *et al.* 1992; Rattray and Symington, 1995). The *srs2* mutant observed very low spore viability which could not be explained by only the reduced formation of CO and NCO, indicating a slight impair in the DSB repair stage of meiosis. The observed low spore viability can be accredited to the presence of abnormal phenotype of Rad51, which forms a condensed structure on the chromosome, termed as the "Rad51 aggregates" in this study. The aggregates are not protein based and are indicative of the presence of chromosome abnormality in the absence of Srs2, as other repair-associated proteins such as RPA and Rad52 were shown to localize at the Rad51 aggregate sites (Sasanuma and Sakurai *et al.*, 2019). The presence

of the ssDNA binding protein, RPA, at the Rad51 aggregates sites indicates the presence of ssDNA tracts that could elicit the Rad51 aggregation phenotype in the absence of Srs2. These aggregates are also not a consequence of DNA morphological changes during chromosome segregation in meiosis I, as shown by the presence of aggregates at the onset of anaphase I in the *CDC20mn* background mutant and by treatment with microtubule de-polymerizing drug, benomyl.

CHEF analysis revealed the presence of DNA damage in the *srs2* mutant, which was also observed to be present in late metaphase/onset of anaphase. However, although cytological analysis indicated 58.4 % (± 8.1 %) of cells were positive for the Rad51 aggregates at 8 h after meiotic induction (Figure 2C), the smear observed through CHEF analysis for 8 h does not appear to reciprocate this figure (Figure 6A). Therefore, it is likely that DNA damage with Rad51 aggregates for late prophase-I does not contain DSBs, which can be detected by CHEF. Thus, it is possible that the DSBs detected by CHEF could be a consequence of further processing of the DNA damage resulting from meiotic divisions. The DNA damage with Rad51 aggregates might be an ssDNA gap in the chromosomes. Further analysis is necessary to understand the exact nature of the DNA damage that enlists Rad51 and causes it to aggregate.

4-2 Dual function of Srs2 in regulation of Rad51 filaments

Srs2's ability to translocate on the ssDNA and it's interaction with Rad51 is essential for the process of dislodging Rad51 from the DNA bound pre-synaptic filaments, shown from the ATPase and Rad51-interaction deficient Srs2 mutants, which observed DNA with undissociated Rad51 *in vitro* and could not prevent recombination *in vivo* (Krejci et al., 2004; Colavito et al., 2009; Antony et al., 2009). During meiotic recombination, the ATP-binding/hydrolysis activity of Srs2 is required for the dismantling of Rad51 *in vivo* however, the Rad51-interaction domain of Srs2 is not required, having a lesser of a role *in vivo* as compared to *in vitro* (Sasanuma *et al.*, 2013b). The translocation of Srs2 along the ssDNA is specific to the dismantling of Rad51 complexes, and not Dmc1 (Sasanuma *et al.*, 2013b). Similarly, the absence of Srs2 results in the aggregation of Rad51 but not Dmc1. Interestingly, the formation of the Rad51 aggregates in the absence of Srs2 is

dependent on the formation of the meiotic DSBs and the following meiotic recombination repair event (Sasanuma and Sakurai *et al.*, 2019). The Rad51 aggregates are also dependent on the Ndt80 function. This study revealed a new role of Srs2 in late meiotic prophase I, which is dependent on the *NDT80* induction. Spo11 catalyzed DSBs are repaired through the Dmc1 mediated recombination repair and the remainder of the breaks are repaired through the Rad51-Rad54 mediated repair (Subramanian *et al.*, 2016). Srs2 functions to regulate Rad51 mediated repair by dislodging the recombinase from ssDNA to prevent recombination when necessary. Before *NDT80* induction (early pachytene), defect in the Rad51 foci formation was observed in the absence of Srs2. In addition to Rad51 foci observed in wild type, the *srs2Δ* mutant observed thin line-like staining in between two or more foci, termed as 'Rad51 bridge'. These Rad51 bridge phenotype may result from multiple-invasion by Rad51 coated ssDNA, connecting the sites of two distinct DSBs. This excess invasion of ssDNA by Rad51 filaments could be prevented by Srs2's translocase activity to dislodge Rad51 filaments to ensure a tight regulation of strand invasion mediated by Rad51 during early meiotic prophase I (Figure 16).

The Rad51 bridge observed in the absence of Srs2 could also be precursor intermediates to form the Rad51 aggregates after the *NDT80* induction. However, analysis with degradable Srs2 protein and inducible *NDT80* system revealed that when functional Srs2 is present till mid pachytene and only degraded after the Ndt80 expression, Rad51 aggregates were observed to be formed (Figure 13). This indicates that independent to Srs2's role pre-Ndt80 function, the protein has a second role during the events following Ndt80 expression, such as resolution of recombination intermediates and the disassembly of the synaptonemal complex (SC), which holds the two homologous chromosomes together during meiosis, and/or chromatin compaction occurring during the transition between prophase I to metaphase I.

The Rad51 aggregate phenotype is also specific to Srs2 as other helicase mutants, such as *sgs1* or *mph1*, do not observe this phenotype. Analysis with *srs2Δ* and meiotic depletion of *SGS1* revealed no changes in the formation of the Rad51 aggregates however, continued plateau after 10 h in the double mutant (Figure 11D) indicated that a small

fraction of the Rad51 aggregates in the absence of Srs2 could have been dissolved by Sgs1 resulting in the downward trend observed in the *srs2Δ* mutant after 10 h into meiosis.

In wild type, after meiotic DSB formation and 5'-end resection, Rad51 and Dmc1 are loaded onto the ssDNA for homology search and strand exchange mediated by Dmc1. Once the Dmc1-mediated meiotic DSB repair is complete, the cell exits prophase I and enters the meiotic division. Srs2 does not play any role in Dmc1-mediated meiotic DSB repair. A small fraction of abnormal recombination intermediates may form during the meiotic repair. Rad51 may bind to these intermediates (Figure 16). These Rad51 protein may be dismantled by Srs2 and the resolution of these intermediates could be mediated by Srs2's DNA translocase activity and unwind the DNA intermediates. In the absence of Srs2, Rad51 remains loaded onto these intermediates and after Ndt80 induction, the resolution event as well as other DNA changes promoted by the disassembly of SC could result in the Rad51 aggregate phenotype observed (Figure 17). Secondly, after the Ndt80 induction, resolvases introduce nicks in the double Holliday junction (dHJ) structure in order to resolve to CO (Figure 16). There nicks create strands of ssDNA, which may be a substrate for Rad51 to bind to. This bound Rad51 is then dislodged by Srs2 and Srs2's translocase activity unwinds DNA to ensure accurate resolution of the intermediates. In the absence of Srs2, these Rad51 bound recombination intermediates could develop into aggregates after Ndt80 induction and the resulting events of resolution and SC disassembly, as mentioned above (Figure 17). In both occasions, Srs2 may play a role in the regulation of Rad51 assembly and strand invasion by Rad51 after the completion of meiotic DSB repair, during which Rad51 and Rad54 is inhibited by the action of Mek1 to inhibit inter-sister recombination. Srs2 may play a role in ensuring efficient Rad51 loading and repair in the middle of resolution of recombination intermediates from Dmc1 mediated repair and the dismantling of the SC, by disrupting Rad51 mediated D-loops to resolve through the SDSA pathway.

4-3 Role of Srs2 and Rad51 mediators in Rad51 assembly

Previous reports have indicated that Rad51 mediators, Rad55-57 and the PCSS complex both antagonize Srs2 (Liu *et al.*, 2011; Bernstein *et al.*, 2011). While *SRS2* deletion is

able to suppress the mitotic defects of the *rad55* or *rad57* mutants, it did not dramatically suppress the meiotic defects related to mutations in Rad55-57 complex or the PCSS (*PSY3*, *CSM2*, *SHU1* and *SHU2*) components (Liu *et al.*, 2011; Sasanuma *et al.*, 2013), thus indicating that the assembly of Rad51 onto the chromatin is more strictly regulated during meiosis than mitosis. Studies in mitosis have revealed that the Rad51 focus formation in the *srs2* mutant was reported to have a reduced requirement for Rad52 activity, suggesting that Srs2 antagonizes Rad52 in the formation of Rad51 filaments (Burgess *et al.*, 2009). As previously reported, *srs2* mutation is synthetically lethal with a mutation of the *RAD54*, which acts in the later stage of recombination, and the lethality of the *srs2Δ rad54Δ* is suppressed by mutation of the *RAD51* gene (Klein, 2001), confirming Srs2's role in post assembly regulation of Rad51. In this study, Rad54 depletion studies in the *srs2Δ* mutant showed that in the absence of Rad54, wild type as well as *srs2Δ* observed Rad51 clumps at several distinct locations in the nuclear spread (Figure 8D). Strangely, these clumps disappear during further incubation (Figure 8E), indicating further processing and/or repair. Although the percentage of cells positive for Rad51 aggregates in the *srs2Δ* mutant upon depletion of Rad54 decrease the percentage plateaus to similar value as compared to *srs2Δ* (Figure 8H). This indicates that Rad54 does not function in the pathway in which Srs2 functions which leads to the prevention of the Rad51 aggregate formation. However, Rad54's role in early strand invasion step by Rad51 appears to be downstream of the event leading to the Rad51 aggregate formation in the absence of Srs2. This would explain the decrease in Rad51 aggregate formation in the earlier hours. It has been reported that, during mitosis upon depletion of Srs2, Rad54, thus possibly Rad51, loads onto the chromatin even in the absence of Rad52, which functions prior to Rad51 assembly (Burgess *et al.*, 2009).

Similar to 'Rad51 clumps' observed when Rad54 was depleted, similar phenotype was observed in the *rad55Δ* mutant, raising question whether Rad51 mediators play a role in the prevention of Rad51 filaments entangling while invading the donor template strand. Interestingly in the *rad55Δ srs2Δ* mutant, where assembly of Rad51 is impaired during early prophase I, Rad51 aggregates formation was delayed in late meiosis. This suggests that the Rad55-57 stabilized-Rad51 filaments may not be involved as the pre-requisite structures that form the Rad51 aggregates in the absence of Srs2.

4-4 Conservation of Srs2 functions in higher eukaryotes

In higher eukaryotes, although a clear Srs2 sequence homolog is still not known, many functional homologs have thus far been reported such as, RTEL1, FBH1, RECQL5 and PCNA-associated recombination inhibitor protein (PARI) (Barber *et al.*, 2008; Simandlova *et al.*, 2013; Paliwal *et al.*, 2014; Moldovan *et al.*, 2012). RTEL1 is reported to inhibit recombination in human cells (Barber *et al.*, 2008) and although it is a functional analog of Srs2, it is a member of a different RAD3 helicase family (Srs2 belongs to UvrD helicase family). Additionally, unlike Srs2, RTEL1 dismantles RAD51 from D-loops rather than the presynaptic nucleofilaments (Barber *et al.*, 2008). PARI, on the other hand, unlike other functional homologs, similar to the yeast Srs2 contains a UvrD-like domain, SUMO- and PCNA-interacting domains. In yeast, it is reported that *SRS2* deletion can suppress the DSB repair of HR-deficient *rad57* mutants (Fung *et al.*, 2009), while similarly PARI depletion has been reported to suppress the genomic instability of BRCA2-mutated and FANCJ-mutated cancer cells deficient in HR (Moldovan *et al.*, 2012).

This study on the effect of *srs2* deletion on meiosis can be applied to the higher eukaryotes. As the sequence homolog of Srs2 is not apparent in the genomes of higher eukaryotes, it has thus been suggested that Srs2's role in negatively regulating HR and ensuring genome stability is replaced by several different helicases which work in combination. Srs2's role in meiosis to prevent the DNA damage which appear in minority after the generation of the recombination products may as well be shared amongst the several helicases regulating HR. Currently, RTEL1 appears to be a sound candidate as RTEL1 observes synthetic lethality with BLM (Barber *et al.*, 2008), which is a homolog of Sgs1, whose deletion is also reported to show synthetic lethality with *srs2* (Lee *et al.*, 1999; Wang *et al.*, 2001), while the inviability was found to be associated with the accumulation of toxic HR intermediates as deletion of *rad51* or *rad54* was able to rescue the lethality (Gangloff *et al.*, 2000; Klein 2001). It has also been reported that *Rtel1*$^{-/-}$ null mice have decreased reproducibility and chromosomal abnormalities (Ding *et al.*, 2004). In *C. elegans rtel-1* mutant is reported to observe slightly higher Rad51 foci and thus DSBs (Youds *et al.*, 2010). *C. elegans* RTEL-1 is reported to enforce crossover interference and homeostasis by channeling the extra DSBs, other than those which are processed to be 'obligate'

crossovers (COs), towards the SDSA pathway and thus forming non-crossovers (NCOs) (Youds *et al.*, 2010). It can be hypothesized that these anti-recombinases ensure accurate disassembly of RAD51 from the chromatin after the meiotic DSB repair is complete. Particularly, RTEL1 may prevent RAD51 from localizing excessively at points of breaks after the completion of DMC1-mediated homologous recombination during meiosis, by dislodging RAD51 at the D-loop sites. Studying the effect of knocking down or knocking out RTEL1 in mice or human cells would help to better understand the role of antirecombinases and helicases in the processing of minor DSBs in higher eukaryotic organisms during meiosis.

Figure 1

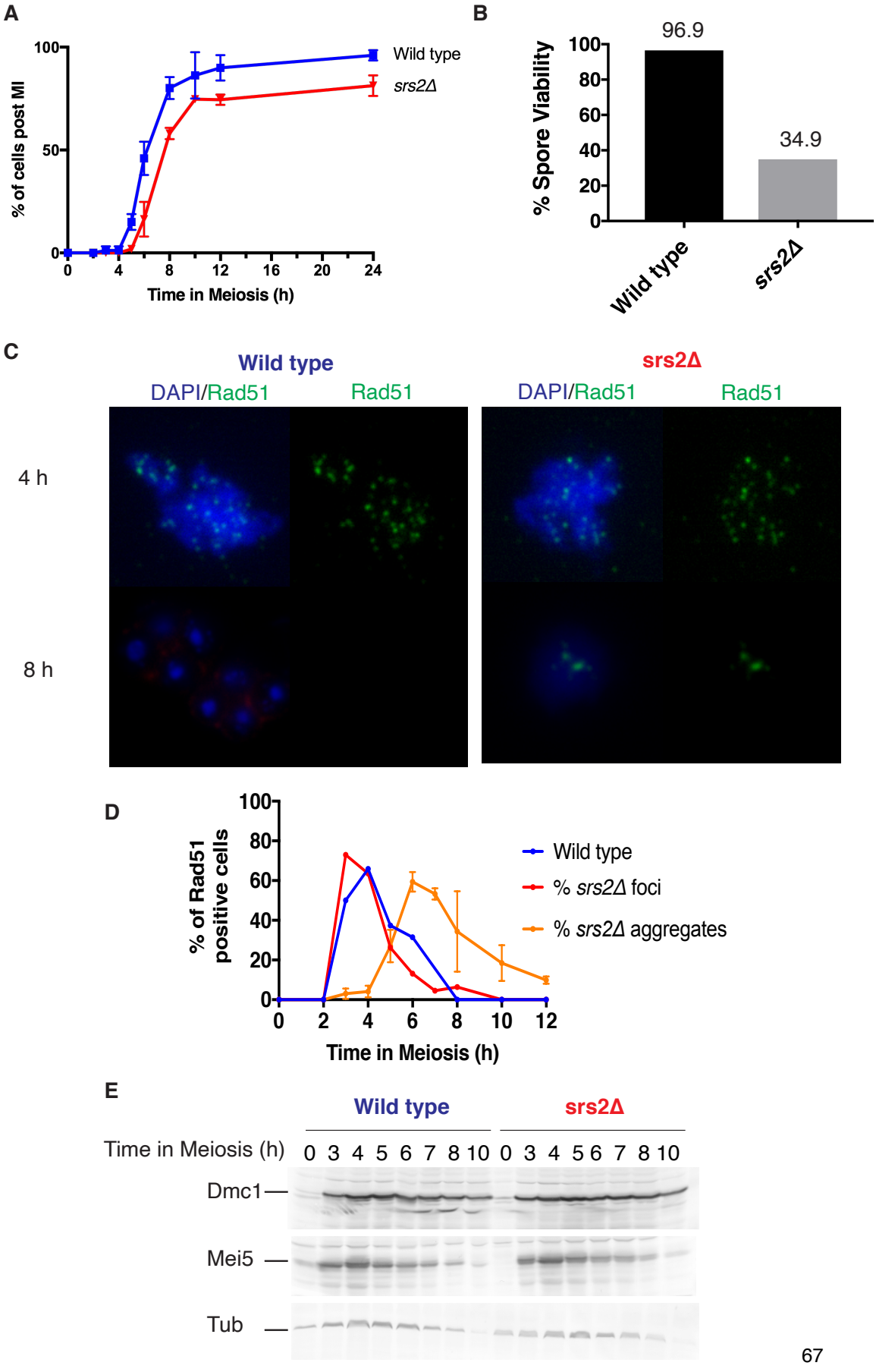
A
% of cells post MI
Time in Meiosis (h)
Wild type
srs2Δ
B
% Spore Viability
96.9
34.9
Wild type
srs2Δ
C
Wild type
srs2Δ
DAPI/Rad51
Rad51
4 h
8 h
D
% of Rad51 positive cells
Time in Meiosis (h)
Wild type
% srs2Δ foci
% srs2Δ aggregates
E
Wild type
srs2Δ
Time in Meiosis (h)
0 3 4 5 6 7 8 10 0 3 4 5 6 7 8 10
Dmc1
Mei5
Tub

Figure 1: Rad51 aggregates form in late time in meiosis in the *srs2*Δ mutant.

A. Meiotic progression of wild type (NKY-1303/1543) and the *srs2Δ* (HYS 13/14) mutant was observed by counting DAPI (DNA dye) stained, 1, 2 or 4, DAPI bodies. More than 200 cells were counted, error bar indicates S.D. p = 0.021, n = 3, unpaired t-test with Welch's correction.

B. Spore viability of wild type (NKY-1303/1543) and the *srs2Δ* (HYS 13/14). More than 100 tetrads were dissected to calculate spore viability.

C. Representative images of chromosome spreads from wild type (NKY-1303/1543) and *srs2Δ* (HYS 13/14) strains, which were stained with anti-Rad51 (green) and DAPI (blue), at 4 h and 8 h. Scale bar indicates 1 μm.

D. Kinetics of chromosome spreads positive for Rad51 foci observed in wild type (NKY-1303/1543) and *srs2Δ* (HYS 13/14) mutant. More than 100 nuclei were counted at each time point in these mutants, error bars indicate S.D, n = 3.

E. Expression of various meiotic proteins was verified by western blotting. At each time point, cells were fixed with TCA and cell lysates were subject to the analysis. Representative western blot images of wild type (NKY1303/1543) and *srs2Δ* (HYS 13/14) are shown. Dmc1, Mei5 and Tubulin (Tub, control) are shown by bars on the left.

Figure 2

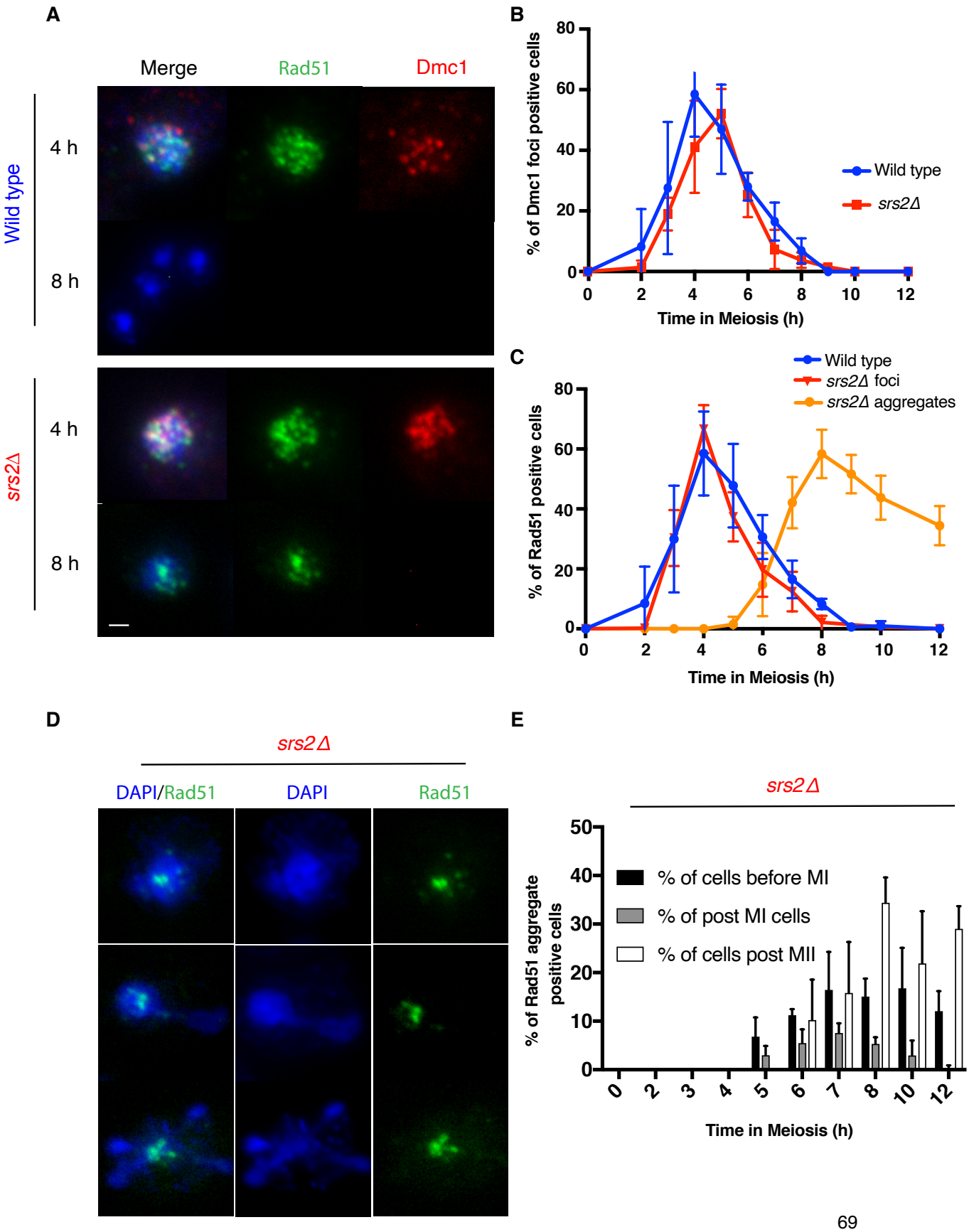
A
Merge
Rad51
Dmc1
Wild type
4 h
8 h
srs2Δ
4 h
8 h
B
% of Dmc1 foci positive cells
Time in Meiosis (h)
Wild type
srs2Δ
C
% of Rad51 positive cells
Time in Meiosis (h)
Wild type
srs2Δ foci
srs2Δ aggregates
D
srs2Δ
DAPI/Rad51
DAPI
Rad51
E
srs2Δ
% of Rad51 aggregate positive cells
Time in Meiosis (h)
% of cells before MI
% of post MI cells
% of cells post MII

Figure 2: Rad51 aggregates formed in late time in meiosis in the *srs2*Δ mutant carries on to the cells undergoing meiosis I and II.

A. Representative images of whole cell from wild type (NKY-1303/1543) and *srs2Δ* (HYS 13/14) strains, which were stained with anti-Dmc1 (red), anti-Rad51 (green) and DAPI (blue), at 4 h and 8 h. Scale bar indicates 1 μm.

B. Kinetics of whole cell positive for Dmc1 foci observed in wild type (NKY-1303/1543) and *srs2Δ* (HYS 13/14) mutant. More than 100 nuclei were counted at each time point in these mutants, error bars indicate S.D.

C. Kinetics of whole cell positive for Rad51 foci observed in wild type (NKY-1303/1543) and Rad51 foci and aggregates observed in the *srs2Δ* (HYS 13/14) mutant. More than 100 nuclei were counted at each time point in these mutants, error bars indicate S.D, n = 3.

D. Representative images of whole cell from *srs2Δ* (HYS 13/14) strains, which were stained with anti-Rad51 (green) and DAPI (blue), at 6 h, undergoing prophase, meiosis I (MI) and meiosis II (MII). Scale bar indicates 1 μm.

E. Distribution of Rad51 aggregate positive cells before meiosis I (MI), post MI and post meiosis II (MII) in the *srs2Δ* (HYS 13/14) strains. More than 100 nuclei were counted at each time point in these mutants, error bars indicate S.D, n = 3.

Figure 3

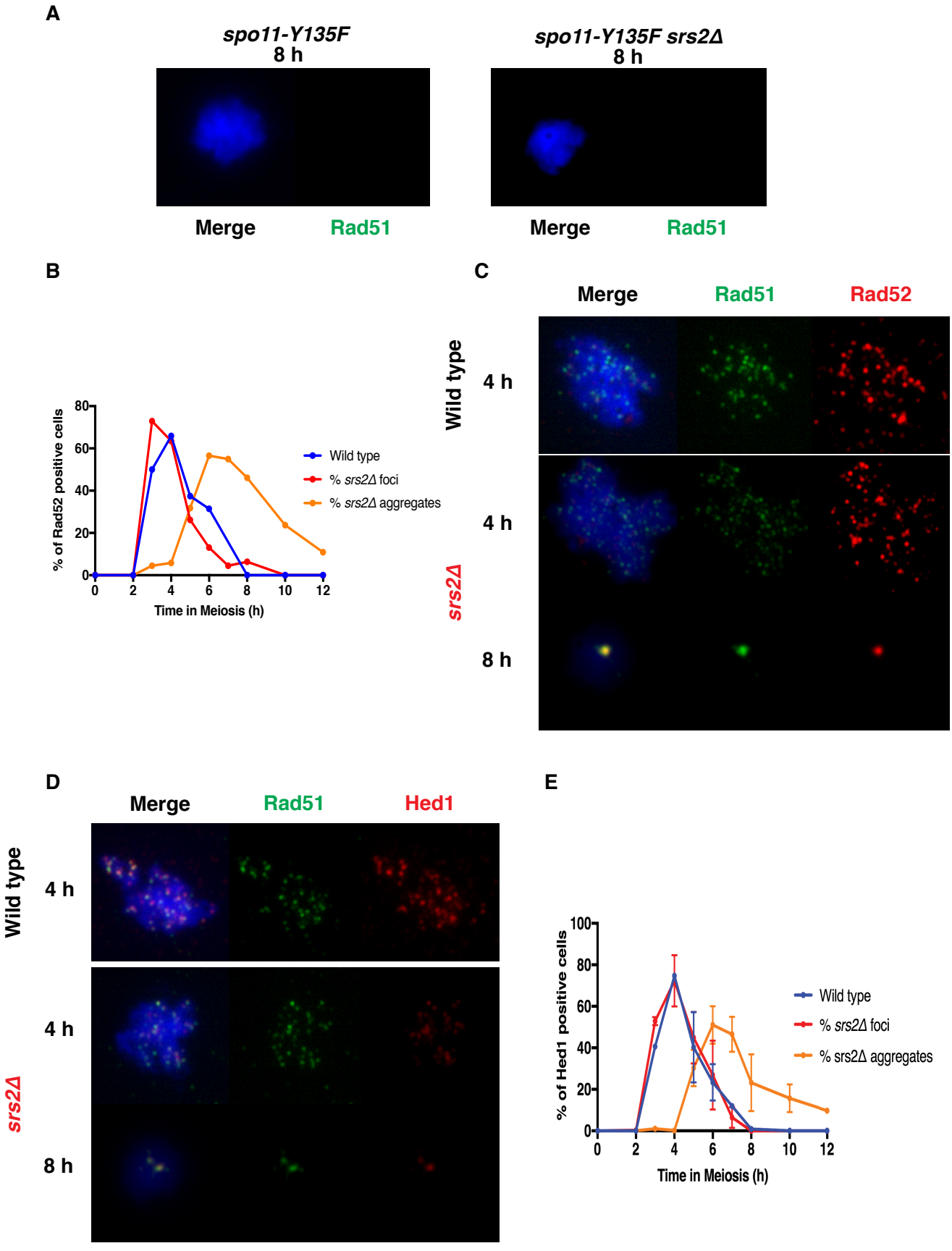
A
spo11-Y135F
8 h
spo11-Y135F srs2Δ
8 h
Merge
Rad51
Merge
Rad51
B
% of Rad52 positive cells
Time in Meiosis (h)
Wild type
% srs2Δ foci
% srs2Δ aggregates
C
Merge
Rad51
Rad52
Wild type
4 h
4 h
srs2Δ
8 h
D
Merge
Rad51
Hed1
Wild type
4 h
4 h
srs2Δ
8 h
E
% of Hed1 positive cells
Time in Meiosis (h)
Wild type
% srs2Δ foci
% srs2Δ aggregates

Figure 3: Rad51 aggregates in the *srs2Δ* mutant is dependent on meiotic DSBs and associates with Rad51 interacting proteins.

A. Representative images of chromosome spreads from *spo11-Y135F* (HYS 92/93) and *spo11-Y135F srs2Δ* (HYS 94/95) strains, which were stained with anti-Rad51 (green) and DAPI (blue), at 8 h. Scale bar indicates 1 μm.

B. Kinetics of chromosome spreads positive for Rad52 observed in wild type (NKY-1303/1543) and *srs2Δ* (HYS 13/14) mutant. More than 100 nuclei were counted at each time point in these mutants, n = 1.

C. Representative images of chromosome spreads from wild type (NKY-1303/1543) and *srs2Δ* (HYS13/14) strains, which were stained with anti-Rad51 (green), anti-Rad52 (red) and DAPI (blue), at 4 h and 8 h. Scale bar indicates 1 μm.

D. Representative images of chromosome spreads from wild type (NKY-1303/1543) and *srs2Δ* (HYS 13/14) strains, which were stained with anti-Rad51 (green), anti-Hed1 (red) and DAPI (blue), at 4 h and 8 h. Scale bar indicates 1 μm.

E. Kinetics of chromosome spreads positive for Hed1 observed in wild type (NKY-1303/1543) and *srs2Δ* (HYS 13/14) mutant. More than 100 nuclei were counted at each time point in these mutants, error bars indicate S.D, n = 3.

Figure 4

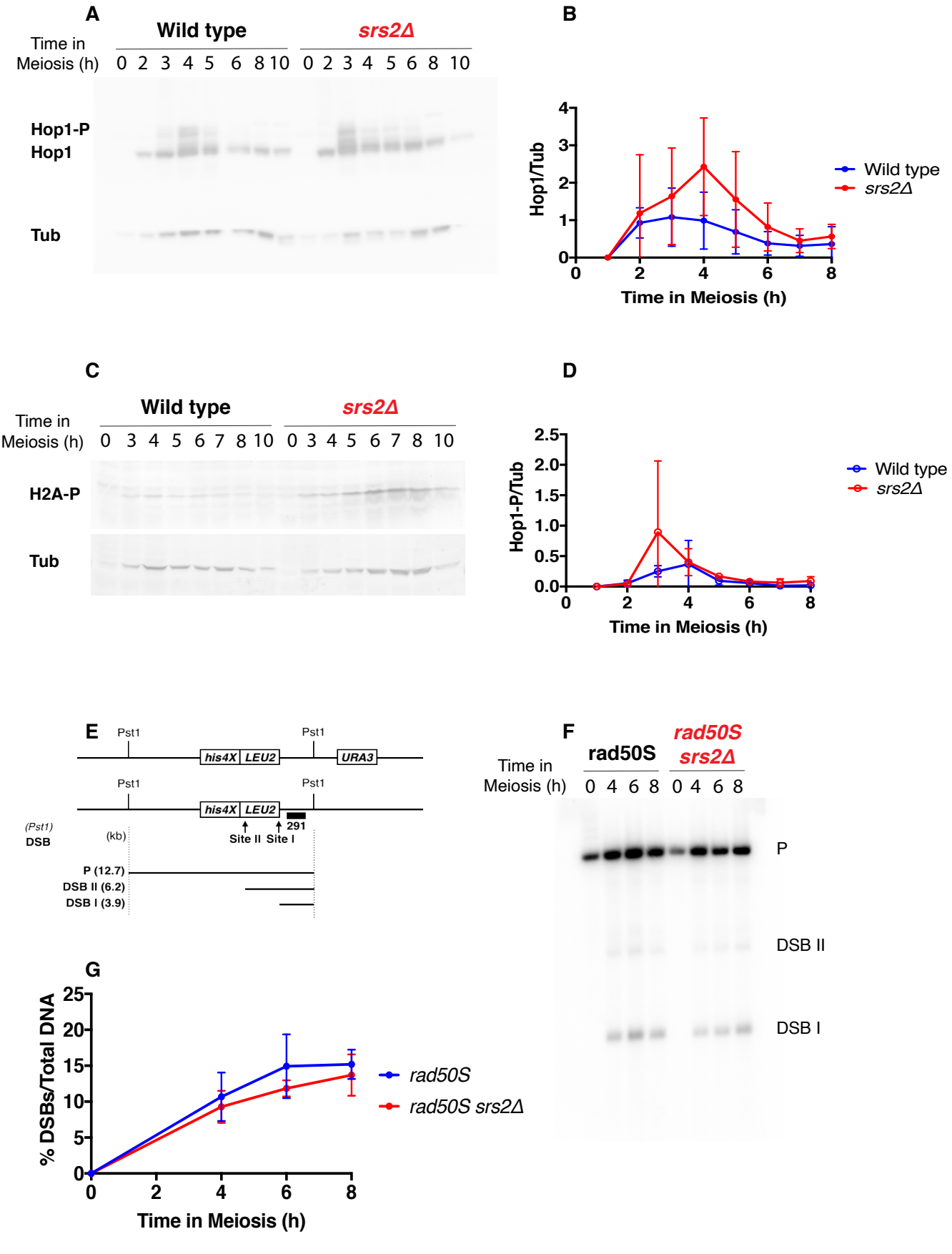
A
Time in Meiosis (h)
Wild type
srs2Δ
0 2 3 4 5 6 8 10 0 2 3 4 5 6 8 10
Hop1-P
Hop1
Tub
B
Hop1/Tub
Time in Meiosis (h)
Wild type
srs2Δ
C
Time in Meiosis (h)
Wild type
srs2Δ
0 3 4 5 6 7 8 10 0 3 4 5 6 7 8 10
H2A-P
Tub
D
Hop1-P/Tub
Time in Meiosis (h)
Wild type
srs2Δ
E
Pst1
his4X
LEU2
URA3
(Pst1)
DSB
(kb)
Site II
Site I
291
P (12.7)
DSB II (6.2)
DSB I (3.9)
F
Time in Meiosis (h)
rad50S
rad50S srs2Δ
0 4 6 8 0 4 6 8
P
DSB II
DSB I
G
% DSBs/Total DNA
Time in Meiosis (h)
rad50S
rad50S srs2Δ

Figure 4: DSB turnover and repair associated checkpoint is not altered in the *srs2Δ* mutant.

A. Expression of various meiotic proteins was verified by western blotting. At each time point, cells were fixed with TCA and cell lysates were subject to the analysis. Representative western blot images of wild type (NKY-1303/1543) and *srs2Δ* (HYS 13/14) are shown. Hop1, phosphorylated Hop1 (Hop1-P) and Tubulin (Tub, control) are indicated on the left.

B Quantification of protein expression for Hop1. The ratio of Hop1 protein to Tubulin was calculated, n = 3, error bars indicate S.D.

C. Expression of various meiotic proteins was verified by western blotting. At each time point, cells were fixed with TCA and cell lysates were subject to the analysis. Representative western blot images of wild type (NKY-1303/1543) and *srs2Δ* (HYS 13/14) are shown. Phosphorylated H2A (H2A-P) and Tubulin (Tub, control) are indicated on the left.

D. Quantification of protein expression for phosphorylated Hop1. The ratio of phosphorylated Hop1 protein to Tubulin was calculated, n = 3, error bars indicate S.D.

E. Schematic representation of the *HIS4-LEU2* locus. Sizes of fragments for DSB (DSB I and DSB II) and parental fragments (P) are shown with lines below.

F. DSB formation and repair at the *HIS4-LEU2* locus in *rad50S* (HYS 197) and *rad50S srs2Δ* (HYS 189/193) were verified by Southern blotting. Genomic DNAs were digested with *Pst*I and analyzed by Southern blotting. A representative image of the blots is shown.

G. Kinetics of % of DSBs over the total DNA. Quantification of total % DSBs (DSB I + DSB II) fragment to a parental fragment was quantified and plotted. The values are the mean values, error bar indicates S.D, n = 3.

Figure 5

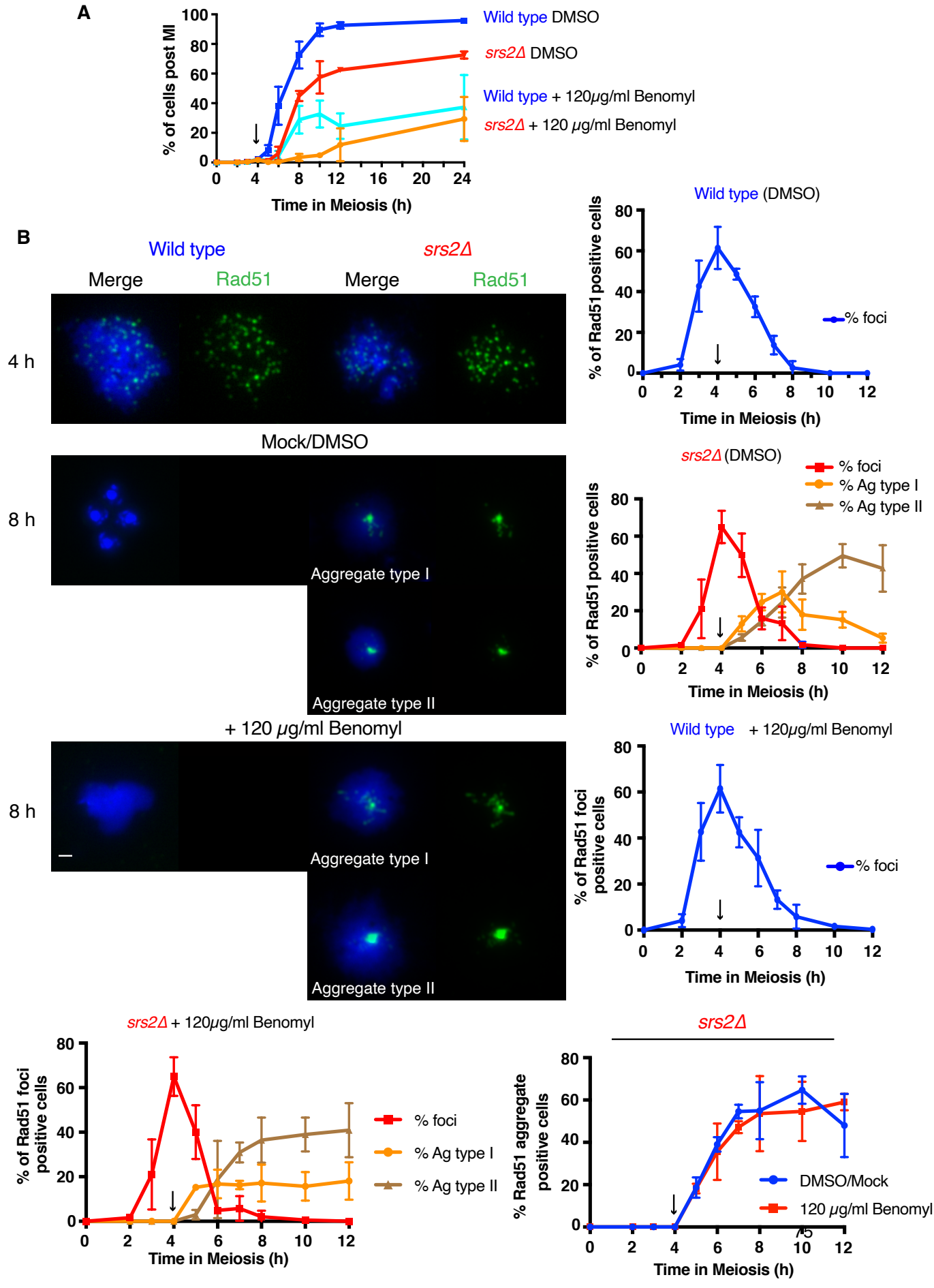
A
% of cells post MI
Time in Meiosis (h)
Wild type DMSO
srs2Δ DMSO
Wild type + 120μg/ml Benomyl
srs2Δ + 120 μg/ml Benomyl
B
Wild type
srs2Δ
Merge
Rad51
4 h
Mock/DMSO
8 h
Aggregate type I
Aggregate type II
+ 120 μg/ml Benomyl
Wild type (DMSO)
% of Rad51 positive cells
% foci
srs2Δ (DMSO)
% Ag type I
% Ag type II
Wild type + 120μg/ml Benomyl
% of Rad51 foci positive cells
srs2Δ + 120μg/ml Benomyl
srs2Δ
% Rad51 aggregate positive cells
DMSO/Mock
120 μg/ml Benomyl

Figure 5: Chromosome tension by microtubules does not contribute to the formation of Rad51 aggregates in the *srs2Δ* mutant.

A. Meiotic progression of wild type (NKY-1303/1543) and *srs2Δ* (HYS 13/14) mutant was observed by counting DAPI (DNA dye) stained, 1, 2 or 4, DAPI bodies. DMSO or 120 µg/ml Benomyl was added at 4 h indicated by arrow. More than 200 cells were counted, error bars indicate S.D, n = 3.

B. Representative images of nuclear spreads from wild type (NKY-1303/1543) and *srs2Δ* (HYS 13/14) strains, which were stained with anti-Rad51 (green) and DAPI (blue), at 4 h. DMSO or 120 µg/ml Benomyl was added at 4 h indicated by arrow. Scale bar indicates 1 µm.

C. Kinetics of nuclear spreads positive for Rad51 foci observed in wild type (NKY-1303/1543), DMSO was added at 4 h indicated by arrow. More than 100 nuclei were counted at each time point in these mutants, error bars indicate S.D, n = 3.

D. Kinetics of nuclear spreads positive for Rad51 foci and aggregates type I and type II observed in *srs2Δ* (HYS 13/14) mutant. DMSO was added at 4 h indicated by arrow. More than 100 nuclei were counted at each time point in these mutants, error bars indicate S.D.

E. Kinetics of nuclear spreads positive for Rad51 foci observed in wild type (NKY-1303/1543). 120 µg/ml Benomyl was added at 4 h indicated by arrow. More than 100 nuclei were counted at each time point in these mutants, error bars indicate S.D, n = 3.

F. Kinetics of nuclear spreads positive for Rad51 aggregates type I and type II observed in *srs2Δ* (HYS 13/14) mutant. 120 µg/ml Benomyl was added at 4 h indicated by arrow. More than 100 nuclei were counted at each time point in these mutants, error bars indicate S.D, n = 3.

G. Kinetics of nuclear spreads positive for both Rad51 aggregates type I and type II observed in *srs2Δ* (HYS 13/14) mutant. DMSO (0.2%) or 120 µg/ml Benomyl was added at 4 h indicated by arrow. More than 100 nuclei were counted at each time point in these mutants, error bars indicate S.D, n = 3.

Figure 6

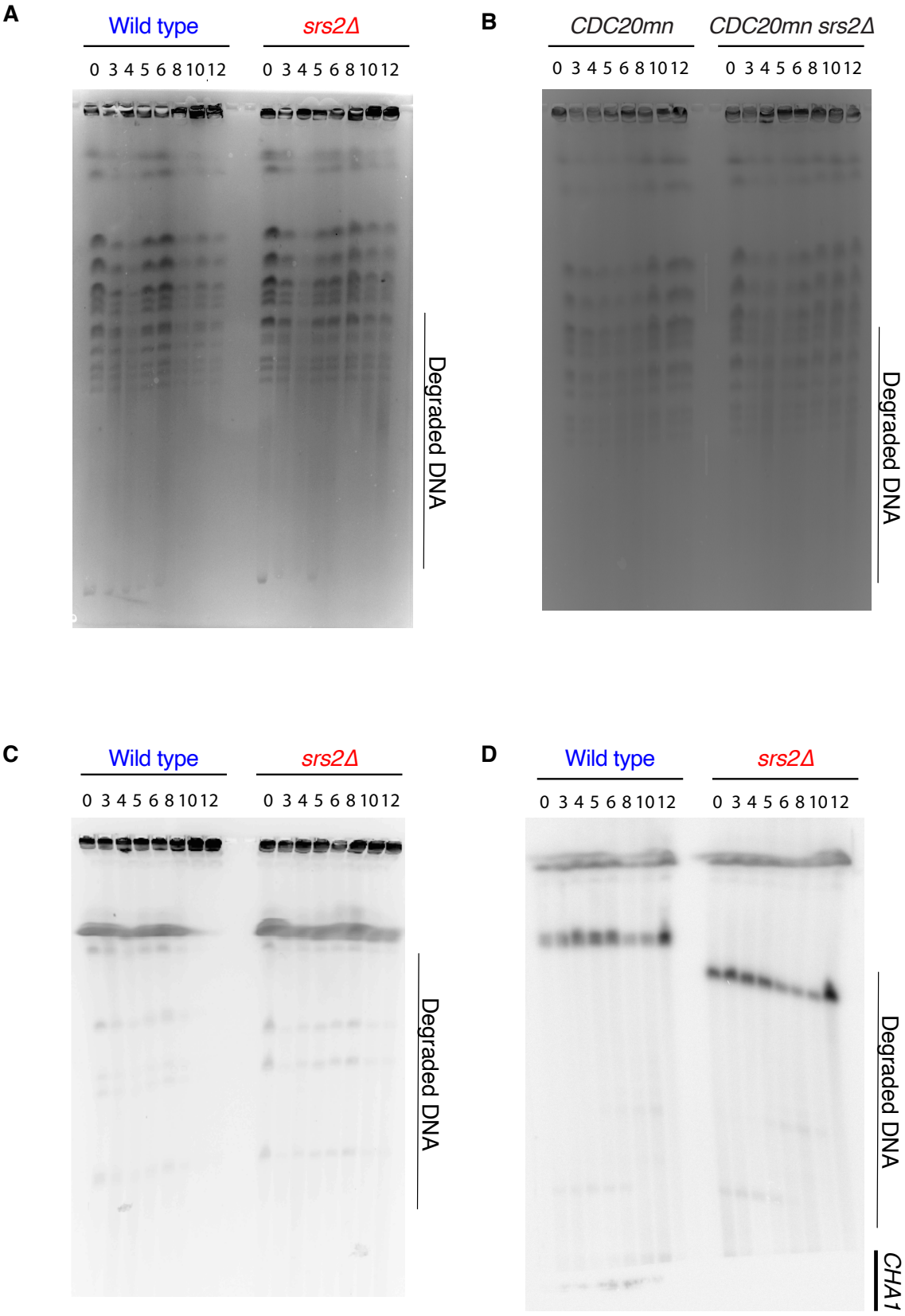
A
Wild type
srs2Δ
0 3 4 5 6 8 10 12
0 3 4 5 6 8 10 12
Degraded DNA
B
CDC20mn
CDC20mn srs2Δ
0 3 4 5 6 8 10 12
0 3 4 5 6 8 10 12
Degraded DNA
C
Wild type
srs2Δ
0 3 4 5 6 8 10 12
0 3 4 5 6 8 10 12
Degraded DNA
D
Wild type
srs2Δ
0 3 4 5 6 8 10 12
0 3 4 5 6 8 10 12
Degraded DNA
CHA1

Figure 6: *srs2Δ* mutant observes accumulation of DNA damage at late time in meiosis.

A. A representative image of CHEF electrophoresis analysis for all chromosome detection of wild type (NKY-1303/1543) and *srs2Δ* (HYS 13/14) mutant. Stained with ethidium bromide (0.5 μg/ml).

B. A representative image of CHEF electrophoresis analysis for all chromosome detection of *CDC20mn* (HYS 45/46) and *CDC20mn srs2Δ* (HYS 47/48) mutant. Stained with ethidium bromide (0.5 μg/ml).

C. A representative image of CHEF electrophoresis analysis for short chromosome detection of wild type (NKY-1303/1543) and *srs2Δ* (HYS 13/14) mutant. Stained with ethidium bromide (0.5 μg/ml).

D. Replication status at chromosome III (*CHA1*) in wild type (HYS26/27) and *srs2Δ* (HYS13/14) was verified by Southern blotting. A representative image of the blots is shown.

Figure 7

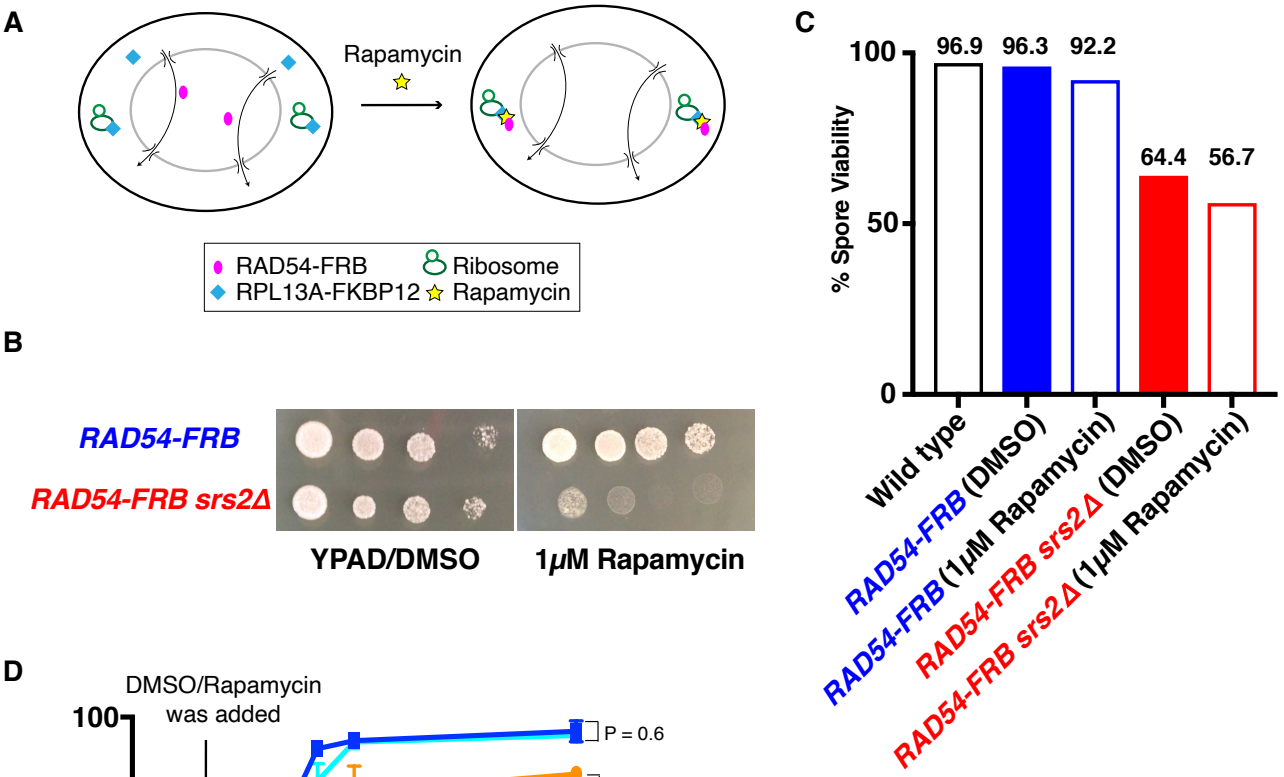
A
Rapamycin
RAD54-FRB
RPL13A-FKBP12
Ribosome
Rapamycin
B
RAD54-FRB
RAD54-FRB srs2Δ
YPAD/DMSO
1μM Rapamycin
C
% Spore Viability
100
50
0
96.9
96.3
92.2
64.4
56.7
Wild type
RAD54-FRB (DMSO)
RAD54-FRB (1μM Rapamycin)
RAD54-FRB srs2Δ (DMSO)
RAD54-FRB srs2Δ (1μM Rapamycin)

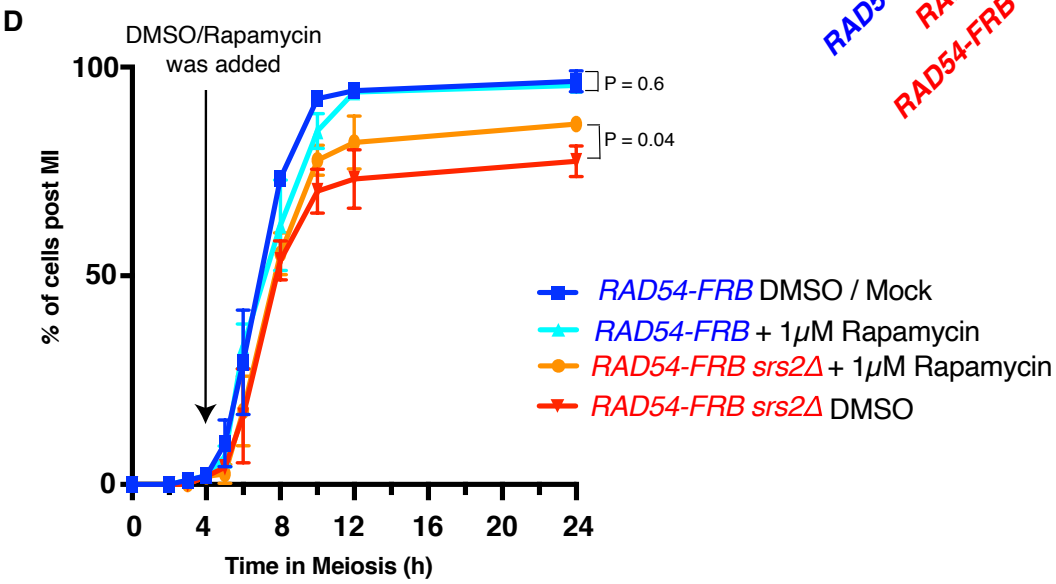
D
DMSO/Rapamycin
was added
% of cells post MI
100
50
0
0
4
8
12
16
20
24
Time in Meiosis (h)
P = 0.6
P = 0.04
RAD54-FRB DMSO / Mock
RAD54-FRB + 1μM Rapamycin
RAD54-FRB srs2Δ + 1μM Rapamycin
RAD54-FRB srs2Δ DMSO

Figure 7: *RAD54-FRB* is a conditional mutant.

A. Diagrammatic representation of conditional nuclear depletion and inactivation by the anchor away technique (adapted from Haruki *et al.*, 2008 Figure 1).

B. Drug dilution assay for haploid *RAD54-FRB* (H7791) and *RAD54-FRB srs2Δ* (HYS 71) in the presence of 1 μM Rapamycin and DMSO (control).

C. Spore viability of *RAD54-FRB* (H7790/7791) and *RAD54-FRB srs2Δ* (HYS 71/82). 0.2 % DMSO or 1 μM Rapamycin was added at 4 h. 100 tetrads were dissected and the spore viability was calculated.

D. Meiotic progression of *RAD54-FRB* (H7790/7791) and *RAD54-FRB srs2Δ* (HYS 71/82). 0.2 % DMSO or 1 μM Rapamycin was added at 4 h indicated by arrow. More than 200 cells were counted, error bar indicates S.D, n = 3, indicated p-value calculated with unpaired t-test with Welch's correction.

Figure 8

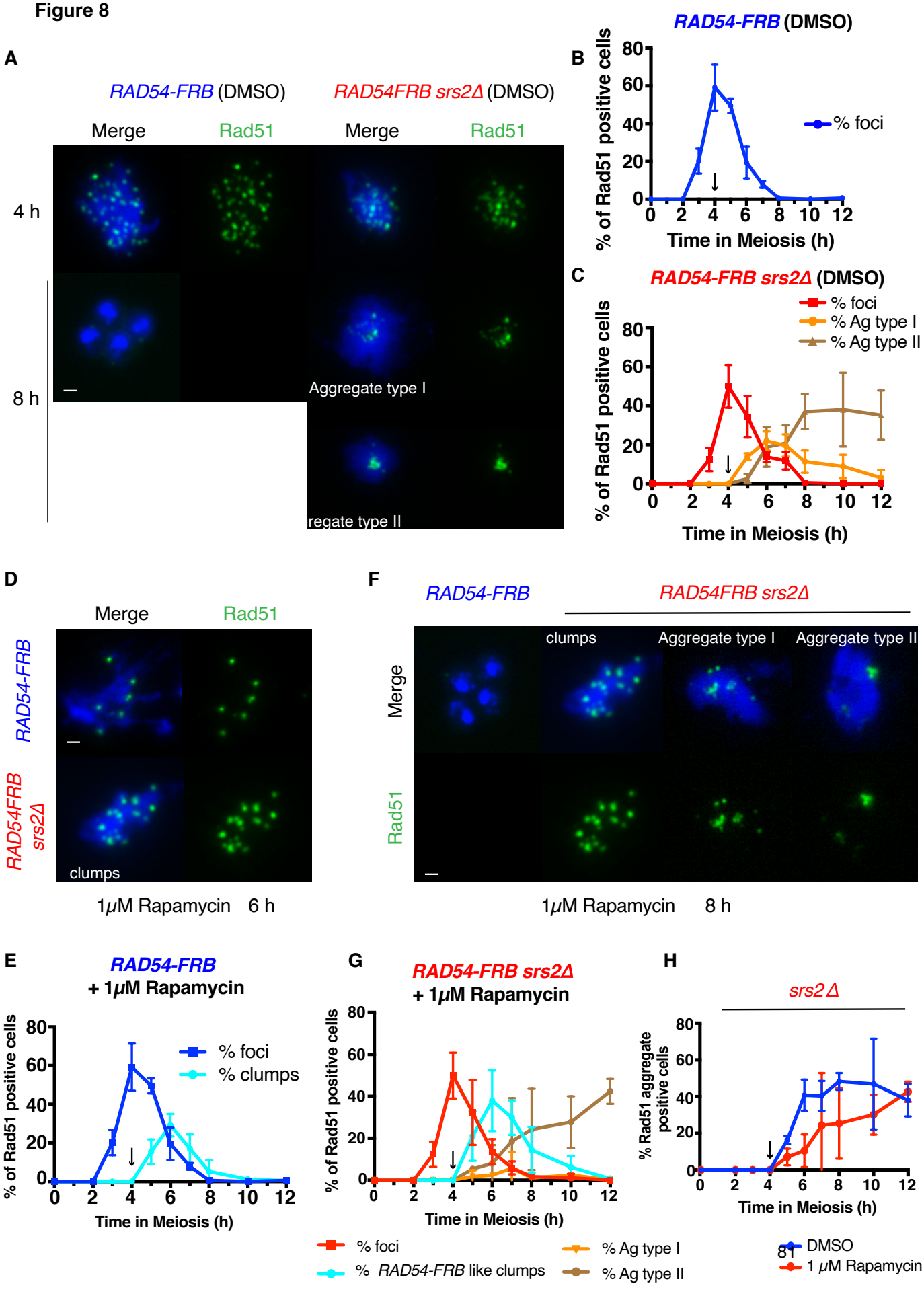
A
RAD54-FRB (DMSO)
RAD54FRB srs2Δ (DMSO)
Merge
Rad51
Merge
Rad51
4 h
8 h
Aggregate type I
regate type II
B
RAD54-FRB (DMSO)
% of Rad51 positive cells
% foci
Time in Meiosis (h)
C
RAD54-FRB srs2Δ (DMSO)
% foci
% Ag type I
% Ag type II
% of Rad51 positive cells
Time in Meiosis (h)
D
Merge
Rad51
RAD54-FRB
RAD54FRB srs2Δ
clumps
1μM Rapamycin 6 h
F
RAD54-FRB
RAD54FRB srs2Δ
clumps
Aggregate type I
Aggregate type II
Merge
Rad51
1μM Rapamycin 8 h
E
RAD54-FRB
+ 1μM Rapamycin
% of Rad51 positive cells
% foci
% clumps
Time in Meiosis (h)
G
RAD54-FRB srs2Δ
+ 1μM Rapamycin
% of Rad51 positive cells
Time in Meiosis (h)
H
srs2Δ
% Rad51 aggregate positive cells
Time in Meiosis (h)
% foci
% RAD54-FRB like clumps
% Ag type I
% Ag type II
DMSO
1 μM Rapamycin

Figure 8: Rad54 depletion decreases aggregates in the *srs2Δ* mutant.

A. Representative images of nuclear spreads from *RAD54-FRB* (H7790/7791) and *RAD54-FRB srs2Δ* (HYS 71/82) strains, which were stained with anti-Rad51 (green) and DAPI (blue), at 4 h and 8 h. DMSO was added at 4 h. Scale bar indicates 1 μm.

B. Kinetics of nuclear spreads positive for Rad51 foci observed in *RAD54-FRB* (H7790/7791). DMSO was added at 4 h indicated by arrow. More than 100 nuclei were counted at each time point in these mutants, error bars indicate S.D, n = 3.

C. Kinetics of nuclear spreads positive for Rad51 foci and aggregates type I and type II observed in *RAD54-FRB srs2Δ* (HYS 71/82) mutant. DMSO was added at 4 h indicated by arrow. More than 100 nuclei were counted at each time point in these mutants, error bars indicate S.D, n = 3.

D. Representative images for Rad51 clumps observed in nuclear spreads from *RAD54-FRB* (H7790/7791) and *RAD54-FRB srs2Δ* (HYS 71/82), which were stained with anti-Rad51 (green) and DAPI (blue), at 6 h. 1 μM Rapamycin was added at 4 h. Scale bar indicates 1 μm.

E. Kinetics of nuclear spreads positive for Rad51 foci and clumps observed in *RAD54-FRB* (H7790/7791). 1 μM Rapamycin was added at 4 h indicated by arrow. More than 100 nuclei were counted at each time point in these mutants, error bars indicate S.D, n = 3.

F. Representative images of nuclear spreads from *RAD54-FRB* (H7790/7791) and *RAD54-FRB srs2Δ* (HYS 71/82), which were stained with anti-Rad51 (green) and DAPI (blue), at 8 h. 1 μM Rapamycin was added at 4 h. Scale bar indicates 1 μm.

G. Kinetics of nuclear spreads positive for Rad51 foci and aggregates observed in *RAD54-FRB srs2Δ* (HYS 71/82). 1 μM Rapamycin was added at 4 h indicated by arrow. More than 100 nuclei were counted at each time point in these mutants, error bars indicate S.D, n = 3.

H. Kinetics of nuclear spreads positive for both Rad51 aggregates type I and type II observed in *RAD54-FRB srs2Δ* (HYS 71/82) mutant. 0.2 % DMSO or 1 μM Rapamycin was added at 4 h indicated by arrow. More than 100 nuclei were counted at each time point in these mutants, error bars indicate S.D, n = 3.

Figure 9

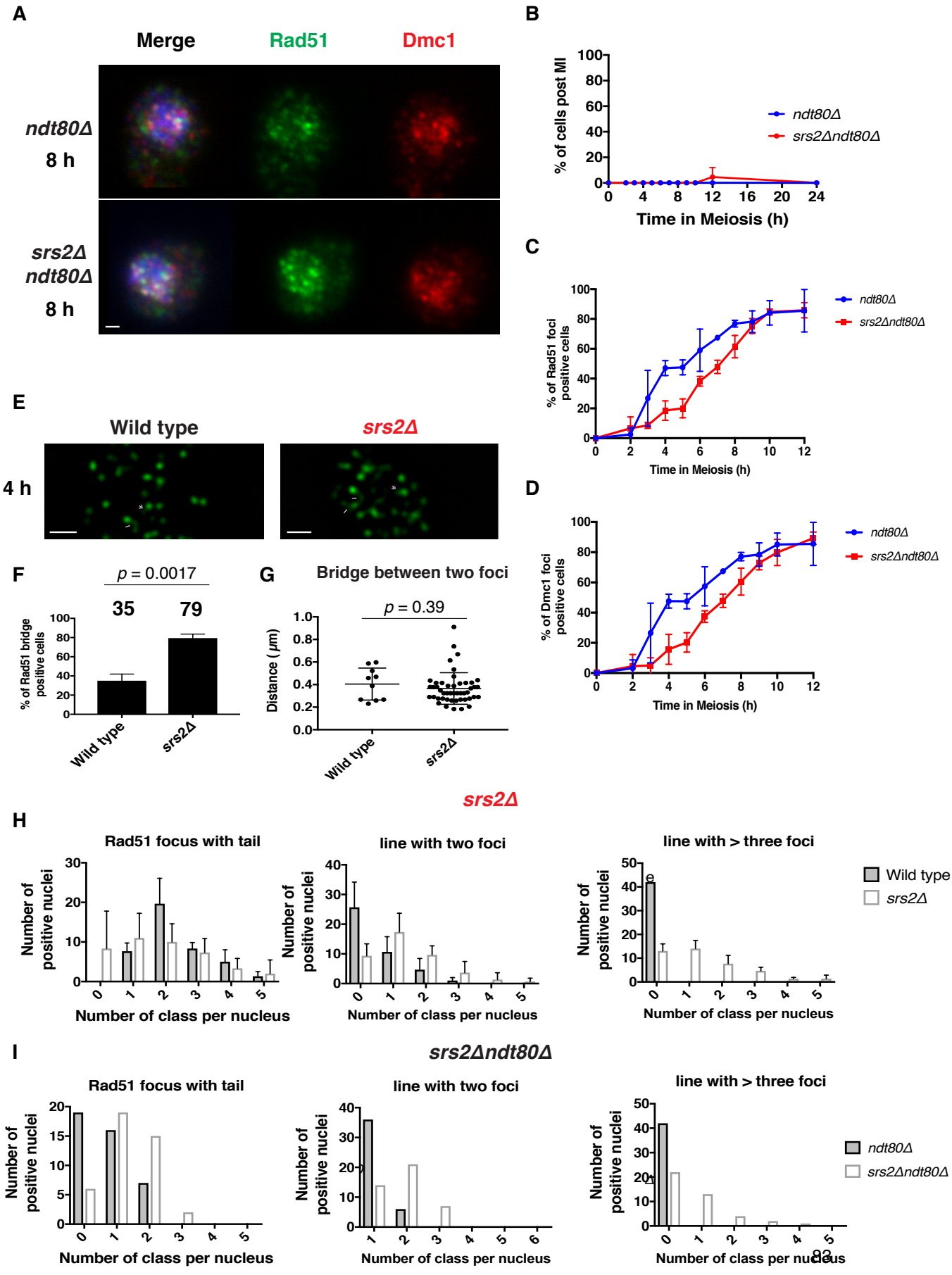
A
Merge
Rad51
Dmc1
ndt80Δ
8 h
srs2Δ
ndt80Δ
8 h
B
% of cells post MI
Time in Meiosis (h)
ndt80Δ
srs2Δndt80Δ
C
% of Rad51 foci positive cells
Time in Meiosis (h)
ndt80Δ
srs2Δndt80Δ
D
% of Dmc1 foci positive cells
Time in Meiosis (h)
ndt80Δ
srs2Δndt80Δ
E
Wild type
srs2Δ
4 h
F
p = 0.0017
35
79
% of Rad51 bridge positive cells
Wild type
srs2Δ
G
Bridge between two foci
p = 0.39
Distance (μm)
Wild type
srs2Δ
srs2Δ
H
Rad51 focus with tail
line with two foci
line with > three foci
Number of positive nuclei
Number of class per nucleus
Wild type
srs2Δ
srs2Δndt80Δ
I
Rad51 focus with tail
line with two foci
line with > three foci
Number of positive nuclei
Number of class per nucleus
ndt80Δ
srs2Δndt80Δ

Figure 9: Rad51 aggregates formation in *srs2Δ* is dependent on the mid-pachytene exit and loss of Srs2 results in Rad51 loading defect in early prophase.

A. Representative images of nuclear spreads from *ndt80Δ* (HYS 20/23) and *srs2Δ ndt80Δ* (HYS 18/19), which were stained with anti-Rad51 (green) and DAPI (blue), at 8 h. Scale bar indicates 1 μm.

B. Meiotic progression of *ndt80Δ* (HYS 20/23) and *srs2Δ ndt80Δ* (HYS 18/19). More than 200 cells were counted, error bar indicates S.D, n = 3

C. Kinetics of nuclear spreads positive for Rad51 observed in *ndt80Δ* (HYS 20/23) and *srs2Δ ndt80Δ* (HYS 18/19). More than 100 nuclei were counted at each time point in these mutants, error bars indicate S.D, n = 3.

D. Kinetics of nuclear spreads positive for Dmc1 observed in *ndt80Δ* (HYS 20/23) and *srs2Δ ndt80Δ* (HYS 18/19). More than 100 nuclei were counted at each time point in these mutants, error bars indicate S.D, n = 3.

E. Representative images of chromosome spreads from wild type (NKY-1303/1543) and *srs2Δ* (HYS 13/14) strains, which were stained with anti-Rad51 (green) at 4 h. Rad51 tail and bridge are indicated with double headed and single headed arrows respectively. Scale bar indicates 1 μm.

F. Distribution of percentage of nuclei positive for Rad51 bridge phenotype observed in wild type (NKY-1303/1543) and *srs2Δ* (HYS 13/14). More than 100 nuclei were counted at each time point in these mutants, error bars indicate S.D, n = 3, indicated p-value calculated with unpaired t-test with Welch's correction.

G. Length of Rad51 bridge between two Rad51 foci in wild type (NKY-1303/1543) and *srs2Δ* (HYS 13/14). Indicated p-value was calculated with Mann Whitney U test.

H. Distribution of Rad51 focus with tail, line with two foci (=Rad51 bridge between two foci), line with > three foci (= Rad51 bridge between more than 3 foci) in wild type (NKY-1303/1543) and *srs2Δ* (HYS 13/14) strain. 42 nuclei were counted, error bars indicate S.D, n = 3.

I. Distribution of Rad51 focus with tail, line with two foci (=Rad51 bridge between two foci), line with > three foci (= Rad51 bridge between more than 3 foci) in *ndt80Δ* (HYS 20/23) and *srs2Δ ndt80Δ* (HYS 18/19) strains. 42 nuclei were counted, n = 1.

Figure 10

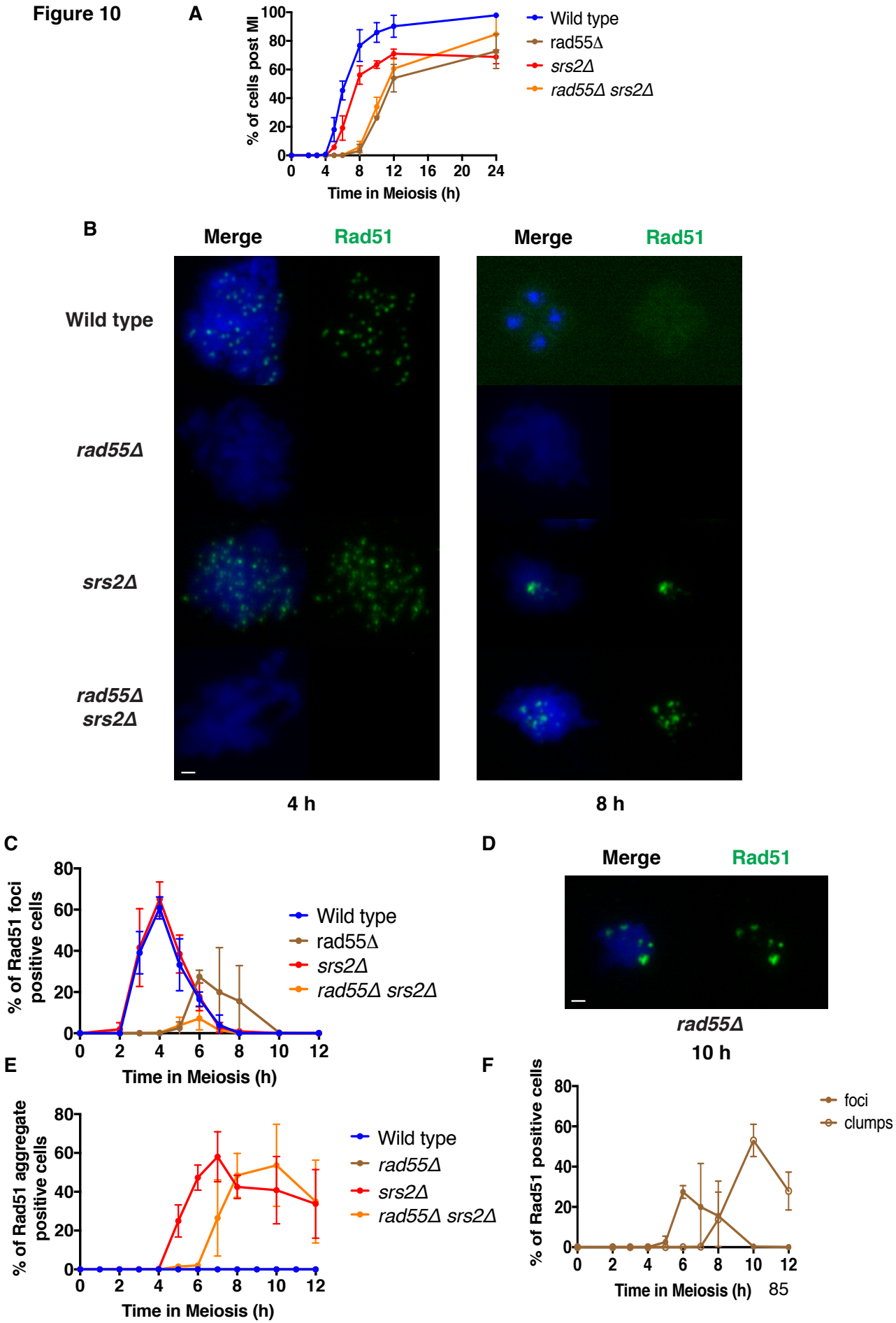
A
% of cells post MI
Time in Meiosis (h)
Wild type
rad55Δ
srs2Δ
rad55Δ srs2Δ
B
Merge
Rad51
Wild type
rad55Δ
srs2Δ
rad55Δ srs2Δ
4 h
8 h
C
% of Rad51 foci positive cells
Time in Meiosis (h)
D
rad55Δ
10 h
E
% of Rad51 aggregate positive cells
F
% of Rad51 positive cells
foci
clumps

Figure 10: Rad51 aggregate formation is not dependent of Rad55/57-mediated Rad51 assembly.

A. Meiotic progression of wild type (NKY-1303/1543), *rad55Δ* (HYS 102/103), *srs2Δ* (HYS 13/14) and *rad55Δ srs2Δ* (HYS 161/165). More than 200 cells were counted, error bar indicates S.D, n = 3

B. Representative images of nuclear spreads from wild type (NKY-1303/1543), *rad55Δ* (HYS 102/103), *srs2Δ* (HYS 13/14) and *rad55Δ srs2Δ* (HYS 161/165), which were stained with anti-Rad51 (green) and DAPI (blue), at 4 h and 8 h. Scale bar indicates 1 μm.

C. Kinetics of nuclear spreads positive for Rad51 foci observed in wild type (NKY-1303/1543), *rad55Δ* (HYS 102/103), *srs2Δ* (HYS 13/14) and *rad55Δ srs2Δ* (HYS 161/165). More than 100 nuclei were counted at each time point in these mutants, error bars indicate S.D, n = 3.

D. Representative images of nuclear spreads from *rad55Δ* (HYS 102/103), which were stained with anti-Rad51 (green) and DAPI (blue), at 10 h. Scale bar indicates 1 μm.

E. Kinetics of nuclear spreads positive for Rad51 aggregates observed in wild type (NKY-1303/1543), *rad55Δ* (HYS 102/103), *srs2Δ* (HYS 13/14) and *rad55Δ srs2Δ* (HYS 161/165). More than 100 nuclei were counted at each time point in these mutants, error bars indicate S.D, n = 3.

F. Kinetics of nuclear spreads positive for Rad51 observed in *rad55Δ* (HYS 102/103). More than 100 nuclei were counted at each time point in these mutants, error bars indicate S.D, n = 3.

Figure 11

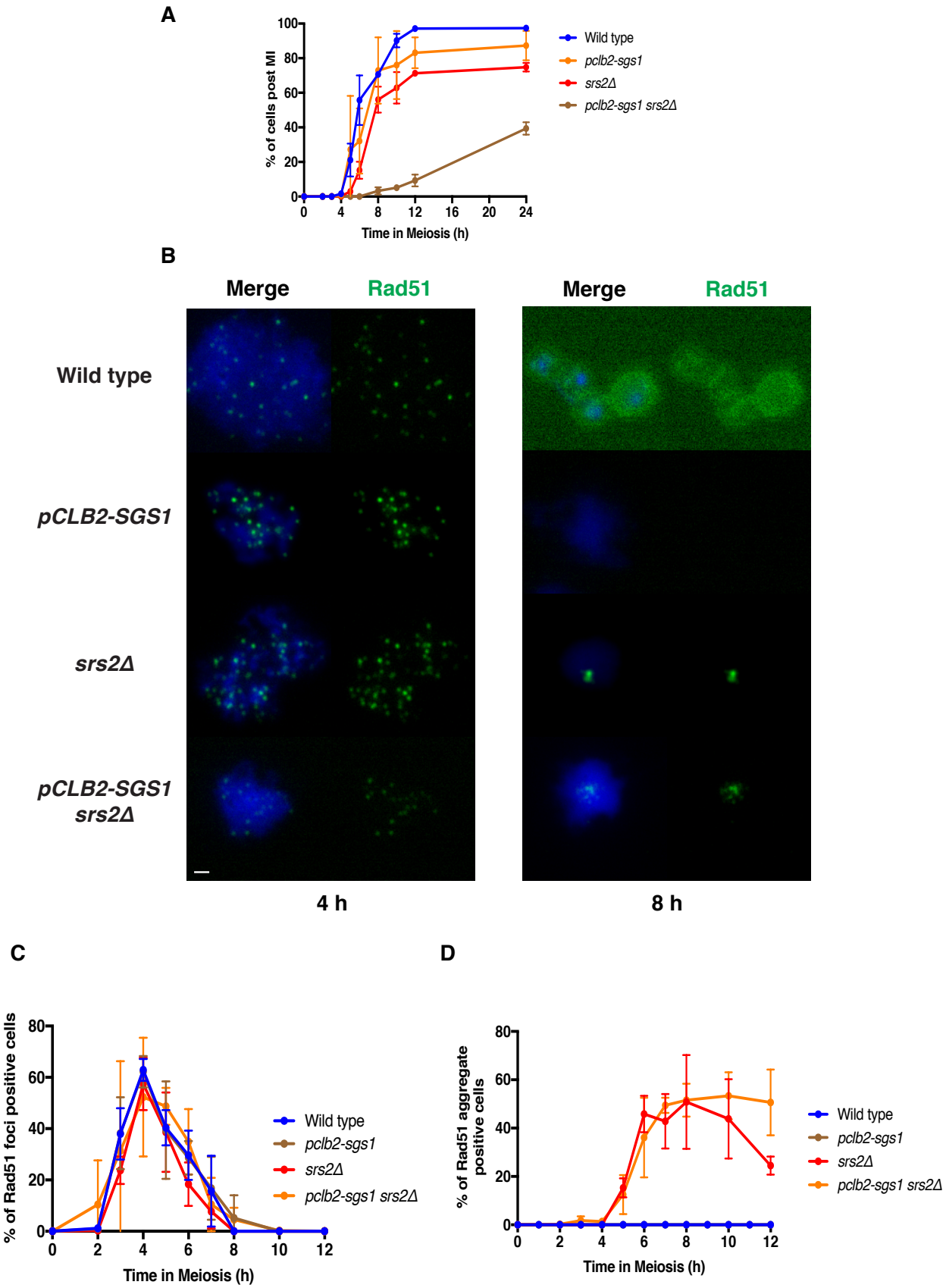
A
% of cells post MI
Time in Meiosis (h)
Wild type
pclb2-sgs1
srs2Δ
pclb2-sgs1 srs2Δ
B
Merge
Rad51
Wild type
pCLB2-SGS1
srs2Δ
pCLB2-SGS1
srs2Δ
4 h
8 h
C
% of Rad51 foci positive cells
Time in Meiosis (h)
D
% of Rad51 aggregate positive cells
Time in Meiosis (h)

Figure 11: Dissolution by Sgs1 is not associated with the formation of Rad51 aggregate in the absence of Srs2.

A. Meiotic progression of wild type (NKY-1303/1543), *pCLB2-SGS1* (HYS 100/101), *srs2Δ* (HYS 13/14) and *pCLB2-SGS1 srs2Δ* (HYS 124/122). More than 200 cells were counted, error bar indicates S.D, n = 3

B. Representative images of nuclear spreads from wild type (NKY-1303/1543), *pCLB2-SGS1* (HYS 100/101), *srs2Δ* (HYS 13/14) and *pCLB2-SGS1 srs2Δ* (HYS 124/122), which were stained with anti-Rad51 (green) and DAPI (blue), at 4 h and 8 h. Scale bar indicates 1 μm.

C. Kinetics of nuclear spreads positive for Rad51 foci observed in wild type (NKY-1303/1543), *pCLB2-SGS1* (HYS 100/101), *srs2Δ* (HYS 13/14) and *pCLB2-SGS1 srs2Δ* (HYS 124/122), More than 100 nuclei were counted at each time point in these mutants, error bars indicate S.D, n = 3.

D. Kinetics of nuclear spreads positive for Rad51 aggregates observed in wild type (NKY-1303/1543), *pCLB2-SGS1* (HYS 100/101), *srs2Δ* (HYS 13/14) and *pCLB2-SGS1 srs2Δ* (HYS 124/122). More than 100 nuclei were counted at each time point in these mutants, error bars indicate S.D, n = 3.

Figure 12

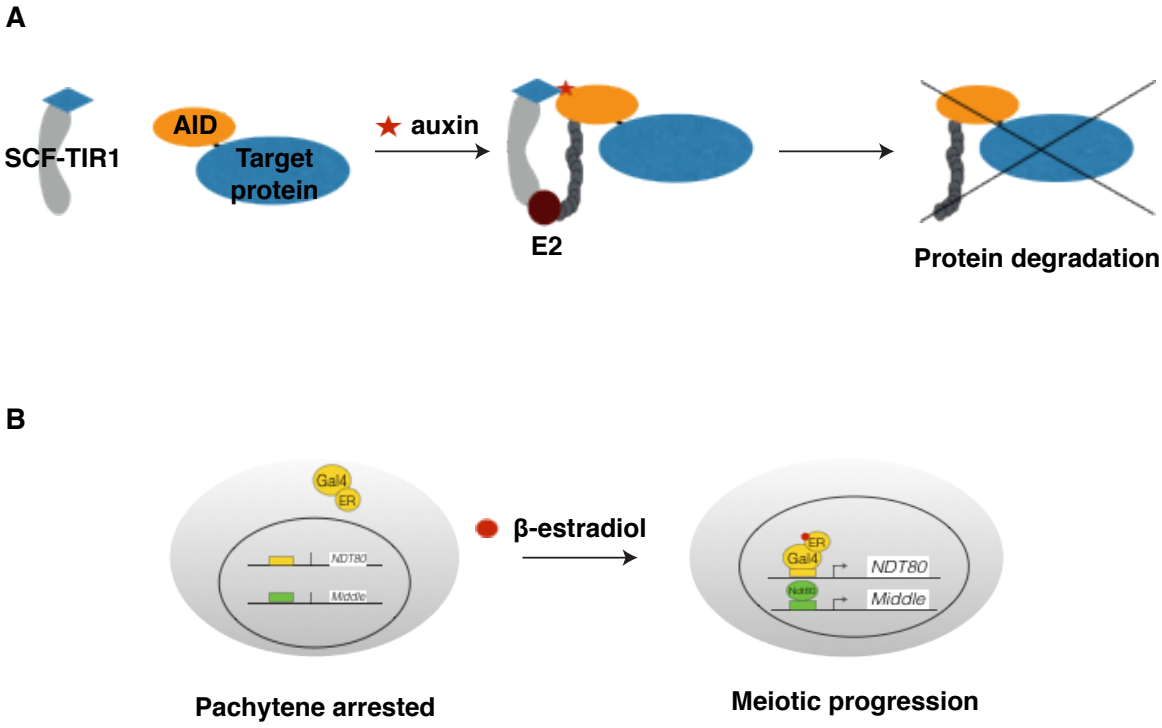
A
SCF-TIR1
AID
Target protein
auxin
E2
Protein degradation
B
Gal4
ER
NDT80
Middle
β-estradiol
Pachytene arrested
Meiotic progression

Figure 12: Degradable SRS2 and inducible Ndt80 system.

A. Diagrammatic representation of conditional protein degradation by the Auxin induced degron (AID) system (adapted from Nishimura *et al.*, 2009, Figure 1).

B Diagrammatic representation of conditional pachytene cell arrest by inducible Ndt80 protein expression by GAL promoter-estradiol system (adapted from Carlile and Amon, 2008, Figure 1A).

Figure 13

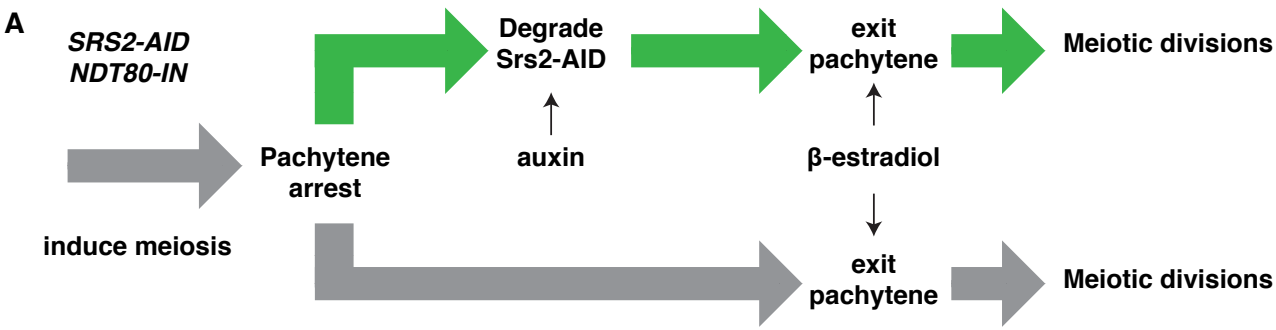
A
SRS2-AID
NDT80-IN
induce meiosis
Pachytene
arrest
Degrade
Srs2-AID
auxin
exit
pachytene
β-estradiol
Meiotic divisions
exit
pachytene
Meiotic divisions

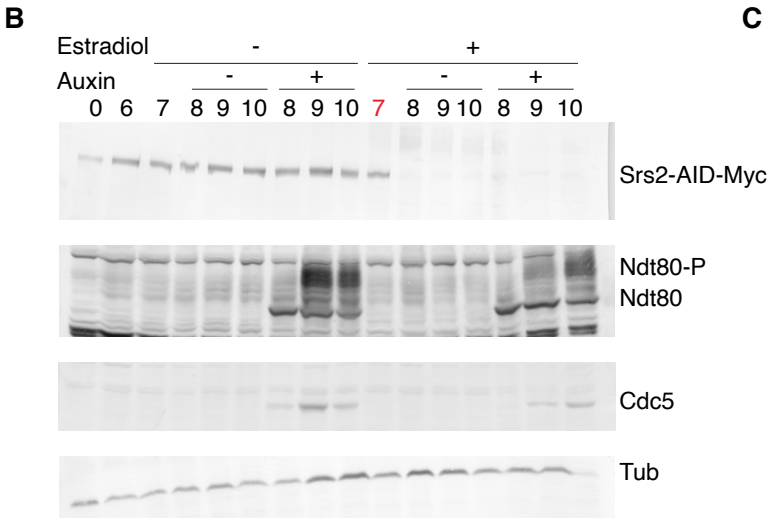
B
Estradiol - +
Auxin - + - +
0 6 7 8 9 10 8 9 10 7 8 9 10 8 9 10
Srs2-AID-Myc
Ndt80-P
Ndt80
Cdc5
Tub

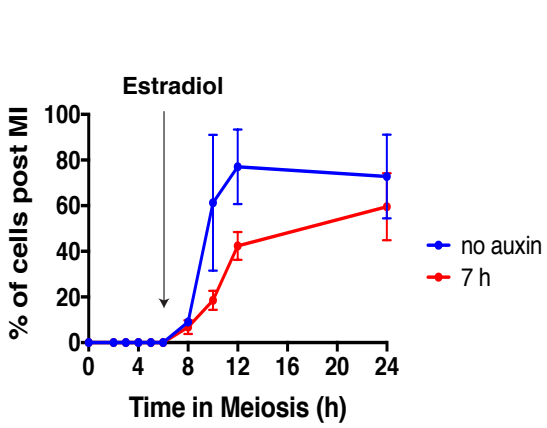
C
Estradiol
% of cells post MI
100
80
60
40
20
0
0 4 8 12 16 20 24
Time in Meiosis (h)
no auxin
7 h

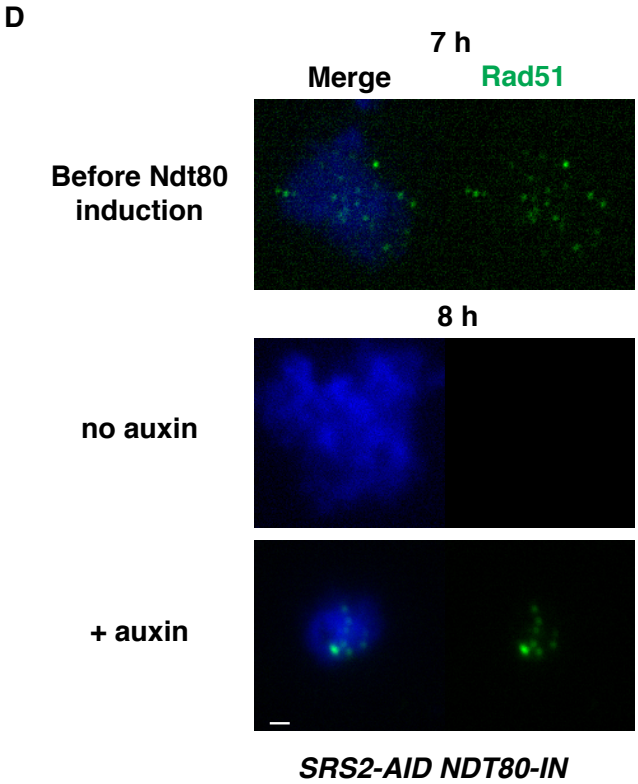
D
7 h
Merge
Rad51
Before Ndt80
induction
8 h
no auxin
+ auxin
SRS2-AID NDT80-IN

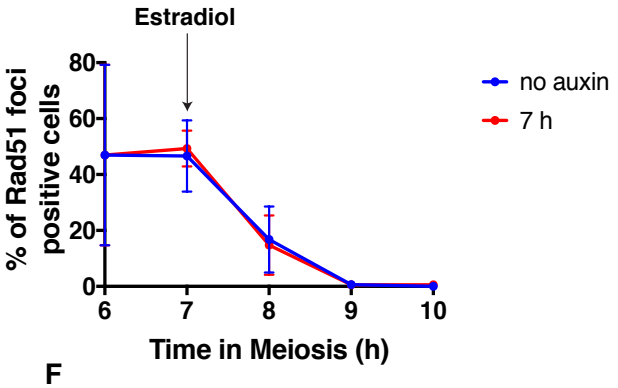
E
Estradiol
% of Rad51 foci
positive cells
80
60
40
20
0
6 7 8 9 10
Time in Meiosis (h)
no auxin
7 h

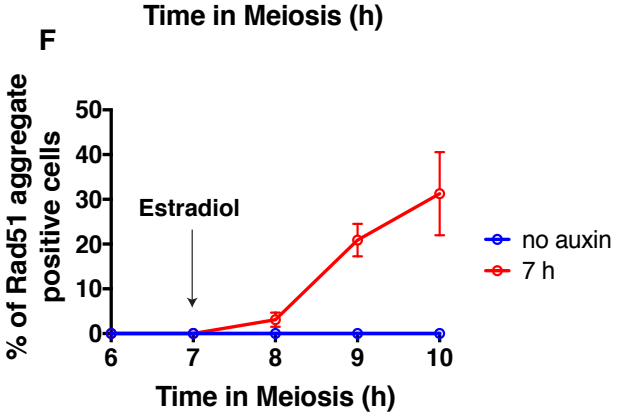
F
% of Rad51 aggregate
positive cells
50
40
30
20
10
0
Estradiol
6 7 8 9 10
Time in Meiosis (h)
no auxin
7 h

Figure 13: Srs2 degradation at the onset of Ndt80 expression gives Rad51 aggregat formation.

A. Schematic representation of meiotic time course set up with the addition of auxin and estradiol at the same time (7 h into meiosis).

B. Expression of various meiotic proteins was verified by western blotting. At each time point, cells were fixed with TCA and cell lysates were subject to the analysis. Representative western blot images of *SRS2-AID-9Myc NDT80-IN* (HYS 295/296) are shown. Srs2-AID-9Myc (anti-myc), Ndt80, phosphorylated Ndt80, Cdc5 and Tubulin (Tub, control) are shown by bars on the left.

B. Meiotic progression of *SRS2-AID-9Myc NDT80-IN* (HYS 295/296) with the addition of auxin or DMSO (control) at 7 h. Estradiol was added at 7 h (indicated by arrow). More than 200 cells were counted, error bar indicates S.D, n = 3

C. Representative images of nuclear spreads from *SRS2-AID-9Myc NDT80-IN* (HYS 295/296) with the addition of auxin or DMSO (control) at 7 h. which were stained with anti-Rad51 (green) and DAPI (blue), before Ndt80 induction (7 h) and after Ndt80 induction (8 h). Estradiol was added at 7 h. Scale bar indicates 1 μm.

D. Kinetics of nuclear spreads positive for Rad51 foci observed in *SRS2-AID-9Myc NDT80-IN* (HYS 295/296) with the addition of auxin or DMSO (control) at 7 h. Estradiol was added at 7 h (indicated by arrow). More than 100 nuclei were counted at each time point in these mutants, error bars indicate S.D, n = 3.

E. Kinetics of nuclear spreads positive for Rad51 aggregates observed in *SRS2-AID-9Myc NDT80-IN* (HYS 295/296) with the addition of auxin or DMSO (control) at 7 h. Estradiol was added at 7 h (indicated by arrow). More than 100 nuclei were counted at each time point in these mutants, error bars indicate S.D, n = 3.

Figure 14

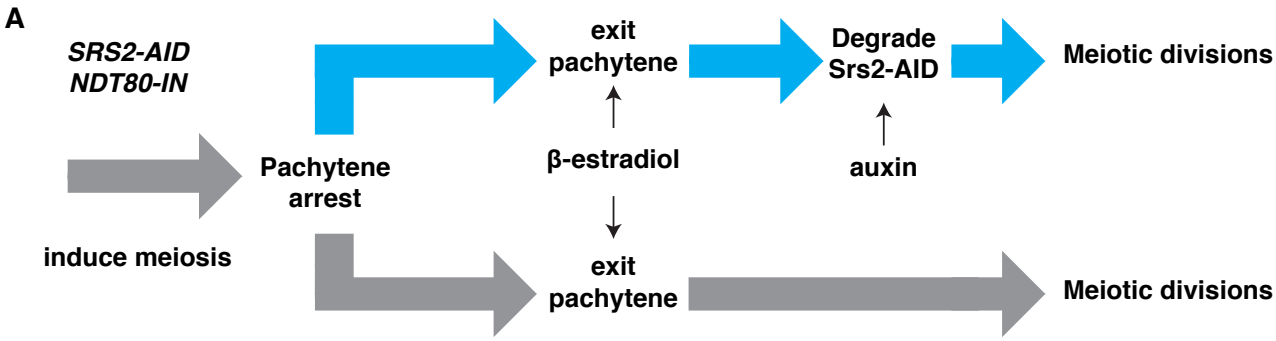
A
SRS2-AID
NDT80-IN
induce meiosis
Pachytene
arrest
exit
pachytene
β-estradiol
exit
pachytene
Degrade
Srs2-AID
auxin
Meiotic divisions
Meiotic divisions

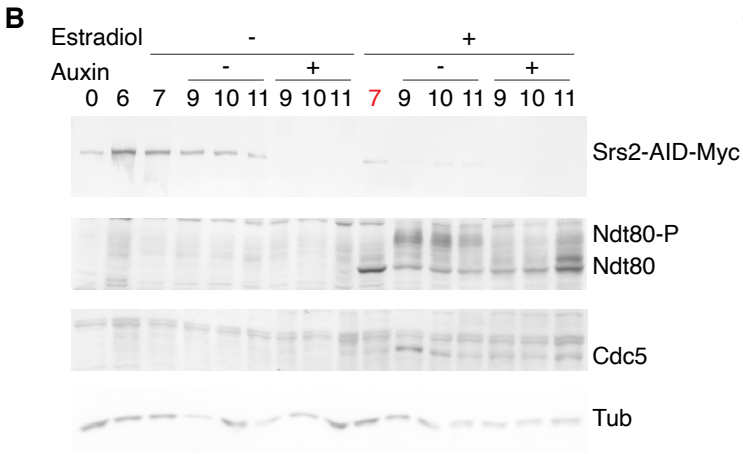
B
Estradiol
Auxin
0 6 7 9 10 11 9 10 11 7 9 10 11 9 10 11
Srs2-AID-Myc
Ndt80-P
Ndt80
Cdc5
Tub

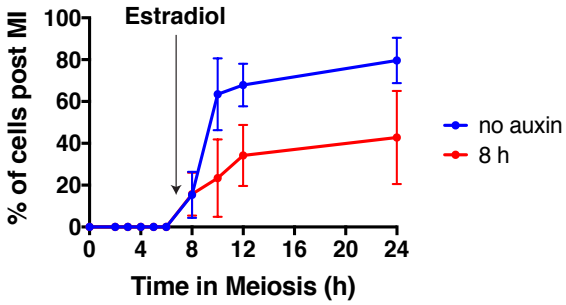
C
Estradiol
% of cells post MI
Time in Meiosis (h)
no auxin
8 h

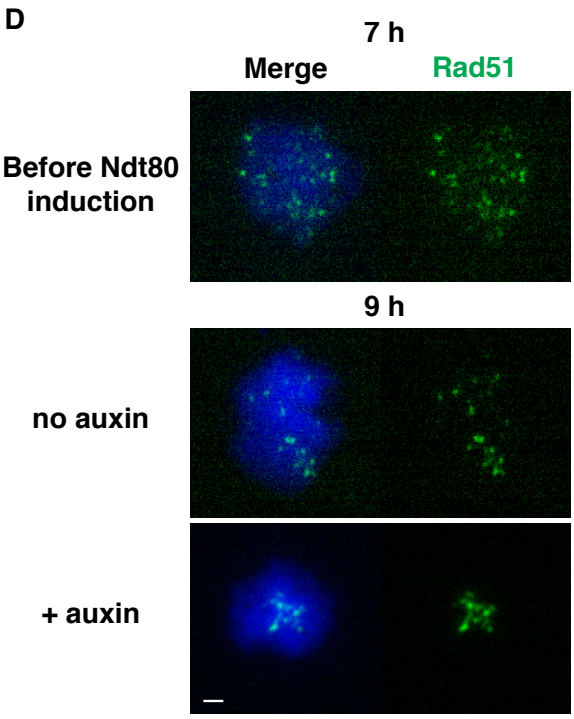
D
7 h
Merge
Rad51
Before Ndt80
induction
9 h
no auxin
+ auxin
SRS2-AID NDT80-IN

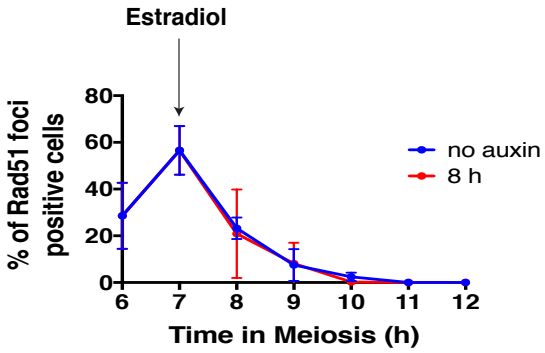
E
Estradiol
% of Rad51 foci
positive cells
Time in Meiosis (h)
no auxin
8 h

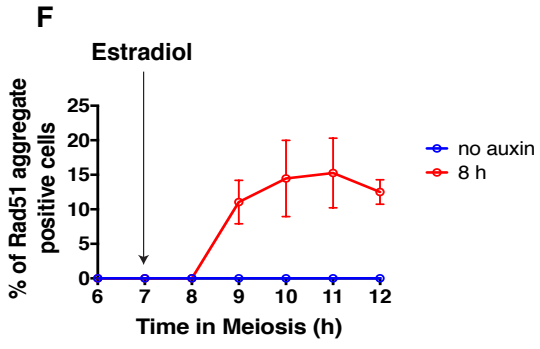
F
Estradiol
% of Rad51 aggregate
positive cells
Time in Meiosis (h)
no auxin
8 h

Figure 14: Srs2 degradation after Ndt80 expression observes reduced level of Rad51 aggregate formation.

A. Schematic representation of meiotic time course set up with the addition of auxin at 8 h after the addition of estradiol at 7 h into meiosis.

B. Expression of various meiotic proteins was verified by western blotting. At each time point, cells were fixed with TCA and cell lysates were subject to the analysis. Representative western blot images of *SRS2-AID-9Myc NDT80-IN* (HYS 295/296) are shown. Srs2-AID-9Myc (anti-myc), Ndt80, phosphorylated Ndt80, Cdc5 and Tubulin (Tub, control) are shown by bars on the left.

B. Meiotic progression of *SRS2-AID-9Myc NDT80-IN* (HYS 295/296) with the addition of auxin or DMSO (control) at 8 h. Estradiol was added at 7 h (indicated by arrow). More than 200 cells were counted, error bar indicates S.D, n = 3

C. Representative images of nuclear spreads from *SRS2-AID-9Myc NDT80-IN* (HYS 295/296) with the addition of auxin or DMSO (control) at 8 h. which were stained with anti-Rad51 (green) and DAPI (blue), before Ndt80 induction (7 h) and after Ndt80 induction (9 h). Estradiol was added at 7 h. Scale bar indicates 1 μm.

D. Kinetics of nuclear spreads positive for Rad51 foci observed in *SRS2-AID-9Myc NDT80-IN* (HYS 295/296) with the addition of auxin or DMSO (control) at 8 h. Estradiol was added at 7 h (indicated by arrow). More than 100 nuclei were counted at each time point in these mutants, error bars indicate S.D, n = 3.

E. Kinetics of nuclear spreads positive for Rad51 aggregates observed in *SRS2-AID-9Myc NDT80-IN* (HYS 295/296) with the addition of auxin or DMSO (control) at 8 h. Estradiol was added at 7 h (indicated by arrow). More than 100 nuclei were counted at each time point in these mutants, error bars indicate S.D, n = 3.

Figure 15

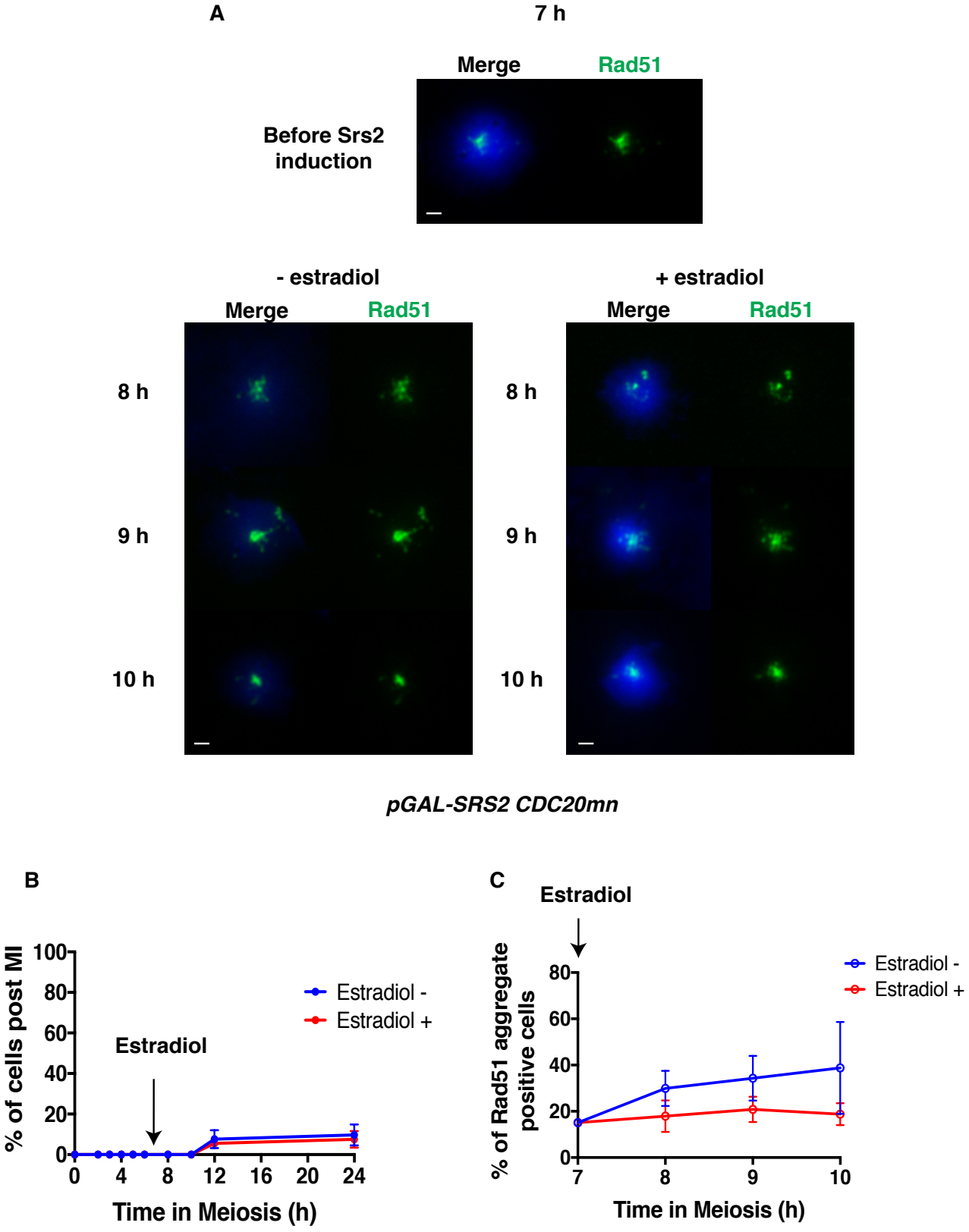
A
7 h
Merge
Rad51
Before Srs2 induction
- estradiol
+ estradiol
Merge
Rad51
8 h
9 h
10 h
pGAL-SRS2 CDC20mn
B
% of cells post MI
100
80
60
40
20
0
Estradiol
Estradiol -
Estradiol +
0
4
8
12
16
20
24
Time in Meiosis (h)
C
Estradiol
% of Rad51 aggregate positive cells
80
60
40
20
0
Estradiol -
Estradiol +
7
8
9
10
Time in Meiosis (h)

Figure 15: Srs2 induction at late meiosis reduces the Rad51 aggregates observed.

A. Representative image of nuclear spreads from *pGAL-SRS2 CDC20mn* (HYS 324/325) with the addition of estradiol at 7 h. which were stained with anti-Rad51 (green) and DAPI (blue), before Srs2 induction (7 h) and after Srs2 induction (8, 9 and 10 h). Scale bar indicates 1 μm.

B. Meiotic progression *pGAL-SRS2 CDC20mn* (HYS 324/325) with the addition of estradiol at 7 h (indicated by arrow). More than 200 cells were counted, error bar indicates S.D, n = 3.

C. Kinetics of nuclear spreads positive for Rad51 foci observed in *pGAL-SRS2 CDC20mn* (HYS 324/325) with the addition of estradiol at 7 h (indicated by arrow). More than 100 nuclei were counted at each time point in these mutants, error bars indicate S.D, n = 3.

Figure 16. Model for dual function of Srs2 during Meiosis

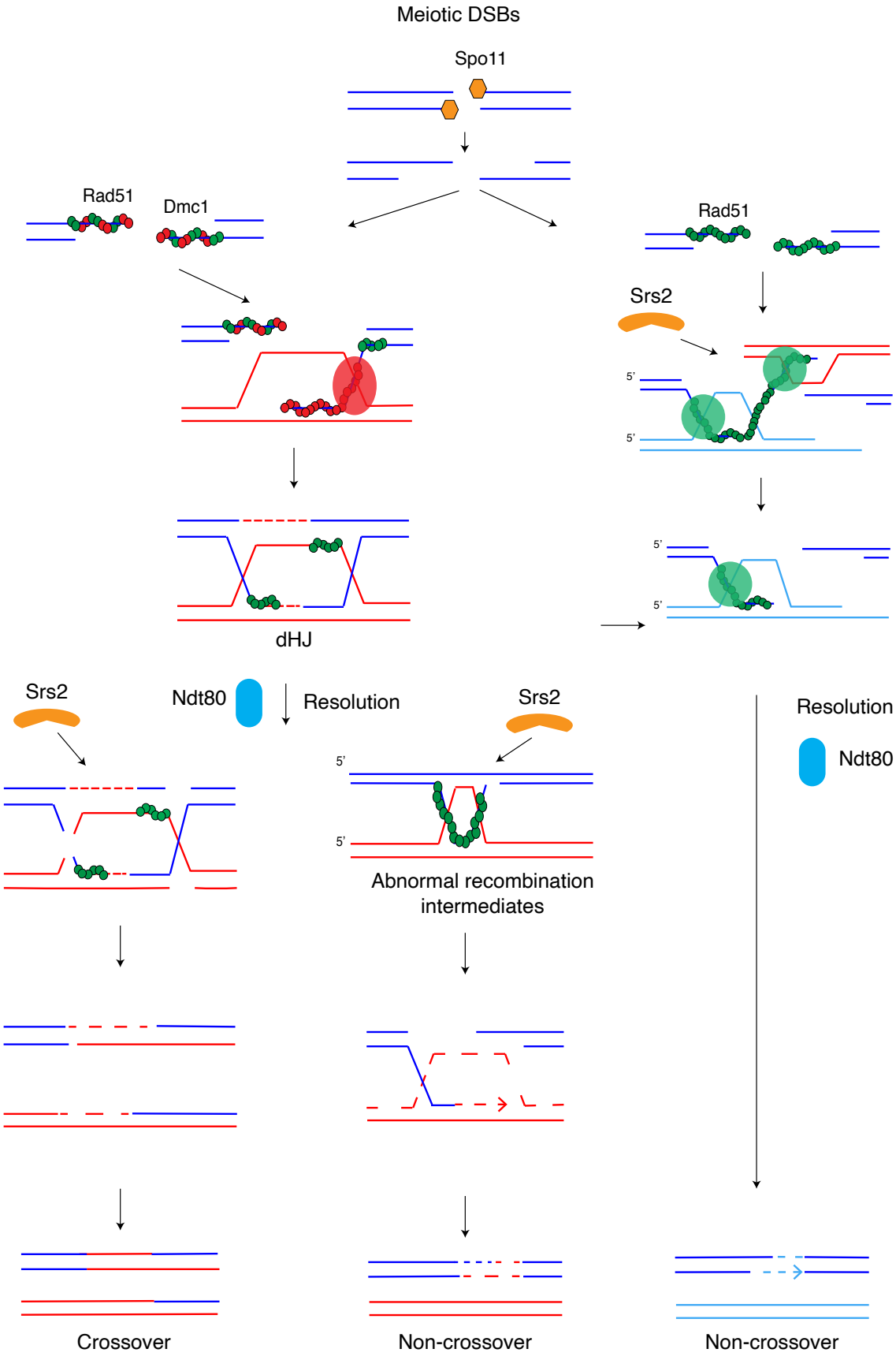

Figure 17. Model for formation of Rad51 aggregates in the absence of Srs2.

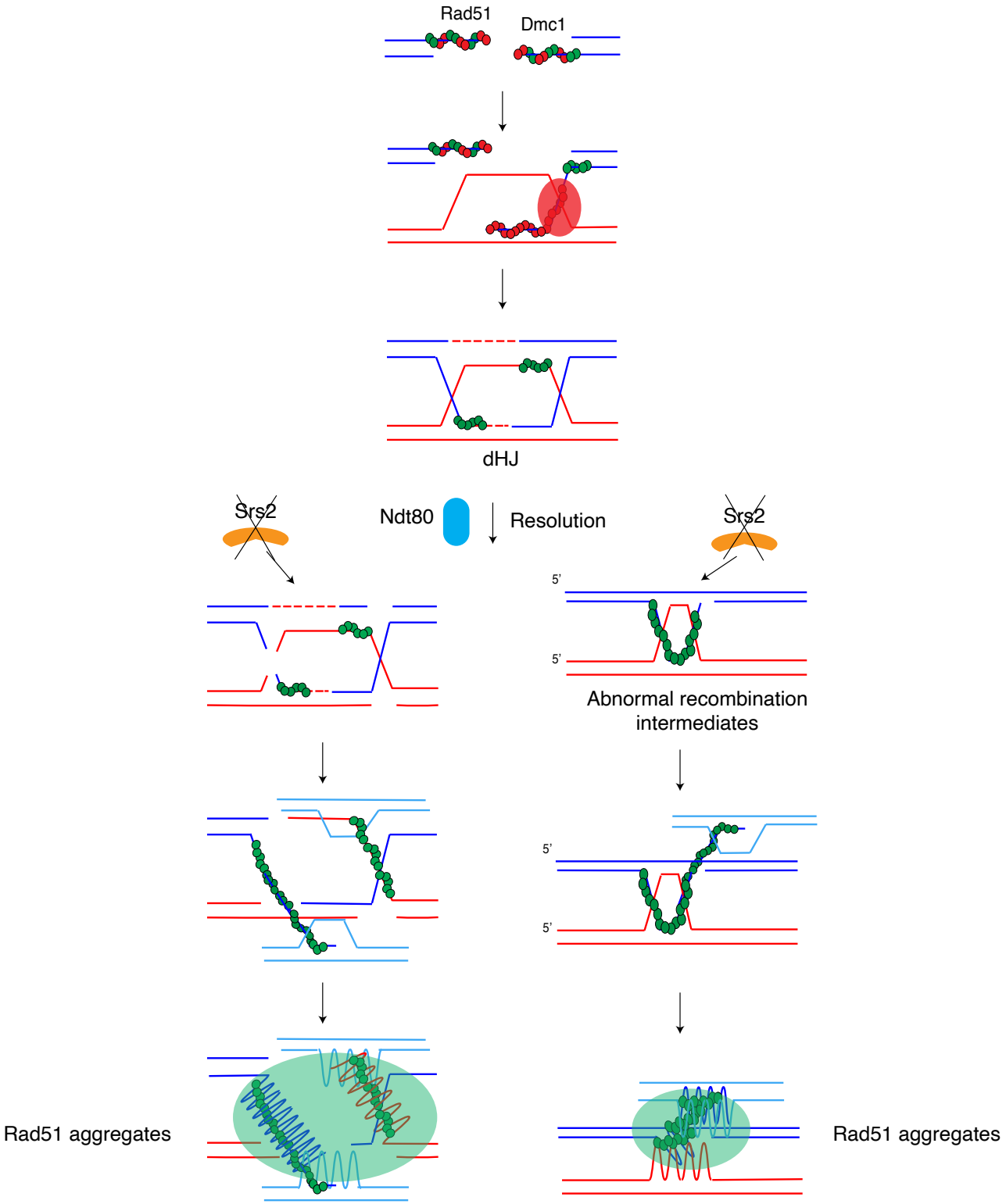

Table 1: Strain list

Strain no.	Genotype
MSY-833	MAT a, ho::LYS2, ura3, leu2::hisG, trp1::hisG, lys2
MSY-832	MAT α, ho::LYS2, ura3, leu2::hisG, trp1::hisG, lys2
NKY-1303	MAT a, ho::LYS2, ura3, leu2::hisG, lys2, his4B-LEU2(MluI), arg4-bgl
NKY-1543	MAT α, ho::LYS2, ura3, leu2::hisG, lys2, his4X-LEU2(BamHI)-URA3, arg4-NSP
HYS 13	NKY-1303 with *srs2::TRP1*
HYS 14	NKY-1543 with *srs2::TRP1*
HYS 38	MSY-833 with *srs2::TRP1*
HYS 39	MSY-832 with *srs2::TRP1*
HYS 92	MSY-833 with *spo11-Y135F::KanMX*
HYS 93	MSY-832 with *spo11-Y135F::KanMX*
HYS 94	MSY-833 with *spo11-Y135F::KanMX*, *srs2::TRP1*
HYS 95	MSY-832 with *spo11-Y135F::KanMX*, *srs2::TRP1*
HYS 197	NKY-1303/NKY-1543 with *rad50S::URA3*
HYS 189	NKY-1303 with *rad50S::URA3*, *srs2::TRP1*
HYS 193	NKY-1543 with *rad50S::URA3*, *srs2::TRP1*
HYS 45	MSY-833 with *pCLB2-CDC20::KanMX4*
HYS 46	MSY-832 with *pCLB2-CDC20::KanMX4*
HYS 47	MSY-833 with *pCLB2-CDC20::KanMX4*, *srs2::TRP1*
HYS 48	MSY-832 with *pCLB2-CDC20::KanMX4*, *srs2::TRP1*
H7790	MATa, ho::LYS2, lys2, URA3, leu2::hisG, his3::hisG, trp1::hisG, RPL13A-2xFKBP12::TRP1, fpr1::KanmX4, tor1-1::HIS3, RAD54-FKB::KanMX6
H7791	MAT α, ho::LYS2, lys2, ura3, LEU2, his3::hisG, trp1::hisG, RPL13A-2xFKBP12::TRP1, fpr1::KanmX4, tor1-1::HIS3, RAD54-FRB::KanMX6
HYS 71	H7790 with *srs2::TRP1*
HYS 82	H7791 with *srs2::TRP1*
HYS 20	MSY-833 with *ndt80::LEU2*
HYS 23	MSY-832 with *ndt80::LEU2*
HYS 18	MSY-833 with *srs2::TRP1*, *ndt80::LEU2*
HYS 19	MSY-832 with *srs2::TRP1*, *ndt80::LEU2*
HYS 102	NKY-1303 with *rad55::URA3*
HYS 103	NKY-1543 with *rad55::URA3*
HYS 161	NKY-1303 with *rad55::URA3*, *srs2::TRP1*
HYS 165	NKY-1543 with *rad55::URA3*, *srs2::TRP1*
HYS 100	NKY-1303 with *pCLB2-3HA-SGS1::KanMX*

HYS 101	NKY-1543 with *pCLB2-3HA-SGS1::KanMX*
HYS 124	NKY-1303 with *pCLB2-3HA-SGS1::KanMX*, *srs2::TRP1*
HYS 122	NKY-1543 with *pCLB2-3HA-SGS1::KanMX*, *srs2::TRP1*
HYS 295	MSY-833 with *lys2::pCUP1-1-OsTir1-9Myc::URA3*, *SRS2-AID-9Myc::Hygro*, *pGAL1-NDT80::Hygro*, *ura3::pGPD1-GAL4(848)-ER::URA*
HYS 296	MSY-832 with *lys2::pCUP1-1-OsTir1-9Myc::URA3*, *SRS2-AID-9Myc::Hygro*, *pGAL1-NDT80::Hygro*, *ura3::pGPD1-GAL4(848)-ER::URA*
HYS 324	MSY-833 with *pGAL-SRS2::KanMX*, *ura3::pGPD1-GAL4-ER::URA3*
HYS 325	MSY-832 with *pGAL-SRS2::KanMX*, *ura3::pGPD1-GAL4-ER::URA3*

Table 2: Primer list

Checking primers:

srs2Δ

F; 5'-GCTTAGGCTACCTTCGCAGAG-3'

R; 5'-GCTCATTCATAGCTGTCATATCGG-3'

RAD54-FRB

F; 5'-ATTTTGCGAGGGCGTGATGCTGATGCTAC-3'
R; 5'-ATTTCCCTGACAGCGTGAGATTTTCTTGCC-3'

RPL13A-2xFKBP12

F; 5'- CTAGTCGGAATAATCACAGTAGAGGTGTGG-3'
R; 5'- TTGTGCTCGAAGGAAAAGCCTGCAAACCTG-3'

fpr1Δ

F; 5'- ACATTATAGTGCCGTTCAATTCCCCTCACC-3'
R; 5'- TGCCACAAGAGTTTCCAGCAGGCTACGAAA-3'

tor1-1

F; 5'- CTACGGTGAGTAATTCCCTTTTGTCGTTGC-3'
R; 5'- CAGATTTAGGCGACAATGGAATAGCCGGGT-3'

SRS2-AID construction primers:

F; 5'-
TTTTCTCAGCTGTCACGTGCGAAAAAAAAGTCAAAATTAAACAACGGTGAA
ATCATAGTCATCGAT CGTACGCTGCAGGTCGAC

R; 5'-
TATGTGCTTTAAATAAAAATTATAAACCGCCTCCAATAGTTGACGTAGTCAG
GCATGAAAGTGCTA ATCGATGAATTCGAGCTCG

Chromosome III probe, *CHA1* gene

F; 5'-GTGGTTCCTACAGCGACAAAG-3'

R; 5'-CCAACGCTTCT TCCAAGTCC-3'

References

Abeysinghe, S. S., Chuzhanova, N., and Cooper, D. N. (2006). Gross deletions and translocations in human genetic disease. *Genome Dyn., 1*, 17-34.

Aboussekhra, A., Chanet, R., Adjiri, A., and Fabre, F. (1992). Semidominant suppressors of Srs2 helicase mutations of Saccharomyces cerevisiae map in the RAD51 gene, whose sequence predicts a protein with similarities to procaryotic RecA proteins, *Mol. Cell. Biol.*, *12*, 3224–3234.

Aboussekhra, A., Chanet, R., Zgaga, Z., Cassier-Chauvat, C., Heude, M., and Fabre, F. (1989). *RADH*, a gene of Saccharomyces cerevisiae encoding a putative DNA helicase involved in DNA repair. Characteristics of radH mutants and sequence of the gene. *Nucleic Acids Res., 17*, 7211–7219.

Aguilera, A., and Klein, H. L. (1988). Genetic control of intrachromosomal recombination in *Saccharomyces cerevisiae*: I. Isolation and genetic characterization of hyper-recombination mutations. *Genetics*, *119*, 779 –790

Akamatsu Y, and Jasin M (2010) Role for the Mammalian Swi5-Sfr1 Complex in DNA Strand Break Repair through Homologous Recombination. *PLOS Genetics*, *6* (10): e1001160.

Alani, E. (2008). A mutation in the putative MLH3 endonuclease domain confers a defect in both mismatch repair and meiosis in Saccharomyces cerevisiae. *Genetics*, *179*, 747–55.

Alani, E., Padmore, R., and Kleckner, N. (1990). Analysis of wild-type and rad50 mutants of yeast suggests an intimate relationship between meiotic chromosome synapsis and recombination. *Cell*, *61*(3), 419-436.

Allers, T., and Lichten, M. (2001). Differential timing and control of noncrossover and crossover recombination during meiosis. *Cell*, *106*, 47–57.

Antony, E., Tomko, E. J., Xiao, Q., Krejci, L., Lohman, T. M., and Ellen-berger, T. (2009). Srs2 disassembles Rad51 filaments by a protein-protein interaction triggering ATP turnover and dissociation of Rad51 from DNA. *Mol. Cell*, *35*, 105–115

Arevalo-Rodriguez, M., Wu, X., Hanes, S.D., and Heitman, J. (2004). Prolyl isomerases in yeast. Front. Biosci. 9, 2420–2446.

Armstrong, A. A., Mohideen, F., and Lima, C. D. (2012). Recognition of SUMO modified PCNA requires tandem receptor motifs in Srs2. *Nature*, *483*, 59–63.

Barber, L. J., Youds, J. L., Ward, J. D., Mcllwraith, M. J., O'Neil, N. J., Petalcorin, M. I., Martin, J. S., Collis, S. J., Cantor, S. B., Auclair, M., Tissenbaum, H., West, S. C., Rose, A. M., and Boulton, S. J. (2008). RTEL1 maintains genomic stability by suppressing homologous recombination. *Cell, 135* (2), 261-71.

Barbour, L., and Xiao, W. (2003). Regulation of alternative replication bypass pathways at stalled replication forks and its effects on genome stability: a yeast model. *Mutat. Res.*, *532*, 137–55.

Belshaw, P. J., Ho, S. N., Crabtree, G. R., and Schreiber, S. L. (1996). Controlling protein association and subcellular localization with a synthetic ligand that induces heterodimerization of proteins. *Proc. Natl. Acad. Sci., 93* (10), 4604-7.

Benjamin, K. R., Zhang, C., Shokat, K. M., and Herskowitz, I. (2003). Control of landmark events in meiosis by the CDK Cdc28 and the meiosis-specific kinase Ime2. *Genes Dev*., *17*(12), 1524-1539.

Bergerat, A., de Massy, B., Gadelle, D., Varoutas, P. C., Nicolas, A., and Forterre, P. (1997). An atypical topoisomerase II from Archaea with implications for meiotic recombination. *Nature*, *386*(6623), 414-7.

Bernstein, K. A., Reid, R. J. D., Sunjevaric, I., Demuth, K., Burgess, R. C., and Rothstein, R. (2011). The Shu complex, which contains Rad51 paralogues, promotes DNA repair through inhibition of the Srs2 anti-recombinase. *Mol. Biol. Cell, 22* (9), 1599-1607.

Bishop, D. K., Park, D., Xu, L., and Kleckner, N. (1992). DMC1: a meiosis-specific yeast homolog of E. coli recA required for recombination, synaptonemal complex formation, and cell cycle progression. *Cell, 69* (3), 439-56.

Blackford, A. N., and Jackson, S. P. (2017). ATM, ATR, and DNA-PK: The trinity at the heart of the DNA damage response. *Mol. Cell*, *66*, 801-817.

Borde, V., and de Massy, B. (2013). Programmed induction of DNA double strand breaks during meiosis: setting up communication between DNA and the chromosome structure. *Current opinion in genetics & development*, *23* (2), 147–155.

Bolcun-Filas, E., and Schimenti, J. C. (2012). Genetics of meiosis and recombination in mice. *International review of cell and molecular biology*, *298*, 179–227.

Börner, G. V., Kleckner, N., and Hunter, N., (2004). Crossover/noncrossover differentiation, synaptonemal complex formation, and regulatory surveillance at the leptotene/zygotene transition of meiosis. *Cell*, *117*, 29–45.

Brill, S. J., and Stillman, B. (1991). Replication factor-A from Saccharomyces cerevisiae is encoded by three essential genes coordinately expressed at S phase. *Genes Dev.*, *5*(9), 1589-1600.

Broomfield, S., and Xiao, W. (2002). Sup.pression of genetic defects within the RAD6 path- way by srs2 is specific for error-free post-replication repair but not for damage-induced mutagenesis. *Nucleic Acids Res.*, *30*, 732–739.

Burgess, R. C., Lisby, M., Altmannova, V., Krejci, L., Sung, P., and Rothstein, R. (2009). Localization of recombination proteins and Srs2 reveals anti-recombinase function in vivo. *J. Cell Biol., 185* (6), 969-81.

Burkovics, P., Sebesta, M., Sisakova, A., Plault, N., Szukacsov, V., Robert, T., Pinter, L., Marini, V., Kolesar, P., Haracska, L., Gangloff, S., and Krejci, L. (2013). Srs2 mediates PCNA-SUMO-dependent inhibition of DNA repair synthesis. *EMBO J.*, *32*, 742–755.

Callender, T. L., Laureau, R., Wan, L., Chen, X., Sandhu, R., *et al.*, (2016). Mek1 down regulates Rad51 activity during yeast meiosis by phosphorylation of Hed1. *PLoS Genet.*, *12*, e1006226.

Cao, L., Alani, E., and Kleckner, N. (1990). A pathway for generation and processing of double-strand breaks during meiotic recombination in S. cerevisiae. *Cell*, *61* (6), 1089-1101.

Carballo, J. A., Johnson, A. L., Sedgwick, S. G., and Cha, R. S. (2008). Phosphorylation of the axial element protein Hop1 by Mec1/Tel1 ensures meiotic interhomolog recombination. *Cell*, *132*, 758–770.

Carlile, T. M., and Amon, A. (2008). Meiosis I is established through division-specific translational control of a cyclin. *Cell*, *133* (2), 280-291.

Carpenter A. T. C. (1994). Chiasma function. *Cell, 77*, 959-962.

Carter, S. D., Vigasová, D., Chen, J., Chovanec, M., and Aström, S. U. (2009). Nej1 recruits the Srs2 helicase to DNA double-strand breaks and supports repair by a single-strand annealing-like mechanism. *Proc. Natl. Acad. Sci., 106* (29), 12037-42.

Chanet, R., Heude, M., Adjiri, A., Maloisel, L., and Fabre, F. (1996). Semidominant mutations in the yeast Rad51 protein and their relationships with the Srs2 helicase. *Mol. Cell. Biol.*, *16*, 4782–4789.

Chen, H., Lisby, M., and Symington, L. S. (2013). RPA coordinates DNA end resection and prevents formation of DNA hairpins. *Mol. Cell*, *50*(4), 589-600.

Chen, J., Zheng, X.F., Brown, E.J., and Schreiber, S.L. (1995). Identification of an 11- kDa FKBP12-rapamycin-binding domain within the 289-kDa FKBP12- rapamycin- associated protein and characterization of a critical serine residue. *Proc. Natl. Acad. Sci.*, *92*, 4947–4951.

Chen, X., Gaglione, R., Leong, T., Bednor, L., de los Santos, T., *et al.*, (2018). Mek1 coordinates meiotic progression with DNA break repair by directly phosphorylating and inhibiting the yeast pachytene regulator Ndt80. *PloS Genetics*, *14*(11), e1007832.

Chen, X., Suhandynata, R. T., Sandhu, R., Rockmill, B., Mohibullah, N., *et al.*, (2015). Phosphorylation of the synaptonemal complex protein Zip1 regulates the crossover/noncrossover decision during yeast meiosis. *PLoS Biology*, *13*(12), e1002329.

Chiolo, I., Carotenuto, W., Maffioletti, G., Petrini, J. H., Foiani, M., and Liberi, G. (2005). Srs2 and Sgs1 DNA helicases associate with Mre11 in different subcomplexes following checkpoint activation and CDK1-mediated Srs2 phosphorylation. *Molecular and cellular biology*, *25* (13), 5738–5751.

Chiolo, I., Minoda, A., Colmenares, S. U., Polyzos, A., Costes, S. V., and Karpen, G. H. (2011). Double-strand breaks in heterochromatin move outside of a dynamic HP1a domain to complete recombinational repair. *Cell*, *144* (5), 732–744.

Chiruvella, K. K., Liang, Z., and Wilson, T. E. (2013). Repair of double-strand breaks by end joining. *Cold Spring Harbor perspectives in biology*, *5* (5).

Ciccia, A., and Elledge, S. J. (2010). The DNA damage response: making it safe to play with knives. *Mol. Cell*, *40*, 179-204.

Clarke, D. J., Johnson, R. T., and Downes, C. S. (1993). Topoisomerase II inhibition prevents anaphase chromatid segregation in mammalian cells independently of the generation of DNA strand breaks. *J. Cell Sci., 105* (2), 563-9.

Cloud, V., Chan, Y. L., Grubb, J., Budke, B., and Bishop, D. K. (2012). Rad51 is an accessory factor for Dmc1-mediated joint molecule formation during meiosis. *Science (New York, N.Y.)*, *337* (6099), 1222–1225.

Colavito, S., Macris-Kiss, M., Seong, C., Gleeson, O., Greene, E. C., Klein, H. L., Krejci, L., and Sung, P. (2009). Functional significance of the Rad51-Srs2 complex in Rad51 presynaptic filament disruption. *Nucleic Acids Res.*, *37*, 6754 – 6764.

Cole, G. M., Schild, D., and Mortimer, R. K., (1989). Two DNA repair and recombination genes in Saccharomyces cerevisiae, RAD52 and RAD54, are induced during meiosis. *Mol. Cell Biol.*, *9*(7), 3101-4.

De Muyt, A., Jessop, L., Kolar, E., Sourirajan, A., Chen, J., *et al.*, (2012). BLM helicase ortholog Sgs1 is a central regulator of meiotic recombination intermediate metabolism. *Molecular Cell*, *46*, 43–53.

Difilippantonio, M. J., Zhu, J., Chen, H. T., Meffre, E., Nussenzweig, M. C., Max, E. E., Ried, T., and Nussenzweig, A. (2000). DNA repair protein Ku80 suppresses chromosomal aberrations and malignant transformation. *Nature*, *404* (6777), 510–514.

Ding, H., Schertzer, M., Wu, X., Gertsenstein, M., Selig, S., Kammori, M., Pourvali, R., Poon, S., Vulto, I., Chavez, E., *et al.*, (2004). Regulation of murine telomere length by Rtel: An essential gene encoding a helicase-like protein. *Cell*, *117*, 873–886.

Dong, H., and Roeder, G. S. (2000). Organization of the yeast Zip1 protein within the central region of the synaptonemal complex. *The Journal of Cell Biology*, *148*, 417–426.

Downs, J. A., Lowndes, N. F., and Jackson, S. P. (2000). A role for Saccharomyces cerevisiae histone H2A in DNA repair. *Nature*, *408*(6815), 1001-1004.

Fabre, F., Chan, A., Heyer, W. D., and Gangloff, S. (2002). Alternate pathways involving Sgs1/Top3, Mus81/Mms4, and Srs2 prevent formation of toxic recombination intermediates from single-stranded gaps created by DNA replication. *Proc. Natl. Acad. Sci. U.S.A.*, *99*, 16887–16892.

Falck, J., Coates, J., and Jackson, S. P. (2005). Conserved modes of recruitment of ATM, ATR and DNA-PKcs to sites of DNA damage. *Nature*, *434*, 605-611.

Fink, M., Imholz, D., and Thoma, F. (2007). Contribution of the serine 129 of histone H2A to chromatin structure. *Mol. Cell Biol*., *27*(10), 3589-3600.

Fung, C. W., Mozlin, A. M., and Symington, L. S. (2009). Suppression of the double-strand-break-repair defect of the Saccharomyces cerevisiae rad57 mutant. *Genetics, 181* (4), 1195-1206.

Furuse, M., Nagase, Y., Tsubouchi, H., Murakami-Murofushi, K., Shibata, T., and Ohta, K. (1998). Distinct roles of two separable in vitro activities of yeast Mre11 in mitotic and meiotic recombination. *The EMBO journal*, *17* (21), 6412–6425.

Gangloff, S., Soustelle, C., and Fabre, F. (2000). Homologous recombination is responsible for cell death in the absence of the Sgs1 and Srs2 helicases. *Nat. Genet., 25,* 192–194.

Gari, K., Décaillet, C., Stasiak, A. Z., Stasiak, A. and Constantinou, A. (2008). The Fanconi anemia protein FANCM can promote branch migration of Holliday junctions and replication forks. *Mol. Cell*, *29*, 141–148.

Gasior, S. L., Wong, A. K., Kora, Y., Shinohara, A., and Bishop, D. K. (1998). Rad52 associates with RPA and functions with rad55 and rad57 to assemble meiotic recombination complexes. *Genes Dev*., *12*(14), 2208-2221.

Gorbsky, G. J. (1994). Cell cycle progression and chromosome segregation in mammalian cells cultures in the presence of the topoisomerase II inhibitors ICRF-187 [(+)-1,2-bis(3,5-dioxopiperazinyl-1-yl)propane;ADR-529] and ICRF-159 (Razoxane). *Cancer Res., 54* (4), 1042-8.

Greenwell, P. W., Kronmal, S. L., Porter, S. E., Gassenhuber, J., Obermaier, B., and Petes, T. D. (1995). TEL1, a gene involved in controlling telomere length in S. cerevisiae, is homologous to the human ataxia telangiectasia gene. *Cell*, *82*, 823-829.

Haber, J. E. (2014). Genome Stability: DNA Repair and Recombinaition. New York, NY: Garland Science.

Haruki, H., Nishikawa, J., and Laemmli, U. K. (2008). The Anchor-Away Technique: Rapid, Conditional Establishment of Yeast Mutant Phenotypes. *Molecular Cell, 31*, 925-932.

Harvey, A. C., Jackson, S. P., and Downs, J. A. (2005). Saccharomyces cerevisiae histone H2A Ser122 facilitates DNA repair. *Genetics*, *170* (2), 543-553.

Hawley, R. S., and Arbel, T. (1993). Yeast genetics and the fall of the classical view of meiosis. *Cell*, *72* (3), 301–303.

Hayase, A., Takagi, M., Miyazaki, T., Oshiumi, H., Shinohara, M., and Shinohara, A. (2004). A protein complex containing Mei5 and Sae3 promotes the assembly of the meiosis-specific RecA homolog Dmc1. *Cell*, *119* (7), 927-940.

Hays, S. L., Firmenich, A. A., and Berg P. (1995). Complex formation in yeast double-strand break repair: participation of Rad51, Rad52, Rad55, and Rad57 proteins. *Proc. Natl. Acad. Sci. U S A.*, *92* (15), 6925-9.

Hays, S. L., Firmenich, A. A., Massey, P., Banerjee, R., and Berg, P. (1998). Studies of the interaction between Rad52 protein and the yeast single-stranded DNA binding protein RPA. *Mol. Cell Biol*., *18* (7), 4400-4406.

Hedge, V., and Klein, H. (2000). Requirement for the SRS2 DNA helicase gene in non-homologous end joining in yeast. *Nucleic Acids Res. 28* (14), 2779-83.

Helliwell, S. B., Wagner, P., Kunz, J., Deuter-Reinhard, M., Henriquez, R., and Hall, M. N. (1994). TOR1 and TOR2 are structurally and functionally similar but not identical phosphatidylinositol kinase homologues in yeast. *Mol. Biol. Cell, 5* (1), 105-18.

Henderson, K. A. and Keeney, S. (2004). Tying synaptonemal complex initiation to the formation and programmed repair of DNA double-strand breaks. *Proc Natl Acad Sci*, *101*, 4519–4524.

Heyer, W. D., Li, X., Rolfsmeier, M., and Zhang, X. P. (2006). Rad54: the swiss army knife of homologous recombination? *Nucleic Acids Res., 34* (15), 4115-4125.

Heyting C. (1996). Synaptonemal complexes: structure and function. *Current opinion in cell biology*, *8* (3), 389–396.

Hochwagen, A., Wrobel, G., Cartron, M., Demougin, P., Niederhauser-Wiederkehr, C., Boselli, M. G., Primig, M., and Amon, A. (2005). Novel Response to Microtubule Perturbation in Meiosis. *Mol. Cell Biol., 25* (11) 4767-4781.

Hollingsworth, N. M., and Byers, B., (1989). HOP1: a yeast meiotic pairing gene. *Genetics*, *121*, 445–462.

Hollingsworth, N. M. (2016). Mek1/Mre4 is a master regulator of meiotic recombination in budding yeast. *Microb. Cell, 3* (3), 129-131.

Hong, E. J., and Roeder, G. S. (2002). A role for Ddc1 in signaling meiotic double-strand breaks at the pachytene checkpoint. *Genes & development*, *16* (3), 363–376.

Hunter N. (2015). Meiotic Recombination: The Essence of Heredity. *Cold Spring Harbor perspectives in biology*, *7* (12), a016618.

Hunter, N., and Kleckner, N. (2001). The single-end invasion: an asymmetric intermediate at the double- strand break to double-holliday junction transition of meiotic recombination. *Cell*, *106*, 59–70.

Ira, G., Malkova, A., Liberi, G., Foiani, M., and Haber, J. E. (2003). Srs2 and Sgs1-Top3 suppress crossovers during double-strand break repair in yeast. *Cell*, *115*(4), 401-411.

Islam, M. N., Paquet, N., Fox, D. *et al.* (2012). A variant of the breast cancer type 2 susceptibility protein (BRC) repeat is essential for the RECQL5 helicase to interact with RAD51 recombinase for genome stabilization. *J. Biol. Chem.*, *287*, 23808–18.

Jackson, S. P. (2002). Sensing and repairing DNA double-strand breaks. *Carcinogenesis*, *23*, 687–696.

Karanam, K., Kafri, R., Loewer, A., and Lahav, G. (2012). Quantitative live cell imaging reveals a gradual shift between DNA repair mechanisms and a maximal use of HR in mid S phase. *Molecular cell*, *47* (2), 320–329.

Kaur, H., De Muyt, A., and Lichten, M. (2015). Top3-Rmi1 DNA single-strand decatenase is integral to the formation and resolution of meiotic recombination intermediates. *Mol. Cell*, *57*, 583–594.

Keelagher, R. E., Cotton, V. E., Goldman, A. S. H., and Borts, R. H. (2011). Separable roles for Exonuclease I in meiotic DNA double-strand break repair. *DNA Repair (Amst)*, *10*, 126–37.

Keeney S. (2001). Mechanism and control of meiotic recombination initiation. *Current topics in developmental biology*, *52*, 1–53.

Keeney, S., Giroux, C. N., and Kleckner, N. (1997). Meiosis-specific DNA double-strand breaks are catalyzed by Spo11, a member of a widely conserved protein family. *Cell, 88* (3), 375-84.

Keeney, S., Lange, J., and Mohibullah, N. (2014). Self-organization of meiotic recombination initiation: general principles and molecular pathways. *Annu. Rev. Genet.*, *48*, 187–214.

Kerrest, A., Anand, R. P., Sundararajan, R. *et al.* (2009). SRS2 and SGS1 prevent chromosomal breaks and stabilize triplet repeats by restraining recombination. *Nat. Struct. Mol. Biol.*, *16*, 159–67.

Khanna, K. K., and Jackson, S. P. (2001). DNA double-strand breaks: signaling, repair and the cancer connection. *Nature Genet.*, *27*, 247–254.

Kim, K. P., B. M. Weiner, L. Zhang, A. Jordan, J. Dekker *et al.* (2010). Sister cohesion and structural axis components mediate homolog bias of meiotic recombination. *Cell, 143***,** 924-937.

Klein, H.L. (1997). RDH54, a RAD54 homolog in Saccharomyces cerevisiae, is required for mitotic diploid-specific recombination and repair and for meiosis. *Genetics, 147*, 1533-1543.

Klein, H. L. (2001). Mutations in recombinational repair and in checkpoint control genes suppress the lethal combination of srs2Delta with other DNA repair genes in Saccharomyces cerevisiae. *Genetics, 157* (2), 557-65.

Kobayashi, J. (2004). Molecular mechanism of the recruitment of NBS1/hMRE11/hRAD50 complex to DNA double-strand breaks: NBS1 binds to gamma-H2AX through FHA/BRCT domain. *J. Radiat. Res.*, *45*(4), 473-478.

Kohl, K. P., and Sekelsky, J. (2013). Meiotic and mitotic recombination in meiosis. *Genetics*, *194*, 327–334.

Kolesar, P., Altmannova, V., Silva, S. *et al.* (2016). Pro-recombination role of Srs2 protein requires SUMO (small ubiquitin-like modifier) but is independent of PCNA (proliferating cell nuclear antigen) Interaction. *J. Biol. Chem.*, *291*, 7594–607.

Krejci, L., Macris, M., Li, Y., Van Komen, S., Villemain, J., Ellenberger, T., Klein, H., and Sung, P. (2004). Role of ATP hydrolysis in the antirecombinase function of *Saccharomyces cerevisiae* Srs2 protein. *J. Biol. Chem.*, *279*, 23193–23199.

Krejci, L., Van Komen, S., Li, Y., Villemain, J., Reddy, M. S., Klein, H., Ellenberger, T., and Sung, P. (2003). DNA helicase Srs2 disrupts the Rad51 presynaptic filament. *Nature*, *423*, 305–309.

Krogh, B. O., and Symington, L. S. (2004). Recombination proteins in yeast. *Annu. Rev. Genet., 38*, 233-71.

Lambert, S. and Lopez, B. (2001). Role of *RAD51* in sister-chromatid exchanges in mammalian cells. *Oncogene*, *20***,** 6627–6631.

Lambert, S., Mizuno, K., Blaisonneau, J. *et al.* (2010). Homologous recombination restarts blocked replication forks at the expense of genome rearrangements by template exchange. *Mol. Cell*, 39, 346–59.

Lao, J. P., and Hunter, N. (2010). Trying to avoid your sister. *PLoS Biol.*, *8*, e1000519.

Lawrence, C. W., and Christensen, R. B. (1979). Metabolic suppressors of trimethoprim and ultraviolet light sensitivities of Saccharomyces cerevisiae rad6 mutants. *J. Bacteriol.*, *139*, 866–876.

Le Breton, C., Dupaigne, P., Robert, T. *et al.* (2008). Srs2 removes deadly recombination intermediates independently of its interaction with SUMO-modified PCNA. *Nucleic Acids Res.*, *36*, 4964– 74.

Lee, B. H., and Amon, A. (2003). Role of polo-like kinase CDC5 in programming meiosis I chromosome segregation. *Science, 300* (5618), 482-6.

Lee, S.K., Johnson, R.E., Yu, S.L., Prakash, L., and Prakash, S. (1999). Requirement of yeast *SGS1* and *SRS2* genes for replication and transcription. *Science, 286*, 2339–2342.

Lee, K., and Lee, S. E. (2007). Saccharomyces cerevisiae Sae2- and Tel1-dependent single-strand DNA formation at DNA break promotes microhomology-mediated end joining. *Genetics*, *176* (4), 2003–2014.

Leem, S-H., and Ogawa, H. (1992). The MRE4 gene encodes a novel protein kinase homologue required for meiotic recombination in Saccharomyces cerevisiae. *Nucl. Acids Res.*, *20*, 449–457.

Liu, J., Renault, L., Veaute, X., Fabre, F., Stahlberg, H., and Heyer, W. D. (2011). Rad51 paralogues Rad55-Rad57 balance the antirecombinase Srs2 in Rad51 filament formation. *Nature, 479* (7372), 245-8.

Ljunger, E., Cnattingius, S., Lundin, C., and Annerén, G. (2005). Chromosomal anomalies in first trimester miscarriages. *Acta Obstet. Gynaecol Scand*, *84*, 1103-1107

Lynn, A., Soucek, R., and Borner, G. V. (2007). ZMM proteins during meiosis: crossover artists at work. *Chromosome Res.*, *15*, 591–605.

Marechal, A., and Zou, L. (2013). DNA damage sensing by the ATM and ATR kinases. *Cold Spring Harb. Perspect. Biol.*, *5*(9), a012716.

Marini, V., and Krejci, L. (2012). Unwinding of synthetic replication and recombination substrates by Srs2. *DNA repair*, *11* (10), 789–798.

Martin, V., Chahwan, C., Gao, H., Blais, V., Wohlschlegel, J., Yates, J. R. III, McGowan, C. H., and Russell, P. (2006). Sws1 is a conserved regulator of homologous recombination in eukaryotic cells. *Embo J.*, *25*, 2564– 2574.

Masson, J. Y., Tarsounas, M. C., Stasiak, A. Z., Stasiak, A., Shah, R., McIlwraith, M. J., Benson, F. E., and West, S. C. (2001). Identification and purification of two distinct complexes containing the five RAD51 paralogs. *Genes & development*, *15* (24), 3296–3307.

Matos, J., and West, S. C. (2014). Holliday junction resolution: Regulation in space and time. *DNA Repair (Amst)*, *19*, 176–181.

McKee, A. H., and Kleckner, N. (1997). Mutations in Saccharomyces cerevisiae that block meiotic prophase chromosome metabolism and confer cell cycle arrest at pachytene identify two new meiosis-specific genes SAE1 and SAE3. *Genetics*, *146* (3), 817–834.

McMahill, M. S., Sham, C. W., and Bishop, D. K. (2007). Synthesis-dependent strand annealing in meiosis. *PLoS Biol.*, *5*, 2589-2601.

McVey, M., Kaeberlein, M., Tissenbaum, H. A., and Guarente, L. (2001). The short life span of Saccharomyces cerevisiae sgs1 and srs2 mutants is a composite of normal aging processes and mitotic arrest due to defective recombination. *Genetics*, *157*(4), 1531-1542.

Milne, G. T., Ho, T., and Weaver, D. T. (1995). Modulation of Saccharomyces cerevisiae DNA double-strand break repair by SRS2 and RAD51. *Genetics*, *139*, 1189–1199.

Miura, T., Shibata, T., and Kusano, K. (2013). Putative antirecombinase Srs2 DNA helicase promotes noncrossover homologous recombination avoiding loss of heterozygosity. *P. Natl. Acad. Sci. U.S.A.*, *110*, 16067–72.

Moldovan, G. L., Dejsuphong, D., Petalcorin, M. I. R., Hoffmann, K., Takeda, S., Boulton, S. J., and D'Andrea, A. D. (2012). Inhibition of homologous recombination by the PCNA-interacting protein PARI. *Mol. Cell, 45* (1), 75-86.

Moldovan, G. L., Madhavan, M. V., Mirchandani, K. D., McCaffrey, R. M., Vinciguerra, P., and D'Andrea, A. D. (2010). DNA polymerase POLN participates in cross-link repair and homologous recombination. *Mol Cell Biol.*, *30*, 1088–1096.

Morawska, M., and Ulrich, H. D. (2013). An expanded tool kit for the auxin-inducible degron system in budding yeast. *Yeast*, *30*(9), 341-351.

Moreau, S., Ferguson, J. R., and Symington, L. S. (1999). The nuclease activity of Mre11 is required for meiosis but not for mating type switching, end joining, or telomere maintenance. *Molecular and cellular biology*, *19* (1), 556–566.

Moynahan, M. E., Pierce, A. J., and Jasin, M. (2001). BRCA2 is required for homology- directed repair of chromosomal breaks. *Mol. Cell, 7* (2), 263-72.

Neale, M. J., Pan, J., and Keeney, S. (2005). Endonucleolytic processing of covalent protein-linked DNA double-strand breaks. *Nature*, *436* (7053), 1053–1057.

New, J. H., Sugiyama, T., Zaitseva, E., and Kowalczykowski, S. C. (1998). Rad52 protein stimulates DNA strand exchange by Rad51 and replication protein A. *Nature, 391*, 407- 410.

Nishimura, K., Fukagawa, T., Takisawa, H., Kakimoto, T., and Kanemaki, M. (2009). An auxin-based degron system for the rapid depletion of proteins in nonplant cells. *Nat. Methods*, *6*(12), 917-922.

Niu, H., Li, X., Job, E., Park, C., Moazed, D., Gygi, S. P., *et al.*, (2007). Mek1 kinase is regulated to suppress doublestrand break repair between sister chromatids during budding yeast meiosis. *Mol. Cell Biol.*, *27*(15), 5456–67.

Niu, H., Wan, L., Baumgartner, B., Schaefer, D., Loidl, J., *et al*., (2005). Partner choice during meiosis is regulated by Hop1-promoted dimerization of Mek1. *Mol. Biol. Cell*, *16*, 5804–5818.

Niu, H., Wan, L., Busygina, V., Kwon, Y., Allen, J. A., *et al.*, (2009). Regulation of meiotic recombination via Mek1-mediated Rad54 phosphorylation. *Mol. Cell*, *36*, 393–404.

O'Connor, K. W., *et al.* (2013). PARI overexpression promotes genomic instability and pancreatic tumorigenesis. *Cancer Res.*, *73*, 2529–2539.

Oh, S. D., Lao, J. P., Hwang, P. Y., Taylor, A. F., Smith, G. R., *et al.*, (2007). BLM ortholog, Sgs1, prevents aberrant crossing-over by suppressing formation of multichromatid joint molecules. *Cell*, *130*, 259–272.

Okaz, E., Argüello-Miranda, O., Bogdanova, A., Vinod, P. K., Lipp, J. J., Markova, Z., Zagoriy, L., Novak, B., and Zachariae, W. (2012). Meiotic prophase requires proteolysis of Ama1 M phase regulators mediated by the meiosis-specific APC/C. *Cell, 151* (3), 603-618.

Ooi, S. L., Shoemaker, D. D., and Boeke, J. D. (2003). DNA helicase gene interaction network defined using synthetic lethality analyzed by microarray. *Nat. Genet.*, *35*, 277–86.

Padmore, R., Cao, L., and Kleckner, N. (1991). Temporal comparison of recombination and synaptonemal complex formation during meiosis in S. cerevisiae. *Cell*, *66* (6), 1239–1256.

Page, S. L., and Hawley, R. S. (2004). The genetics and molecular biology of the synaptonemal complex. *Annual review of cell and developmental biology*, *20*, 525–558.

Paliwal, S., Radhkrishnan, K., Sturzenegger, A., Burdova, K., and Janscak, P. (2014). Huamn RECQ5 helicase promotes repair of DNA double-strand breaks by synthesis-dependent strand annealing. *Nucleic Acids Res., 42* (4), 2380-2390.

Palladino, F., and Klein, H. L. (1992). Analysis of mitotic and meiotic defects in Saccharomyces cerevisiae SRS2 DNA helicase mutants. *Genetics, 132* (1), 23-37.

Pan, J., Sasaki, M., Kniewel, R., Murakami, H., Blitzblau, H. G., *et al.*, (2011). A hierarchical combination of factors shapes the genome-wide topography of yeast meiotic recombination initiation. *Cell*, *144*, 719–731.

Papouli, E., Chen, S., Davies, A. A. *et al.* (2005). Crosstalk between SUMO and ubiquitin on PCNA is mediated by recruitment of the helicase Srs2p. *Mol. Cell*, *19*, 123–33.

Peoples, T. L., Dean, E., Gonzalez, O., Lambourne, L., and Burgess, S. M. (2002). Close, stable homolog juxtaposition during meiosis in budding yeast is dependent on meiotic recombination,

occurs independently of synapsis, and is distinct from DSB-independent pairing contacts. *Genes Dev*, *16*, 1682–1695.

Petronczki, M., Matos, J., Mori, S., Gregan, J., Bogdanova, A., Schwickart, M., Mechtler, K., Shirahige, K., Zachariae, W., and Nasmyth, K. (2006). Monopolar attachment of sister kinetochores at meiosis I requires casein kinase 1. *Cell*, *126* (6), 1049–1064.

Petronczki, M., Siomos, M. F. and Nasmyth, K. (2003). Un menage a quatre: the molecular biology of chromosome segregation in meiosis. *Cell, 112*, 423– 440.

Pfander, B., Moldovan, G. L., Sacher, M. *et al.* (2005). SUMO-modified PCNA recruits Srs2 to prevent recombination during S phase. *Nature*, *436*, 428–33.

Picard, D. (1994). Regulation of protein function through expression of chimaeric proteins. *Curr Opin Biotechnol*., *5*(5), 511-515.

Prieler, S., Penkner, A., Borde, V., and Klein, F. (2005). The control of Spo11's interaction with meiotic recombination hotspots. *Genes & development*, *19* (2), 255–269.

Prinz, S., Amon, A., and Klein, F. (1997). Isolation of COM1, a new gene required to complete meiotic double-strand break-induced recombination in Saccharomyces cerevisiae. *Genetics*, *146* (3), 781–795.

Rattray, A. J., and Symington, L. S. (1995). Multiple pathways for homologous recombination in Saccharomyces cerevisiae. *Genetics, 139* (1), 45-56.

Robert, T., Dervins, D., Fabre, F. *et al.* (2006). Mrc1 and Srs2 are major actors in the regulation of spontaneous crossover. *EMBO J.*, *25*, 2837–46.

Rockmill, B., and Roeder, G. S. (1990). Meiosis in asynaptic yeast. *Genetics*, *126*, 563–574.

Rockmill, B., and Roeder, G. S. (1991). A meiosis-specific protein kinase homologue required for chromosome synapsis and recombination. *Genes Dev.*, *5*, 2392–2404.

Roeder, G. S. (1997). Meiotic chromosomes: it takes two to tango. *Genes Dev., 11* (20), 2600-21.

Roeder, G. S., and Bailis, J. M. (2000). The pachytene checkpoint. *Trends in genetics : TIG*, *16* (9), 395–403.

Rogakou, E. P., Pilch, D. R., Orr, A. H., Ivanova, V. S., and Bonner, W. M. (1998). DNA double-stranded breaks induce histone H2AX phosphorylation on serine 139. *J. Biol. Chem*., *273*(10), 5858-5868.

Rong, L., Palladino, F., Aguilera, A., and Klein, H. L. (1991). The hyper-gene conversion hpr5-1 mutation of Saccharomyces cerevisiae is an allele of the SRS2/RADH gene. *Genetics, 127* (1), 75-85.

Saponaro, M., Callahan, D., Zheng, X. *et al.* (2010). Cdk1 targets Srs2 to complete synthesis-dependent strand annealing and to promote recombinational repair. *PLoS Genet.*, *6*, e1000858.

Sasanuma, H., Furihata, Y., Shinohara, M., and Shinohara, A. (2013b). Remodeling of the Rad51 DNA Strand-Exchange Protein by the Srs2 Helicase. *Genetics, 194* (4), 859-872.

Sasanuma, H., Sakurai, H. S. M., Furihata, Y., *et al.*, (2019). Srs2 helicase prevents the formation of toxic DNA damage during late prophase I of yeast meiosis. *Chromosoma*, *128*(3), 453-471.

Sasanuma, H., Tawaramoto, M. S., Lao, J. P., Hosaka, H., Sanda, E., Mamoru, S., Yamashita, E., Hunter, N., Shinohara, M., Nakagawa, A., and Shinohara, A. (2013a). A new protein complex promoting the assembly of Rad51 filaments. *Nature Comm., 4* (1676).

Schiestl, R. H., Gietz, R. D., Hastings, P. J., and Wintersberger, U. (1990). Interchromosomal and intrachromosomal recombination in rad 18 mutants of Saccharomyces cerevisiae. *Molecular & general genetics : MGG*, *222* (1), 25–32.

Schild, D. (1995). Suppression of a new allele of the yeast RAD52 gene by overexpression of RAD51, mutations in srs2 and ccr4, or mating-type heterozygosity. *Genetics*, *140*, 115–127.

Schwacha, A., and Kleckner, N., (1994). Identification of joint molecules that form frequently between homologs but rarely between sister chromatids. *Cell*, *76*, 51–63.

Schwacha, A., and Kleckner, N. (1995). Identification of double Holliday junctions as intermediates in meiotic recombination. *Cell, 83*, 783–791.

Schwendener, S., Raynard, S., Paliwal, S., Cheng, A., Kanagaraj, R., Shevelev, I., Stark, J. M., Sung, P., and Janscak, P. (2010). Physical interaction of RECQ5 helicase with RAD51 facilitates its anti-recombinase activity. *The Journal of biological chemistry*, *285* (21), 15739–15745.

Scully, R., Panday, A., Elango, R., and Willis, N. A. (2019). DNA double-strand break repair-pathway choice in somatic mammalian cells. *Nature reviews*, *20*, 698-714.

Seong, C., Colavito, S., Kwon, Y. *et al.* (2009). Regulation of Rad51 recombinase presynaptic filament assembly via interactions with the Rad52 mediator and the Srs2 anti-recombinase. *J. Biol. Chem.*, *284*, 24363–71.

Shinohara, M., Shita-Yamaguchi, E., Buerstedde, J. M., Shinagawa, H., Ogawa, H., and Shinohara, A. (1997). Characterization of the roles of the Saccharomyces cerevisiae RAD54 gene and a homologue of RAD54, RDH54/TID1, in mitosis and meiosis. *Genetics, 147* (4), 1545-56.

Shinohara, A., Ogawa, H., and Ogawa, T. (1992). Rad51 protein involved in repair and recombination in S. cerevisiae is a RecA-like protein. *Cell, 69* (3), 457-70.

Shinohara, A., and Ogawa, T. (1998). Stimulation of Rad52 of yeast Rad51-mediated recombination. *Nature, 391,* 404-407.

Simandlova, J., Zagelbaum, J., Payne, M. J., Chu, W. K., Shevelev, I., Handa, K., Chatterjee, S., Reid, D. A., Liu, Y., Janscak, P., Rothenberg, E., and Hickson, I. D. (2013). FBH1 helicase disrupts RAD51 filaments in vitro and modulates homologous recombination in mammalian cells. *J. Biol. Chem., 288* (47), 34168-34180.

Smirnova, M., and Klein, H. L. (2003). Role of the error-free damage bypass postreplica- tion repair pathway in the maintenance of genomic stability. *Mutat. Res.*, *532*, (2003) 117–135.

Smith, K. N., and Nicolas, A. (1998). Recombination at work for meiosis. *Curr. Opin. Genet. Dev., 8* (2), 200-11.

Sourirajan, A., and Lichten, M. (2008). Polo-like kinase Cdc5 drives exit from pachytene during buding yeast meiosis. *Genes Dev., 22* (19), 2627-32.

Stafa, A., Donnianni, R. A., Timashev, L. A., Lam, A. F., and Symington, L. S. (2014). Template switching during break-induced replication is promoted by the Mph1 helicase in Saccharomyces cerevisiae. *Genetics*, *196*, 1017–1028.

Subramanian, V. V., and Hochwagen, A. (2014). The meiotic checkpoint network: step-by-step through meiotic prophase. *Cold Spring Harbor Perspect. Biol.*, *6*(10) :a016675.

Subramanian V. V., MacQueen A. J., Vader G., Shinohara M., Sanchez A., Borde V., Shinohara, A., and Hochwagen, A. (2016). Chromosome Synapsis Alleviates Mek1- Dependent Suppression of Meiotic DNA Repair. *PLoS. Biol. 14* (2).

Sung, P. (1997b) Yeast Rad55 and Rad57 proteins form a heterodimer that functions with replication protein A to promote DNA strand exchange by Rad51 recombinase. *Genes Dev.*, *11* (9), 1111-21.

Sung, P. (1997a). Function of yeast Rad52 protein as a mediator between replication protein A and the Rad51 recombinase. *J. Biol. Chem.*, *272* (45), 28194-7.

Suwaki, N., Klarea, K., and Tarsounas, M. (2011). RAD51 paralogs: Roles in DNA damage signaling, recombinational repair and tumorigenesis. *Seminars in Cell & Developmental Biology, 22*, 898-905.

Sym, M., Engebrecht, J., and Roeder, G. S. (1993). ZIP1 is a synaptonemal complex protein required for meiotic chromosome synapsis. *Cell*, *72*, 365–378.

Tang, S., Wu, M. K., Zhang, R., and Hunter, N., (2015). Pervasive and essential roles of the Top3-Rmi1 decatenase orchestrate recombination and facilitate chromosome segregation in meiosis. *Mol. Cell*, *57*, 607–621.

Tessé, S., Storlazzi, A., Kleckner, N., Gargano, S., and Zickler, D. (2003). Localization and roles of Ski8p protein in Sordaria meiosis and delineation of three mechanistically distinct steps of meiotic homolog juxtaposition. *Proc Natl Acad Sci*, *100*, 12865–12870.

Tsubouchi, H., and Ogawa, H. (1998). A novel mre11 mutation impairs processing of double-strand breaks of DNA during both mitosis and meiosis. *Molecular and cellular biology*, *18* (1), 260–268.

Ulrich, H. D. (2001). The srs2 suppressor of UV sensitivity acts specifically on the RAD5- and MMS2-dependent branch of the RAD6 pathway. *Nucleic Acids Res.*, *29*, 3487–3494.

Urulangodi, M., Sebesta, M., Menolfi, D. *et al.* (2015). Local regulation of the Srs2 helicase by the SUMO-like domain protein Esc2 promotes recombination at sites of stalled replication. *Gene Dev.*, *29*, 2067–80.

Usui, T., Ohta, T., Oshiumi, H., Tomizawa, J., Ogawa, H., and Ogawa, T. (1998). Complex formation and functional versatility of Mre11 of budding yeast in recombination. *Cell*, *95* (5), 705–716.

van Gent, D. C., Hoeijmakers, J. H., and Kanaar, R. (2001). Chromosomal stability and the DNA double-stranded break connection. *Nature Rev. Genet.*, *2*, 196–206.

Vaze, M. B., Pellicioli, A., Lee, S. E., Ira, G., Liberi, G., Arbel-Eden, A., Foiani, M., and Haber, J. E. (2002). Recovery from checkpoint-mediated arrest after repair of a double- strand break requires Srs2 helicase. *Mol. Cell, 10* (2), 373-85.

Veaute, X., Jeusset, J., Soustelle, C., Kowalczykowski, S. C., Le Cam, E., and Fabre, F. (2003). The Srs2 helicase prevents recombination by disrupting Rad51 nucleoprotein filaments. *Nature*, *423*, 309 –312.

Wanat, J., Gemici, Z., and Alani, E. (2004). Competing crossover pathways act during meiosis in Saccharomyces cerevisiae. *Genetics*, *168*, 1805–16.

Wang, S.W., Goodwin, A., Hickson, I.D., and Norbury, C.J. (2001). Involvement of Schizosaccharomyces pombe Srs2 in cellular responses to DNA damage. *Nucleic Acids Res., 29*, 2963–2972.

Ward, J. D., Muzzini, D. M., Petalcorin, M. I., Martinez-Perez, E., Martin, J. S., Plevani, P., Cassata, G., Marini, F., and Boulton, S. J. (2010). Overlapping mechanisms promote postsynaptic RAD-51 filament disassembly during meiotic double-strand break repair. *Mol. Cell*, *37*, 259–272.

Watts, F. Z. (2006). Sumoylation of PCNA: Wrestling with recombination at stalled replication forks. *DNA Repair (Amst)*, *5*, 399–403.

Weinert, T. A., Kiser, G. L., and Hartwell, L. H. (1994). Mitotic checkpoint genes in budding yeast and the dependence of mitosis on DNA replication and repair. *Genes Dev.*, *8*, 652-665.

Wooster, R., Neuhausen, S. L., Mangion, J., Quirk, Y., Ford, D., Collins, N., Nguyen, K., Seal, S., Tran, T., Averill, D. *et al.*, (1994). Localization of a breast cancer susceptibility gene, BRCA2, to chromosome 13q12-13. *Science, 265* (5181), 2088-2090.

Wu, L., and Hickson, I. D. (2003). The Bloom's syndrome helicase suppresses crossing over during homologous recombination. *Nature*, *426*(6968), 870-874.

Wu, H. Y., Ho, H. C., and Burgess, S. M. (2010). Mek1 kinase governs outcomes of meiotic recombination and the checkpoint response. *Curr. Bio.*, *20*, 1707–1716.

Xu, L., Ajimura, M., Padmore, R., Klein, C., Kleckner, N. (1995). NDT80, a meiosis- specific gene required for exit from pachytene in Saccharomyces cerevisiae. *Mol. Cell Biol., 15* (12), 6572-6581.

Xu, L., Weiner, B. M., and Kleckner, N. (1997). Meiotic cells monitor the status of the interhomolog recombination complex. *Genes Dev.*, *11*, 106-118.

Youds, J. L., Mets, D. G., Mcllwraith, M. J., Martin, J. S., Ward, J. D., O'Neil, N. J., Rose, A. M., West, S. C., Meyer, B. J., Boulton, S. J. (2010). RTEL-1 enforces meiotic crossover interference and homeostasis. *Science, 327*, 1254-1258.

Zakharyevich, K., Ma, Y., Tang, S., Hwang, P. Y-H., Boiteux, S., and Hunter, N. (2010). Temporally and biochemically distinct activities of Exo1 during meiosis: double-strand break resection and resolution of double Holliday junctions. *Mol. Cell*, *40*, 1001–15.

Zakharyevich, K., Tang, S., Ma, Y., and Hunter, N. (2012). Delineation of joint molecule resolution pathways in meiosis identifies a crossover-specific resolvase. *Cell*, *149*, 334–47.

Zhao, W., Vaithiyalingam, S., San Filippo, J., Maranon, D. G., Jimenez-Sainz, J., Fontenay, G. V., Kwon, Y., Leung, S. G., Lu, L., Jensen, R. B., Chazin, W. J., Wiese, C., and Sung, P. (2015). Promotion of BRCA2-Dependent Homologous Recombination by DSS1 via RPA Targeting and DNA Mimicry. *Molecular cell*, *59* (2), 176–187.

Zickler, D., and Kleckner, N. (1999). Meiotic chromosomes: integrating structure and function. *Annu. Rev. Genet., 33*, 603-754.

Zickler, D., and Kleckner, N. (2015). Recombination, Pairing, and Synapsis of Homologs during Meiosis. *Cold Spring Harbor perspectives in biology*, *7* (6), a016626.

Acknowledgements

I would like to express my gratitude towards my supervisor Prof. Akira Shinohara for his continued guidance, support and encouragement during my PhD research study. I am thankful for having been blessed with a good environment for practicing science and learning to be a good researcher. I am thankful to Dr. Ashok Venkitaraman , Dr. Michael Lichten, Dr. Bernard deMassay and Dr. Valerie Borde for insightful discussion regarding my research project. I would like to especially thank Dr. Michael Lichten for sharing unpublished data. I would like to thank Dr. Andreas Hochwagen and Dr. Neil Hunter for providing the yeast strains and Dr. Michael Lichten for providing the antibodies used in this study.

I would like to express my heartfelt gratitude towards Assistant Professor Kenichiro Matsuzaki for giving me guidance and advices regarding my research study as well as research in science in general. I was blessed to have the opportunity to learn from him. I am also thankful for his help in learning experimental techniques. I would also like to thank Associate Professor Asako Furukohri for her active interest in my research project and for giving insightful comments during the preparation of this thesis and presentation.

I am grateful to Dr. Kiran Challa for teaching me basic yeast techniques. I would also like to thank Dr. Mika Higashide for teaching me CHEF and Southern blotting analysis and also for the very helpful experimental advices.

I would like to thank the lab technicians for their help in making my experience doing experiments in the lab very comfortable. I would like to especially thank Hisako Matsumoto, Hiroko Wakabayashi and Chie Watanabe for their assistance in the lab. I would like to thank the lab secretaries for their generous support to make my life in Japan comfortable. I would like to especially thank Hisako Matsumoto and Miki Akaji for their friendship and support.

I would like to thank the lab members present in the lab during my five years in the lab. I would like to especially thank my lab member Lira Palmer for her friendship and support. I would like to thank my lab PhD batchmate Priyanka Sawant for her continued support during my PhD work.

Lastly, I would to thank for Parents and my siblings for their continued understanding and support during my PhD. I would like to thank my father for supporting me financially and my mother and my siblings for providing emotional support.